Finite Element Analysis of the Application of Synthetic Fiber Ropes to Reduce Blast Response of Frames

By

Michael Rembert Motley

Thesis Submitted to the Faculty of the
Virginia Polytechnic Institute and State University
In Partial Fulfillment of the Requirements for the Degree of

MASTER OF SCIENCE
IN
CIVIL ENGINEERING

Approved by:

_____

Raymond H. Plaut, Chairman

_____ _____

Thomas M. Murray Rakesh K. Kapania

December 2004
Blacksburg, Virginia

Keywords: Blast, Synthetic Fiber Ropes, Frame, Springs, Strain Rate Effects

Finite Element Analysis of the Application of Synthetic Fiber Ropes to Reduce Blast Response of Frames

by

Michael Rembert Motley
Raymond H. Plaut, Committee Chairman
Civil Engineering

(ABSTRACT)

Blast resistance has recently become increasingly relevant for structural engineers. Blast loads are created by explosive devices that, upon detonation, create pressure loads that are much higher than most that a structure would ever experience. While there are many types of blast loads that are impossible to adequately prepare for, methods are presently being developed to mitigate these loads. This research investigates the possibility of using synthetic fiber ropes as a means of blast resistance. This is the third phase of a multi-stage research endeavor whose goal is to analyze Snapping-Cable Energy Dissipators (SCEDs) for reducing the effects of large-scale lateral loads.

Finite element models of portal frames were developed using the commercial finite element program ABAQUS and dynamic models were run for varying blasts and frame systems. Blast pressures of 100, 2,000, and 4,000 psi were applied to a steel portal frame and comparisons were made between unbraced frames and frames braced with springs of different stiffnesses. Additional tests were run to examine the effects of strain rate dependent yield on the results of the models. Parallel research is being conducted on the specific material behavior of the synthetic fiber ropes so that the models developed for this research can be revised for a more accurate determination of the effects of the ropes on structural systems subjected to blast loads.

Acknowledgements

I would initially like to thank my committee chairman and advisor, Dr. Raymond H. Plaut. He was vital in the completion of this research and in guiding me in the right direction throughout the duration of this project and his help is highly appreciated. Furthermore, I would like to thank the members of my committee, Dr. Thomas M. Murray and Dr. Rakesh K. Kapania, for their willingness to participate in this research project.

I would also like to thank those who guided me along the way in the completion of this project. Sangeon Chun and Hitesh Kapoor were very helpful in the initial phases of researching the effects of blasts. The collaborations with John Ryan, Paul Taylor, and Greg Hensley were very helpful in developing an understanding of the finite element programs. Ronald Shope and Soojae Park were integral in the completion of the models.

I would further like to thank the people that I have met and the friends that I have made during my time in Blacksburg. I have met too many good friends to name them all here and they have been very supportive of me as I tried to get used to the area and the snow and everything else. I would also like to thank those whom I left behind from my days at The Citadel, students and faculty included. Without their help I could have easily found myself struggling to succeed rather than pushing myself forward.

Finally, I would like to thank the members of my family who have been behind me every step of the way. Mom and Dad, Mark and Brad, and everyone else back in Charleston have supported me through thick and thin and have made my life easier in many different ways. Most importantly, I would like to thank Melissa, who spent the last 18 months with me in Blacksburg and made more sacrifices for me during that time than I could have ever expected.

This research was supported by the National Science Foundation under Grant No. CMS-0114709, and their support is integral in this process and is greatly appreciated.

Table of Contents

List of Figures

List of Tables

Chapter 1
Introduction and Literature Review

1.1 Introduction

Severe lateral impact loads can cause massive damage to structures and often can result in complete failure of an entire support structure. Blast loads are among the most devastating lateral impact loads that a structure may experience. While it is impractical to design a structure for rare large-scale blasts, engineers are beginning to examine methods to prevent the failures that can result from more common blasts such as vehicular bombs. Initial developments in blast resistant design include pressure-reflecting wall systems and code reevaluation. Many of the innovations for blast design, however, have been instituted for large or important government buildings with relatively high budgets. For smaller buildings, other methods of blast resistance must be developed. Furthermore, affordable methods of retrofit must also be investigated so that existing buildings can be strengthened for the possibility of a blast.

A multi-stage research endeavor has begun to examine the use of synthetic fiber ropes as energy dissipators by connecting them diagonally in a slightly relaxed state as a modified x-brace to structural frames. The initial scope of the research was to analyze the effects of these ropes as passive earthquake dampers known as snapping-cable energy dissipators (SCEDs). This research has been expanded to include other possible uses of the ropes. When a blast occurs, extremely high pressures are exerted upon a structure over a very short time period. The large peak pressures over small time periods produce dynamic loads unlike most loads that a structure will experience. These loads, however, can be extreme in nature and cause high levels of deflection and plastic behavior. The advantage of these restraints is that they can relieve a structure of some of the deflections produced by such large dynamic loads that can lead to plastic behavior in the structure.

The purpose of this research is to utilize previous research on the SCEDs and on blast loads and combine those to examine the effects of the SCEDs on structures subjected to blast loads. The ongoing research includes the examination of the specific dynamic behavior of the SCEDs as a result of snap loadings. Because this research is not complete, the SCEDs were modeled as simple springs for a means of comparison. All modeling of the blast loads was performed in the finite element program ABAQUS. Models were developed with and without springs so that the spread of plasticity and the frame deflections could be compared to determine the effectiveness of the springs with different stiffnesses. Once the actual properties and behavior of the SCEDs are developed, they can be inserted into the ABAQUS program to determine their exact effect on the frame.

1.2 Literature Review

1.2.1 Blast Load Characteristics

When an explosive device is detonated, a reaction takes place within the device that creates extremely high pressures relative to ambient air pressure, and high-speed pressure waves travel from the center of the blast outward in all directions, gradually decaying until the waves either completely dissipate or come into physical contact with an object. The pressures that these objects experience are known as blast loads. The loading diagram for the pressure of an ideal blast wave can be modeled using the Friedlander equation (Fung and Chow 1999) defined as

$$p(t) = p_s\left[1 - \frac{t}{\tau}\right]e^{-\frac{bt}{\tau}} \tag{1.1}$$

where p_s = peak overpressure;

τ = positive phase duration;

b = decay constant.

Furthermore, the characteristics of a specific blast can be defined using the Hopkinson scaling law (Baker 1973) which states that any two explosions will have the same ideal blast characteristics at equal scaled distances. The Hopkinson scaling distance is

$$Z = \frac{R}{W^{\frac{1}{3}}} \tag{1.2}$$

where R = actual distance from the center of the blast to the point on a structure where the blast load is applied;

W = weight of the explosive.

Dharaneepathy et al. (1995) examined the distances of explosions from structures and concluded that there is a "ground-zero distance" for all structures. This distance is the critical distance where the cumulative blast effects are at a maximum for the specific structure. Their study was intended to refute the previously held notion that choosing an arbitrary distance for a blast was adequate for design purposes. They determined that, particularly for tall structures, the "ground-zero distance" should be used as the design distance to include the maximum effects of a blast.

An ASCE task committee (Conrath et al. 1999) published a report on designing structures for physical security that details the relationship between explosive characteristics such as types, weights, and locations and the resulting pressure loads. In general, blast loads are characterized in pounds of trinitrotoluene (TNT), a relatively stable chemical compound that is used in many types of explosives. The pressure of a blast of any type can be converted to a blast size to be defined in pounds of TNT. Beshara (1994) studied the modeling of blast loads on above-ground structures and developed mathematical models used to formulate blast load equations. He explained the conversion of the energy output of a blast relative to that of TNT using the equation

$$W_{INT} = \frac{H_{\exp}}{H_{INT}} w_{\exp} \tag{1.3}$$

where W_{INT} = the equivalent TNT weight;

w_{exp} = the weight of the actual explosive;

$\frac{H_{INT}}{H_{\exp}}$ = TNT equivalent factor (ratio of heat of detonation to heat of explosion).

Williams and Newell (1991) discussed methods for assessing blast response of structures in a paper written when engineers were just beginning to examine possibilities for blast resistance. They discussed some of the initial ideas concerning types of blasts and structural behavior. Blast loads are defined by their incident and reflected overpressures. Due to the increase in air temperature from the incident wave, reflected blast waves are multiplied by an amplification factor between 2 and 8, depending on the incident overpressure. For surface explosions, an amplification factor of 1.8 is used—2.0 factor less 10% of the explosive energy that goes into cratering.

1.2.2 Structural Response to Blast Loads

Because blast loads occur so much more quickly than most loads and can have much higher magnitudes than most loads, many types of studies have taken place examining the effects of blast loads in a range of structural systems. Shope and Plaut (1998,1999) examined critical blast loads on both one-span and two-span compressed steel columns. In their first series of analyses on single-span columns, they determined that for a column subjected to a constant axial load and a uniform blast load, the introduction of residual stresses and strain-rate effects reduces the maximum axial load at low impulses and increases the critical impulse at low axial loads. Their later research examined similar compressed steel columns with two spans. From this work they determined that the critical impulse for the two-span case is considerably higher than that of single-span columns of equal length within the acceptable design range.

Williams and Newell (1991) examined the initial concepts of structural response due to blasts. They explained that when the positive phase duration is much shorter than the natural period of the structure ($\tau \leq 0.1T$), the blast wave can be assumed to have produced an instantaneous velocity to the structure, while blasts with longer positive phase durations ($\tau \geq 6T$) can be treated as static loads. They also stated that as a general

rule, materials loaded at high strain rates exhibit higher yield strengths and more ductility than statically loaded materials. Variations in parameters such as Young's modulus can be neglected. For simple SDOF models, for short duration loads it is common to neglect damping effects because damping can be hard to assess and because, commonly, damping forces achieve significant magnitude only after substantial motion has occurred.

Barker (1997) discussed dynamic material behavior to aid a task committee formed by the ASCE Petrochemical Committee. He explained that dynamic material behavior is a function of material strength as well as deformation, both of which must be taken into account to properly perform blast analysis and design. Dynamic loads generally produce an increase in material strength but may decrease ductility. When dynamic loads are applied to a structural element, the material does not have time to deform at the same rate as the load is applied. Both yield strength and ultimate strength are affected by this strain rate behavior. The increase in yield strength can be in the range of 10-40% which can make a significant difference in blast resistance. Ignoring dynamic effects underestimates member end reactions, leading to inadequate connection design for the development of full flexural resistance and prevention of non-ductile failure modes. He continued by relating that blast design utilizes an ultimate strength approach but eliminates safety factors on loads since the blast load is assumed to be an infrequent, maximum load. Resistance factors are also eliminated to reduce conservatism. Structural elements in blast design are generally allowed to exceed the elastic limit and achieve plastic deformation, allowing the member to absorb a much larger amount of blast energy than a static response. Limits on maximum deflection are generally used to determine the adequacy of a member. The primary deformation parameters are support rotation and ductility ratio. Support rotation is the angle formed between the longitudinal axis of the member and a line drawn from the support to the point of maximum deflection. Ductility ratio is the degree of plasticity achieved in a member. A typical measure of frame response is sidesway, which is the lateral deflection at the top of the frame relative to the supports.

Krauthammer (1999) considered the blast resistance of structural concrete and steel

connections. He concluded that, in general, the rotational deformation capacities of steel connections are governed by not only the rigidity of connections, but also the flexural capacity of the adjoining structural members. For weaker connections, such as in semi-rigid connections, the rotational capacity of the connection might be governed by its internal resistance and deformations as opposed to the flexural capacities of the adjoining members. He also explained that very little emphasis seems to be put on the weak axis deformations, which results in surprisingly large horizontal deflections. Two major concerns were developed in the study of structural steel connections, one being the blast resistance of the connections. It was shown that dead loads have an adverse effect on the behavior of the connections due to the added bending and twisting of the beams once they were deformed by the blast.

Longinow and Mniszewski (1996) studied vehicular bombs and their effect on structural systems. They explained that reflected blast pressures are generally at least twice that of the incident shock wave and are proportional to the strength of the incident shock, which is proportional to the weight of the explosive. Developing a structure that will avoid collapse can be done through the sufficient addition of redundants to effectively redistribute loads when portions of the structure are destroyed. Effective passive protection is also crucial for safety, generally in terms of a closed perimeter that prevents an attack from being close enough to do significant harm to a structure.

1.2.3 Blast Resistance

Events such as the bombing of the Alfred P. Murrah Federal Building in Oklahoma and the 1993 bombing of the World Trade Centers have brought attention to the need for blast load retrofitting of existing buildings and blast design standards for new structures. These events showed that even high-profile structures are not immune to attacks. The role of the design codes quickly expanded to include blast resistance. Building new structures to updated blast design specifications, while at times more costly, would be easier. Cost-effective techniques could be developed for smaller structures. The retrofit

of existing structures was an important task for engineers. Several methods were developed, including reflecting walls and structural dampers.

Mlakar (1996) discussed structural design for vehicular bombs, encouraging a system exhibiting strength, ductility, and redundancy. The selection bears some resemblance to the design against strong earthquake motions. An important factor to consider is the provision for redundant load paths, which can prevent an overall collapse of the structure with associated catastrophic damage in the event of the destruction of an isolated element or elements. He also discussed how retrofitting presents a challenging problem for engineers. While increased standoff distances seem to be the most cost-efficient solution, it is not always practical. Modification of boundary conditions can result in a stronger component, for example changing a boundary condition from simply supported to fixed.

Miyamoto et al. (2000) examined blast loadings of 3000 lb of TNT at standoff distances of 100, 40, and 20 ft. Tests were conducted on a conventional special moment resisting frame (SMRF) and an SMRF with a fluid viscous damper (FVD). The SMRF is considered a bare frame and the frame including the damper is a damped frame. For all cases tested, blast overpressure was assumed to be the most significant cause of failure. Nonlinear analyses indicated that FVDs provided a cost-effective way to control displacement and plastic hinge rotation of lateral load resisting frames under blast loading. FVDs absorb significant amounts of input blast energy throughout the duration of the structural response. Because maximum displacement occurs at a somewhat late stage in the time history, damping energy reduces strain energy contribution, thereby reducing maximum displacement. Large blast loading can overcome kinetic energy and cause inelastic response in the structure. FVDs can greatly increase the performance of non-ductile moment frames by eliminating or reducing inelastic demand.

Pearson (2002) and Hennessey (2003) performed the initial research on which this research is based. They examined the possibility of using snapping-cable energy disspators for controlling structural response to seismic activity. The unique accelerations that ground motions induce are similar to the loads produced by blast loads

in that they are rare, high-strain-rate events that produce loads much larger than those seen on a regular basis. Therefore, the use of these cables in blast resistance is examined in the research herein.

1.3 Scope of Research

The objective of this research is to examine the possible benefits of synthetic fiber ropes as a means of blast resistance in portal frames. The ropes were modeled as springs in the finite element analysis program ABAQUS. Bilinear and nonlinear springs were modeled and the structure was examined with and without the inclusion of rate dependent yield effects. This research utilizes previous research that was performed on the properties of the ropes and is part of a multi-stage research project that examines the structural benefits of Snapping Cable Energy Dissipators (SCEDs).

Chapter two of this thesis discusses the use of the finite element program ABAQUS. The construction of the frame model is explained and the results of static and dynamic verification analyses are discussed.

Chapter three begins to examine the effects of blast loads on the portal frame. The modeling of the blast load in ABAQUS is discussed and key nodes of the frame are identified. The results of the blast analysis are presented in terms of these key nodes for the extent of this research.

Chapter four studies the frame with the inclusion of bilinear springs for the same blast loads as discussed in chapter three. These springs are modeled with some slack in them, which would be expected in a full-scale model. A comparison of the frame with and without springs is performed in detail.

Chapter five of this research examines the inclusion of high strain rate effects on the material behavior of the frame. Comparisons are made between the frames discussed in

chapters three and four with and without the addition of rate dependent yield as a material property.

Chapter six takes information gathered from parallel research regarding the actual behavior of the springs and analyzes a more realistic model with nonlinear springs. Comparisons of the nonlinear springs and bilinear springs are made and the benefits of using particular springs are discussed.

Chapter seven summarizes the entire scope of the research from the previous chapters and conclusions are made. Recommendations for future research are also made regarding SCEDs for blast resistance.

Appendix A includes a set of calculations for the length of the springs and the modeling of the slackness in the ropes. Appendix B contains a series of input files for the ABAQUS models.

Chapter 2
Computer Models for Finite Element Analysis

2.1 ABAQUS

The analysis of a structure's response to blast loadings is a difficult task. To achieve adequate results, a multi-degree-of-freedom (MDOF) model must be used with a very large number of degrees of freedom. An analytical dynamic analysis is suitable for a model with only a few degrees of freedom. By solving the dynamic equilibrium equation, an estimate of the structural response can be obtained. There comes a point where the number of degrees of freedom in a model makes it impractical to derive an analytical solution. The finite element method is the most practical way to analyze a structure when a large number of degrees of freedom is necessary. Finite element analyses can be performed using a number of commercial programs. The finite element program ABAQUS was used for this research.

2.1.1 Frame Model

This research examines the structural response of a portal frame subjected to a blast load. The portal frame (Fig. 2.1) developed has 156-in.-high columns and a 300-in.-long beam. All members are 50-ksi steel and are typical wide flange I-sections. The modulus of elasticity for the steel is 29,000 ksi. The columns are W8 x 40 and the beam is W18 x 35 (Fig. 2.2) (*AISC*, 2001). Strain hardening was neglected by using an elastic-perfectly plastic stress-strain relationship for all steel. The supports at the base of the columns are fixed and it is assumed that there is a rigid connection between the beam and the columns. Damping was neglected in the analysis.

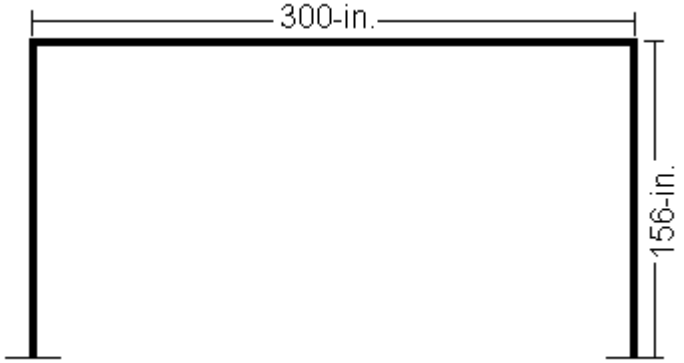

Fig. 2.1. Model of the portal frame (base unit = inch)

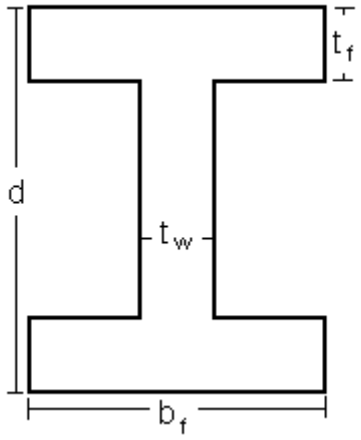

	d	t_w	b_f	t_f	A	I_x	I_y
COLUMN	8.25	0.360	8.07	0.560	11.7	146	49.1
BEAM	17.7	0.300	6.00	0.425	10.3	510	15.3

Fig. 2.2. Typical cross-sections (base unit = inch)

2.1.2 Analysis and Element Type

There are several methods of processing a model in ABAQUS. Due to the nature of the loading, this research used ABAQUS/Explicit as the solver. ABAQUS/Explicit performs explicit dynamic analyses and is recommended for models with high loads over short

time spans. ABAQUS/Explicit uses steps to define the problem history. A step can be programmed using the *STEP command in an input file. It is at this point that the type of analysis is defined. This research utilized a dynamic, explicit analysis. Geometric nonlinearity was considered by specifying an NLGEOM command within the *STEP portion of the input file.

When performing a finite element model, it is important to determine the proper type of element for the model that is being analyzed. ABAQUS contains a large number of different element types, categorized based on family, degrees of freedom, number of nodes, formulation, and integration. For this research, a C3D8R continuum element was used. This type of element is an 8-node linear brick with reduced integration. Three-dimensional brick elements were used to allow for the blast loads to be applied as surface pressures instead of distributed line loads. ABAQUS recommends using continuum elements for complex nonlinear analyses involving plasticity and large deformations, crucial features for blast analysis.

A large number of elements were used to maximize the results. Through an iterative process it was determined that an adequate model is achieved if the column flanges contain 720 elements (40 elements high x 9 elements wide x 2 elements deep), the column webs have 360 elements (40 x 9 x 1), the beam flanges include 1,440 elements (80 x 9 x 2), and the beam web contains 720 elements (80 x 9 x 1). The mesh can be seen in Fig. 2.3 taken from ABAQUS.

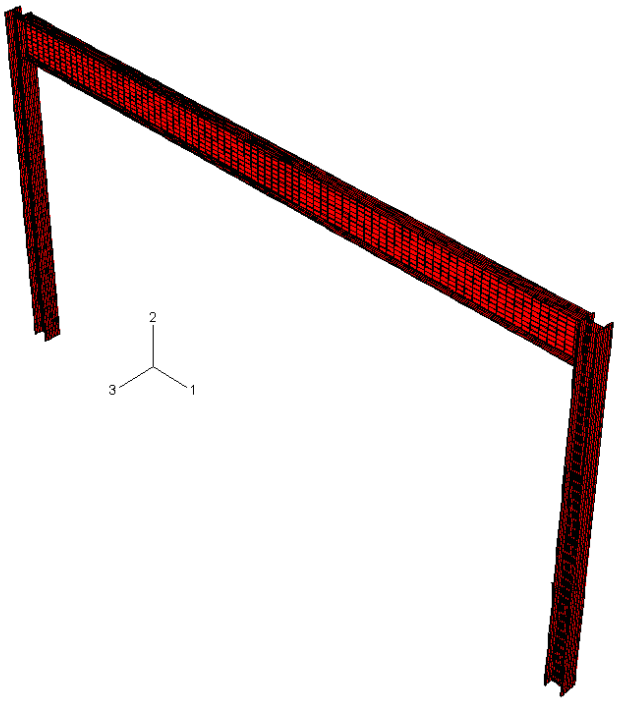

Fig. 2.3. Portal frame mesh taken from ABAQUS

2.2 ABAQUS Verification

The first step in using any commercial software program is the verification of the modeling technique. For this research, two types of verification were performed. An initial static deflection analysis for a cantilevered W8 x 40 column with a concentrated load at the free end was performed to ensure that the continuum elements and the boundary conditions were properly developed. Second, a single-degree-of-freedom dynamic analysis was devised as an estimate of the behavior of a frame subjected to a forced sine wave loading.

2.2.1 Static Analysis

The column used for the static deflection verification was a W8 x 40 with the same input as the columns in the frame in terms of dimensions, material properties, and elements. A concentrated load of 10 kips was placed on the end of the column in the local-1 direction. A static analysis was performed in ABAQUS/Standard—ABAQUS/Explicit is only

applicable for dynamic analyses—and the deflections were compared with the equation for deflection of a cantilevered beam (*AISC*, 2001):

$$\Delta(x) = \frac{P}{6EI}(x^3 - 3l^2x + 2l^3) \tag{2.1}$$

$$\Delta_{max} = \frac{Pl^3}{3EI} \tag{2.2}$$

where P = concentrated load (kip);

E = modulus of elasticity (ksi);

I = moment of inertia about the bending axis (in.^{4});

l = total length of the member (in.).

The maximum deflection of the column in ABAQUS was found to be 3.06 in. while the maximum theoretical deflection is 2.99 in. Fig. 2.4 shows the finite element deflection and the theoretical deflection of the column.

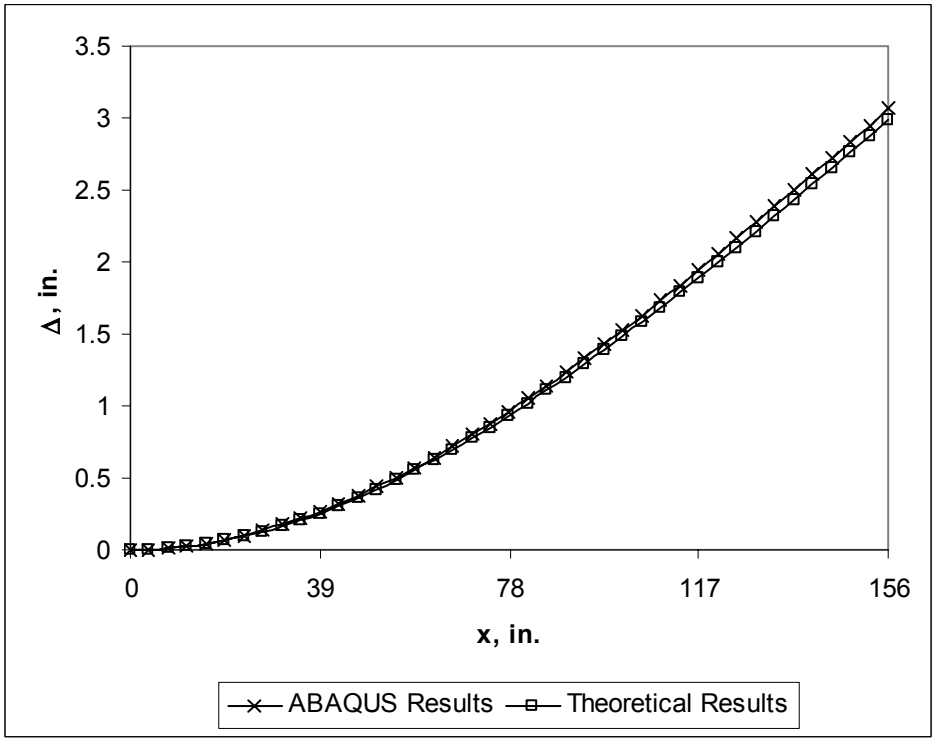

Fig. 2.4. Deflection of a W8 x 40 cantilever subjected to a 10-kip concentrated load on the free end.

The results from the initial ABAQUS verification coincide with the theoretical results very closely throughout the length of the column. This verifies that the continuum elements have been developed such that the boundary conditions and the connections of the elements are valid.

2.2.2 Dynamic Analysis

The second step of the verification process was ensuring that the dynamic solver was consistent with theoretical data for a portal frame. The large number of elements and degrees of freedom in the research model, however, made it unable to perform a parallel theoretical analysis. Instead, a single-degree-of-freedom (SDOF) analysis was developed to compare to the ABAQUS analysis. Chopra (2001) explains the process for analyzing an undamped SDOF frame under harmonic vibration using the equilibrium equation

$$mii + ku = p_o \sin(\omega t) \tag{2.3}$$

where m = mass of the system (kip$*$sec^2/in.);

k = stiffness of the system (kip/in.);

p_o = maximum value of the force (kip);

ω = forcing frequency (rad/sec);

t = time (sec).

Chopra solves this equation for the displacement, and the resulting equation for a system beginning at rest, taking into account the complementary and particular solutions, is

$$u(t) = \frac{p_o}{k} \frac{1}{1-(\omega/\omega_n)^2} \left(\sin(\omega t) - \frac{\omega}{\omega_n} \sin(\omega_n t) \right) \tag{2.4}$$

where ω_n = natural frequency of the system (rad/sec).

For the models, a forcing frequency of 100 rad/sec and an amplitude of 300 kips was used, making the forcing function

$$p(t) = 300 \sin(100t) \tag{2.5}$$

A lumped mass, *m*, of 3.56 lb$*$sec^2/in. was calculated based on the material properties of the structure and was taken at the midspan of the beam. Chopra also gives an equation

for the stiffness of a portal frame based on the relationship between the properties of the beam and the columns:

$$k = \frac{24EI_c}{h_c^3}\frac{12\rho + 1}{12\rho + 4} \tag{2.6}$$

where $\rho = \frac{I_b h_c}{I_c h_b}$ (2.7)

I_c = moment of inertia for the column (in.^{4});

I_b = moment of inertia for the beam (in.^{4});

h_c = height of the column (in.);

h_b = length of the beam (in.);

The stiffness of the system is 23.42 kip/in. The natural frequency of an SDOF system is calculated as

$$\omega_n = \sqrt{\frac{k}{m}} \tag{2.8}$$

Once the variables were calculated and used, the theoretical solution matched the ABAQUS solution for the first several cycles, then they diverged slightly (Fig. 2.5). However, because there is such a large difference in the number of degrees of freedom, some variation is to be expected between the two models. The determination of the mass and the stiffness would vary between an SDOF model and a model with many degrees of freedom, thereby changing the natural frequency of the system. Modifications to the mass and stiffness had a noticeable effect on the theoretical behavior of the system. The theoretical behavior was examined after raising the mass by 4% (Fig. 2.6), lowering the stiffness by 4% (Fig. 2.7), and respectively changing both values by 2% (Fig. 2.8). It is evident that a slight change in those values can make up for the variation in the behavior calculated by an SDOF model. The frequency with which the structure moves is nearly identical with the modifications. The difference in amplitude, also seen slightly in the static deflection test, can be attributed to the fact that the number of integration points is so high relative to the SDOF model.

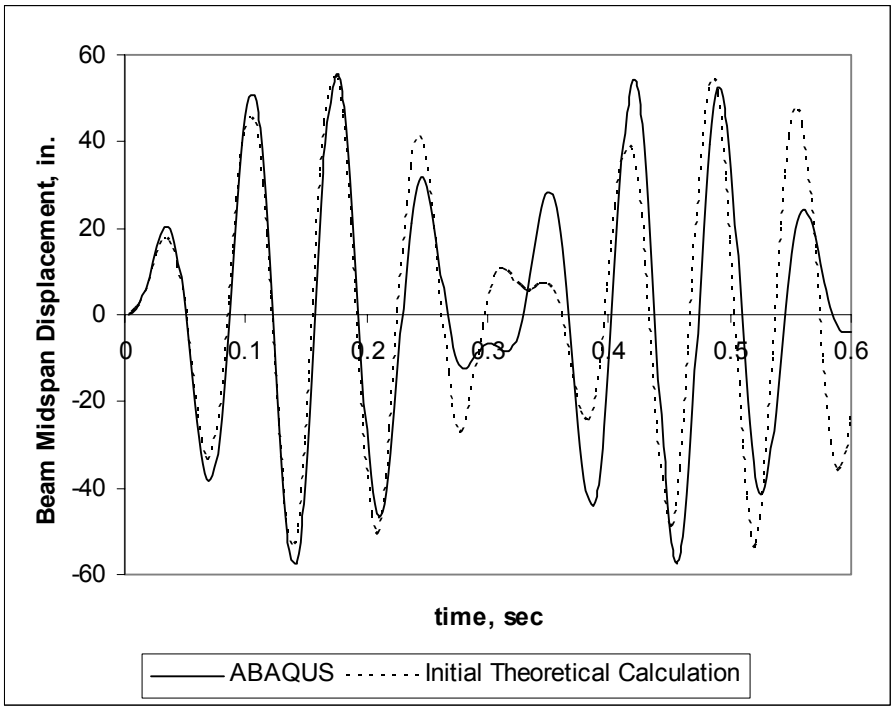

Fig. 2.5. ABAQUS vs. initial theoretical calculation for undamped harmonic excitation of a portal frame

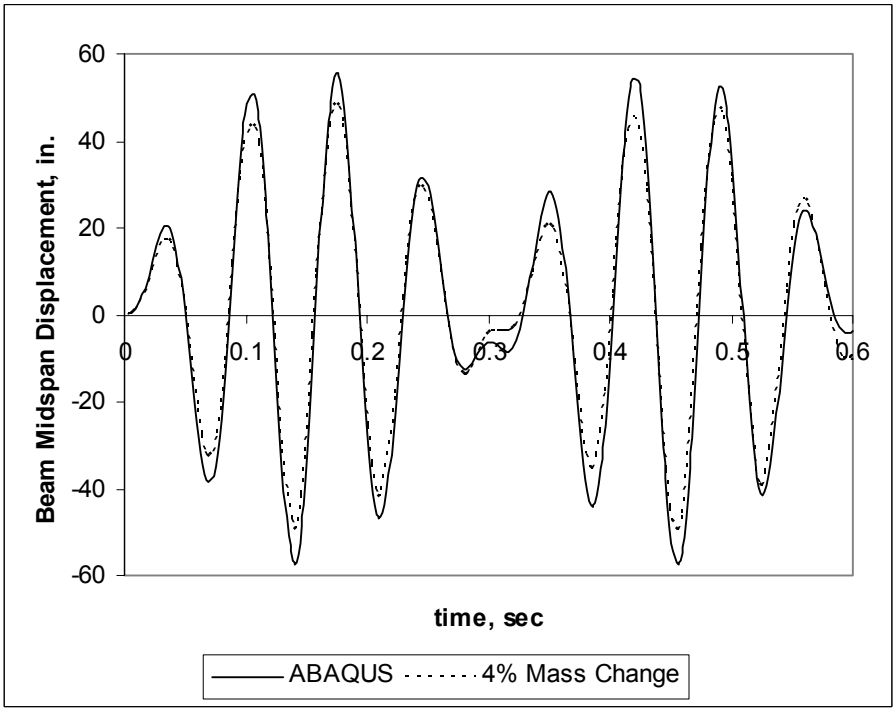

Fig. 2.6. ABAQUS vs. initial theoretical calculation with 4% increase in lumped mass for undamped harmonic excitation of a portal frame

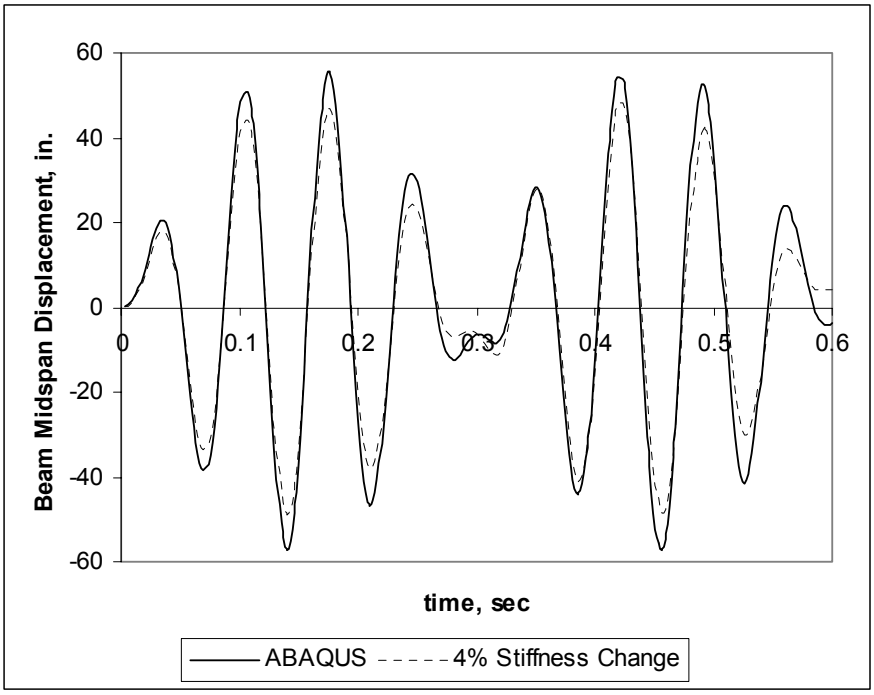

Fig. 2.7. ABAQUS vs. initial theoretical calculation with 4% decrease in stiffness for undamped harmonic excitation of a portal frame

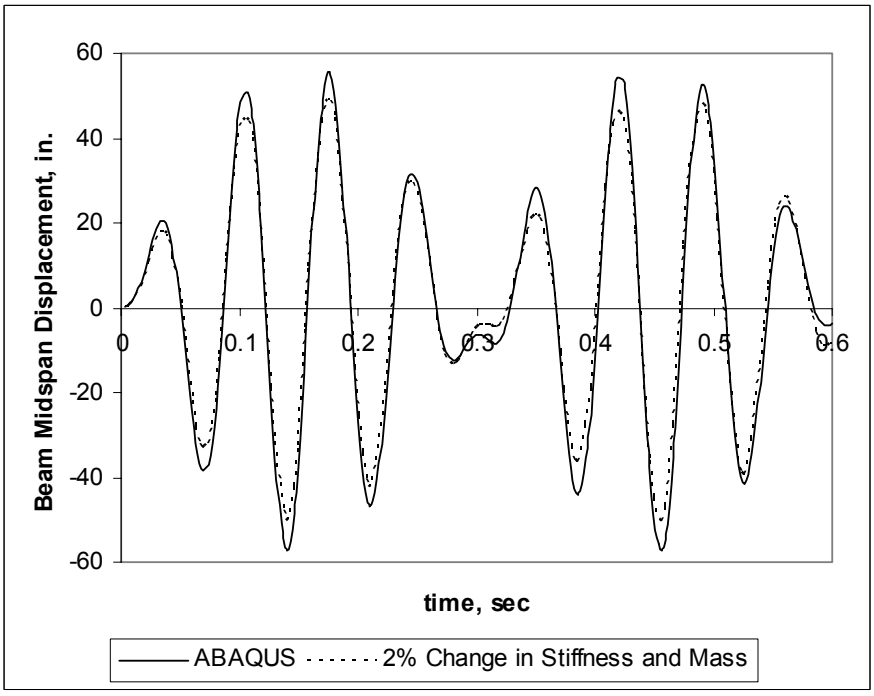

Fig. 2.8. ABAQUS vs. initial theoretical calculation with 2% increase in lumped mass and 2% decrease in stiffness for undamped harmonic excitation of a portal frame

Chapter 3

Blast Loads on a Bare Portal Frame

3.1 Blast Loads

Blast loads are formed when an explosive device is detonated, causing a high speed pressure wave that creates high pressure loads on a structure over a short time span. Blasts can be modeled using pressure time histories or as impulses. For this research, the Friedlander equation (Eq. 1.1) was used. The blast is represented by a unit curve for an ideal blast load multiplied by varying amplitudes (Fig. 3.1).

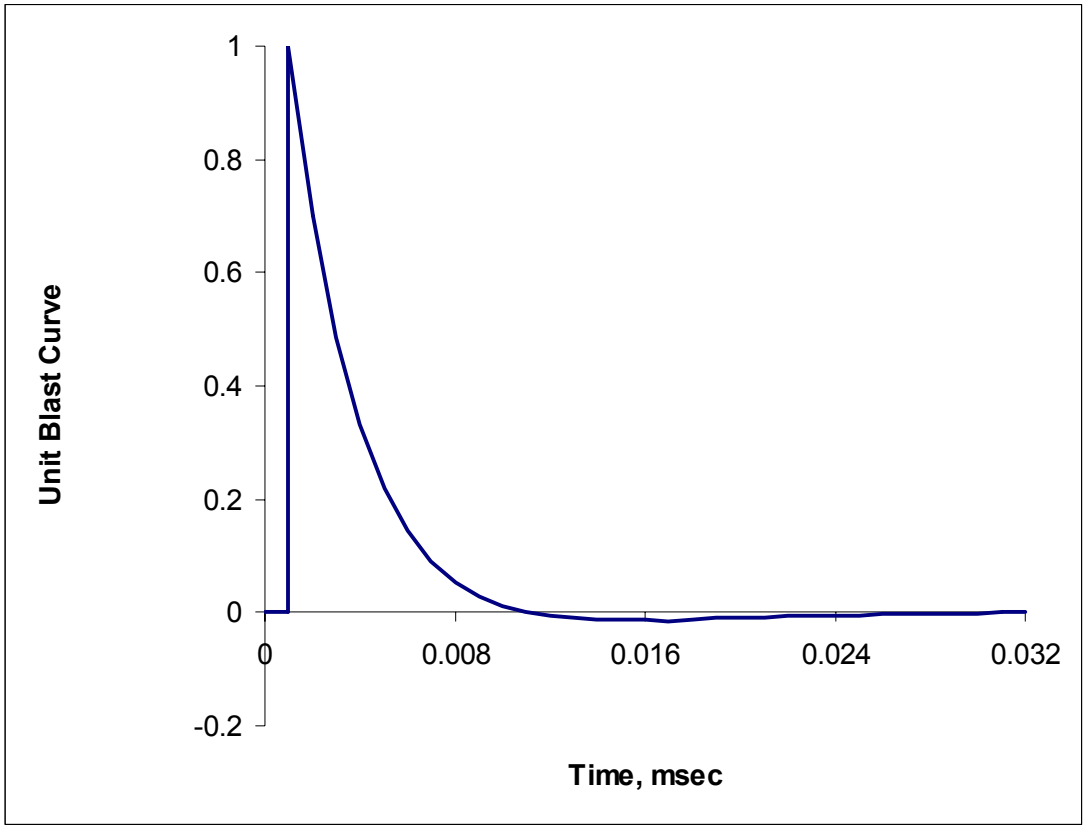

Fig. 3.1. Ideal blast curve used in this research

This curve is defined in the input file and then an amplitude is specified in the *STEP command. The specified amplitude is the peak pressure. All other points on the curve are based on that value. On the curve, 32 points were calculated at a time step of 1 msec. Several amplitudes will be applied to this curve to investigate the behavior of the frame. Miyamoto et al. (2000) examined frames subjected to 3,000 lb TNT blasts at different standoff distances. Their peak pressures at 1 msec are shown in Table 3.1.

Standoff Distance	Peak Reflected Pressure
100 ft	20 psi
40 ft	840 psi
20 ft	4,400 psi

Table 3.1. Peak reflected pressure at 1 msec for 3,000 lb TNT blasts at varying standoff distances (Miyamoto and Taylor 2000)

For this research, blasts will be examined with peak pressures of 100 psi, 2,000 psi, and 4,000 psi. Based on the aforementioned study, this is within a realistic range for blast loads. The load is applied as a lateral pressure along the entire length of the left column of the frame and acts in the global-X direction throughout its duration; therefore, the follower effects of the pressure are not taken into account. This can be seen in Fig. 3.2.

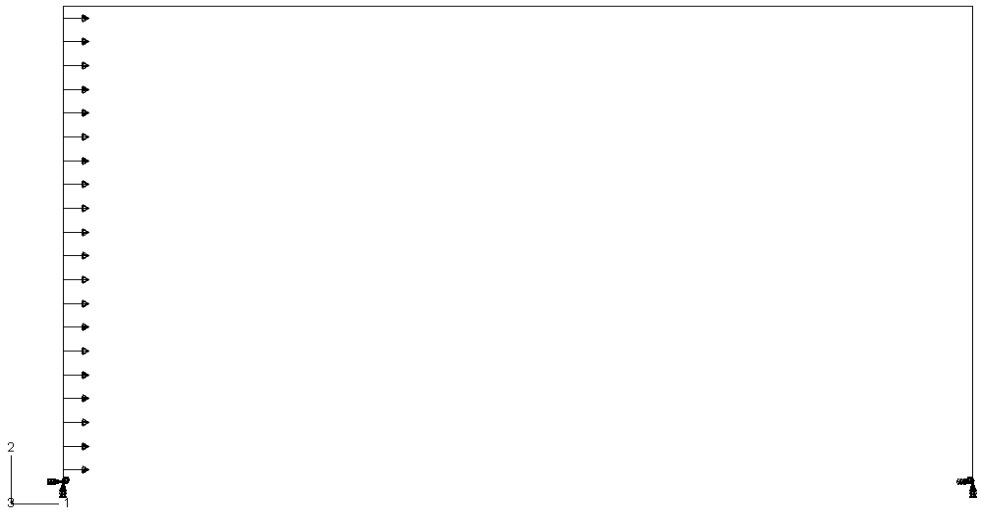

Fig. 3.2. Representation of the blast load on the frame

To achieve an accurate representation of the effects of the blast on the structure, the time period of the ABAQUS analysis was 0.25 seconds for each model. This allowed the structure to experience several cycles of motion before the end of the analysis.

3.2 Bare Frame Models

The purpose of this research is to examine the effects of ropes, modeled as springs, on frames subjected to blasts with varying peak pressures. The first step of the comparison is to examine frames without springs. These frames will be referred to as bare frames throughout the rest of this research. Strain rate effects were ignored for the first series of models. It is important to note that after all of the models were run, several points were determined to be key points of deflection in the frame. These points are the midspan of each column and the top corners of the frame. Nodes were then taken from each area and used to compare the deflections between different models. These nodes are described in Table 3.2 and shown in Fig. 3.3.

Node 205	Midspan of blast side column, midpoint of far left flange
Node 405	Top of blast side column, midpoint of far left flange
Node 11205	Midspan of opposite side column, midpoint of far right flange
Node 11405	Top of opposite side column, midpoint of far right flange

Table 3.2. Location of important nodes in the ABAQUS model

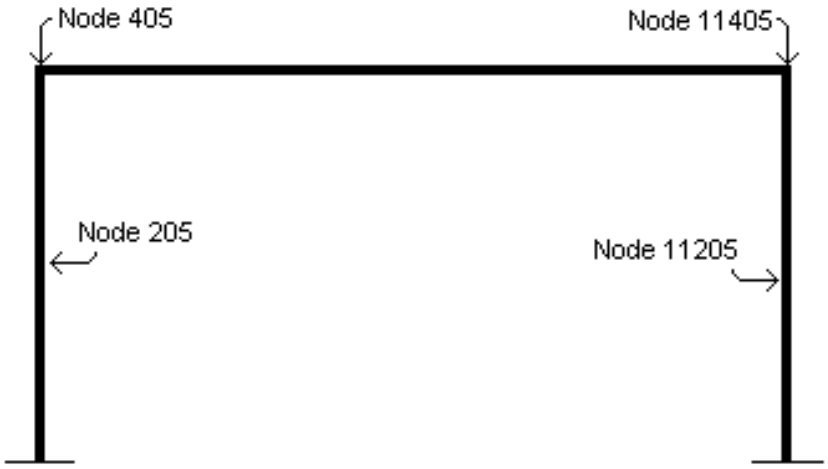

Fig. 3.3. Location of important nodes in the ABAQUS model

3.2.1 Case I – 100 psi blast

The initial blast applied to the model was a 100 psi blast. This blast caused no permanent plastic deformation in the structure and little deflection. The deflection of the structure is small, with a maximum amplitude about 0.2 in. (Figs. 3.4, 3.5). The deflections in these figures are for nodes 405 and 11405 (see Table 3.2). These small deflections result in small stresses that do not reach the elastic limit of the material. A model of the von Mises stresses in the frame can be found in Fig. 3.6. The range of contours in all stress plots is linear from 0 psi to 50,000 psi. It is noted that there is little change in color in the 100 psi stress diagram as the stresses did not reach high enough values on the applicable scale. There is some change from the darker blue region of 0 stress to a lighter blue region that signifies small stress changes in the model.

3.2.2 Case II – 2,000 psi blast

A 2,000 psi blast caused much more drastic results than the 100 psi blast. This blast caused significant plastic deformation, especially in the blast side column. Analyzing the results of this model led to the decision that the midpoint of the blast side column (node

205) was a crucial point in the behavior of the system. As a means of comparison, deflection data were collected from the midpoint of the opposite column (node 11205). The maximum deflection from the 2,000 psi blast was 8.68 in. at node 205, while deflections only reached 7.21 in. and 7.40 in. at nodes 405 and 11405, respectively (Figs. 3.7, 3.8, 3.9). Fig. 3.10 shows the deflection time-history of node 11205. The slight variation in deflections at nodes 405 and 11405 can be attributed to two factors—the location of the nodes on the column and the deflected shape of the frame. The large deflection at the midspan of the blast side column caused the blast side flange to camber outward toward the blast, reducing the total deflection at node 405. Likewise, the bending in the opposite column caused the outer flange to camber outward, increasing total deflection at node 11405.

Stresses in the frame were analyzed and are shown in Fig. 3.11. The stresses in the frame for Case II are substantially different from those in Case I. The permanent plastic deformation in the frame subjected to the 2,000 psi blast is shown in Fig. 3.12. Plastic deformation was considered to occur when equivalent plastic strain occurred in the frame. As the blast passed over the frame, plasticity developed initially at the midspan of the blast side column, at the supports, and at the connections. As the load decayed, the plasticity spread to its final permanent distribution.

3.2.3 Case III – 4,000 psi blast

The final blast that was considered was a 4,000 psi blast. The deflections caused by this blast were much greater than those caused by the other blasts (Figs. 3.13, 3.14, 3.15, and 3.16) with permanent deflection of roughly 18 in. at the corners of the frame and a maximum deflection of 37.61 in. at node 205. Comparative time histories for each of the three cases are shown in Figs 3.17 and 3.18. Fig. 3.19 shows a sample von Mises stress distribution of the frame. This blast caused plastic deformation across the majority of the blast side column and a substantial portion of the beam (Fig. 3.20). Also evident in this figure is the deflection of the blast side column relative to the rest of the frame.

Significant bending can be seen at the midspan and in the flanges at the support (Fig. 3.22). The total time of the blast load was not long enough to force total failure of the beam. Note the equivalent plastic strain in the member in the area. There is substantial plastic strain in the web of the blast side column just above the support; however, these values do not reach the failure strain of the material.

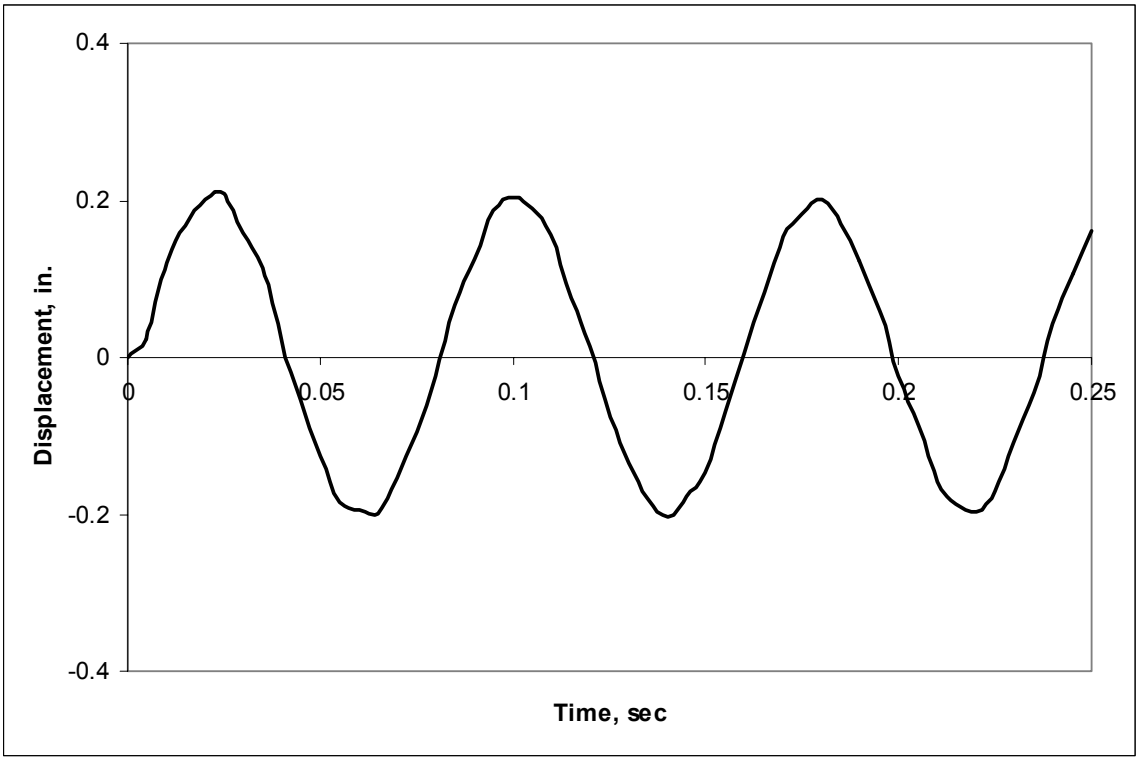

Fig. 3.4. Deflection time-history of node 405 for a 100 psi blast

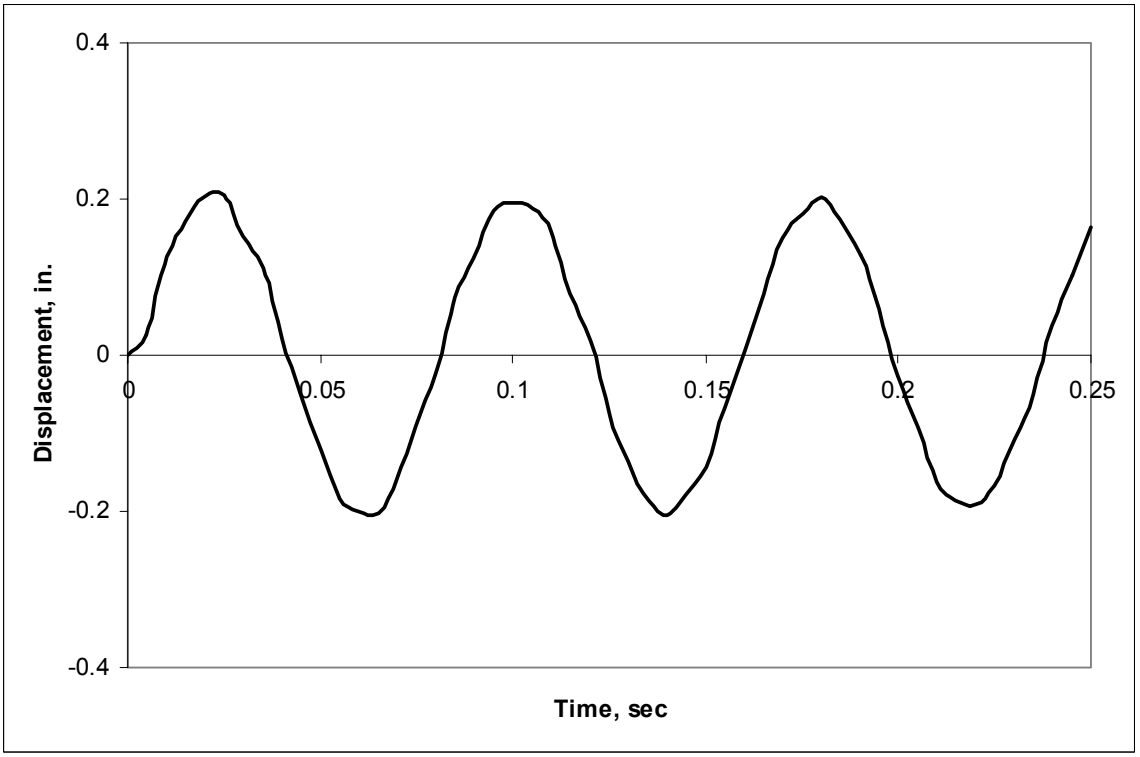

Fig. 3.5. Deflection time-history of node 11405 for a 100 psi blast

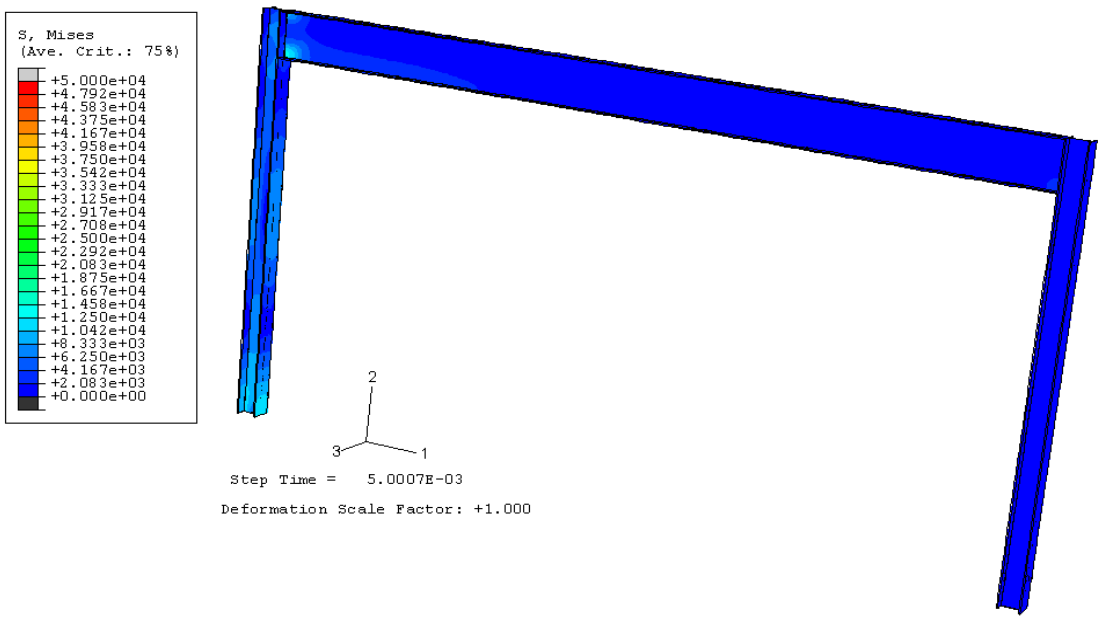

Fig. 3.6. Sample of von Mises stress distribution in the portal frame subjected to a 100 psi blast load

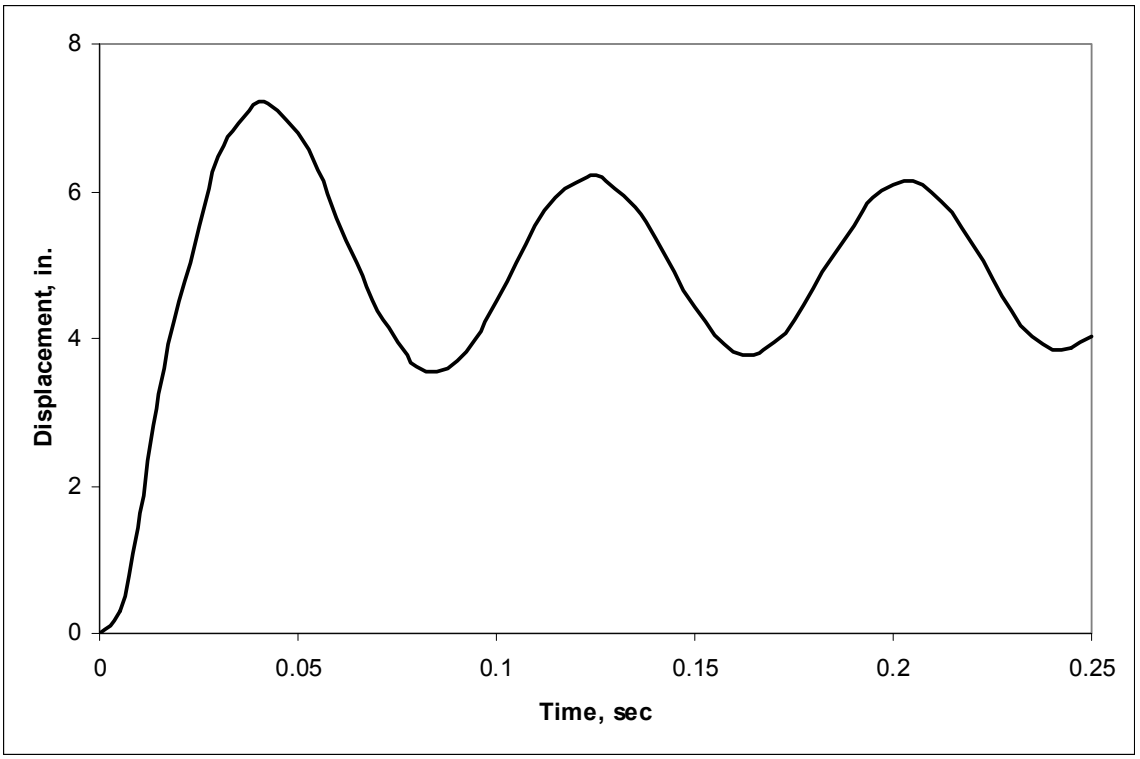

Fig. 3.7. Deflection time-history of node 405 for a 2,000 psi blast

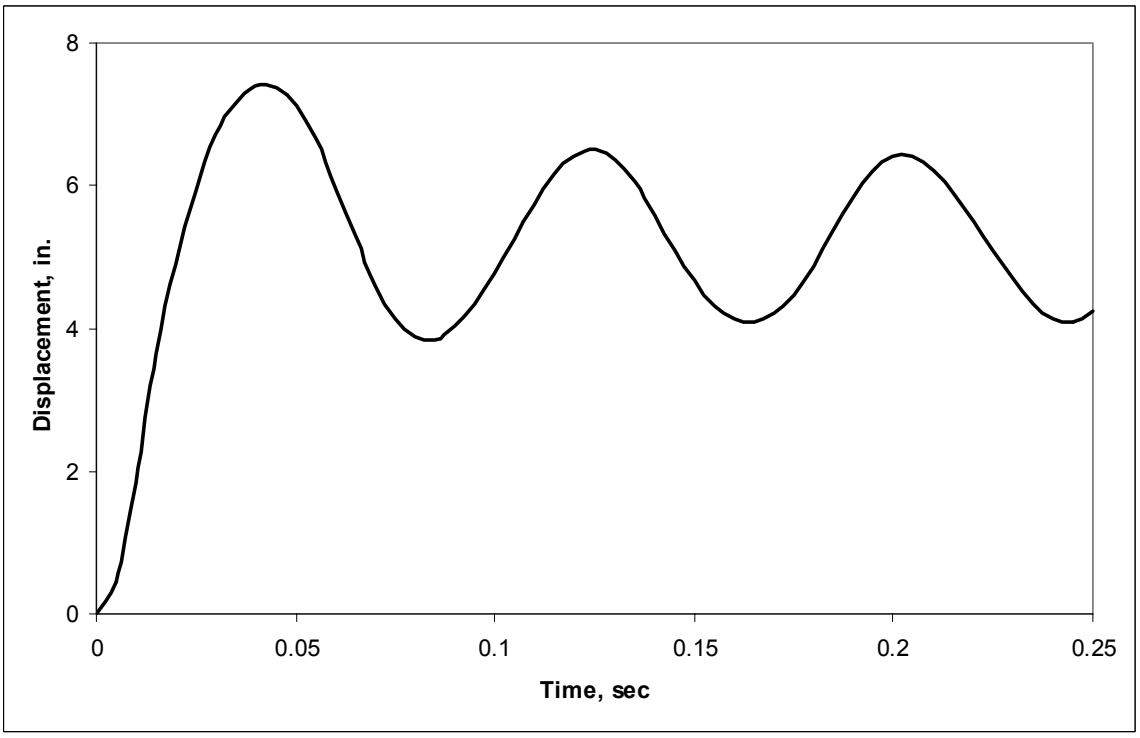

Fig. 3.8. Deflection time-history of node 11405 for a 2,000 psi blast

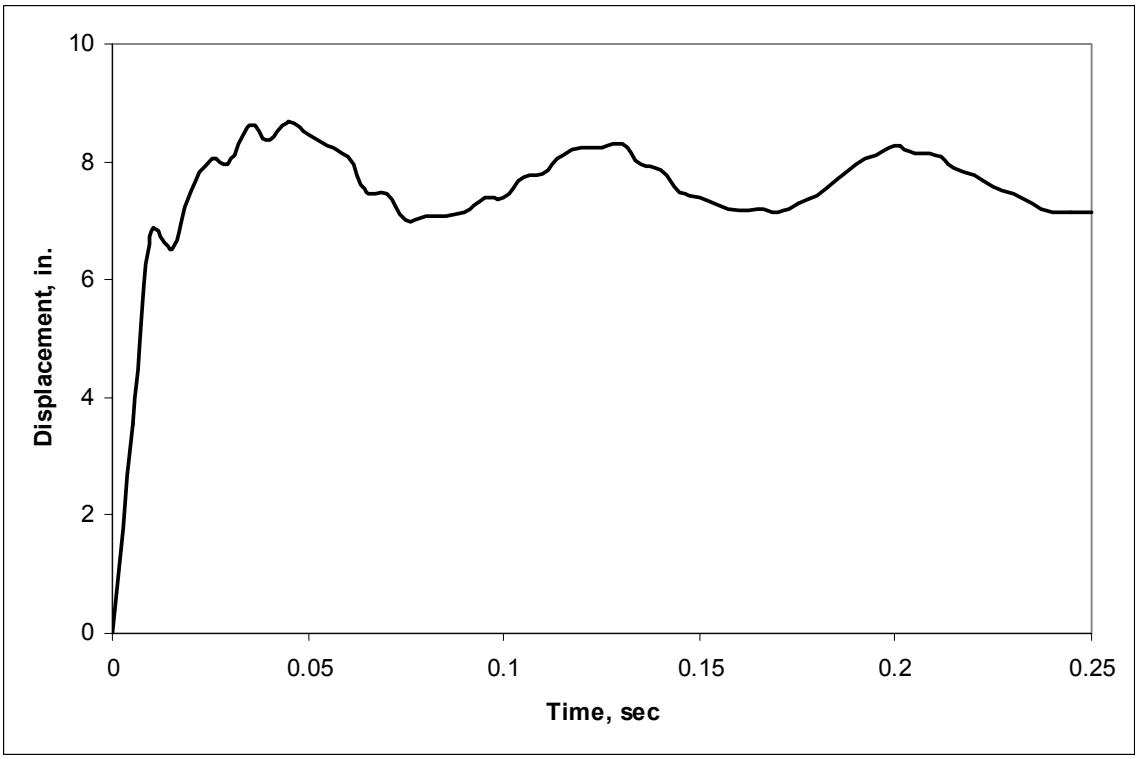

Fig. 3.9. Deflection time-history of node 205 for a 2,000 psi blast

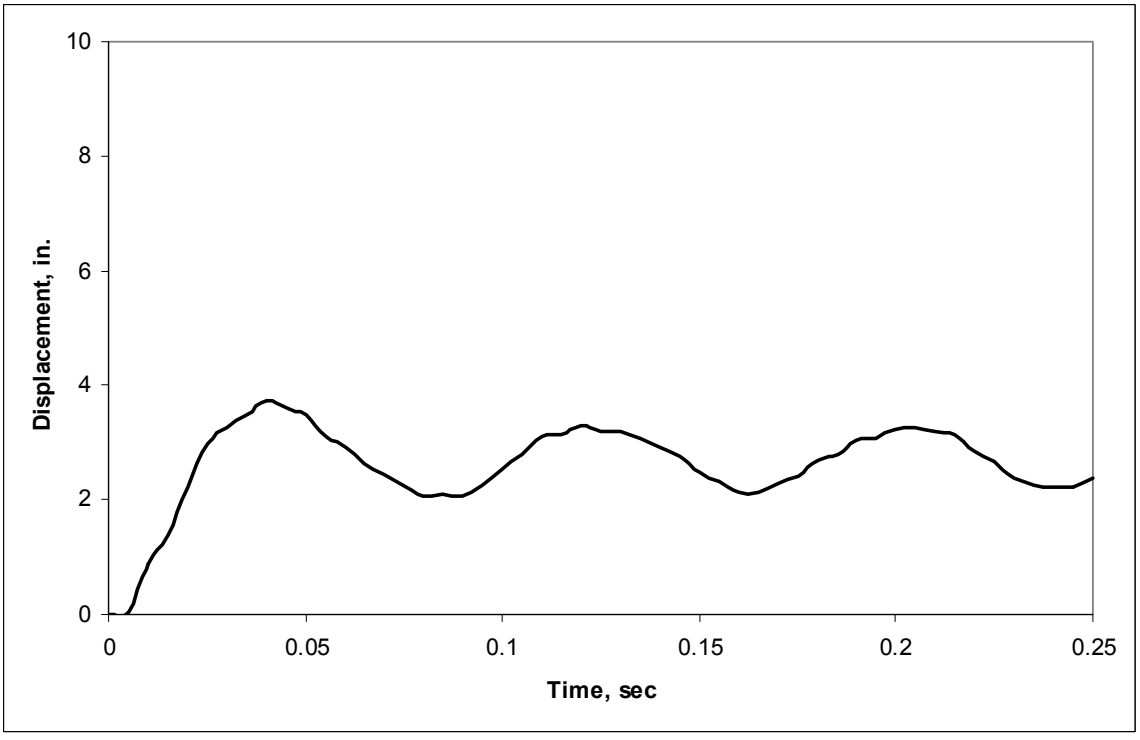

Fig. 3.10. Deflection time-history of node 11205 for a 2,000 psi blast

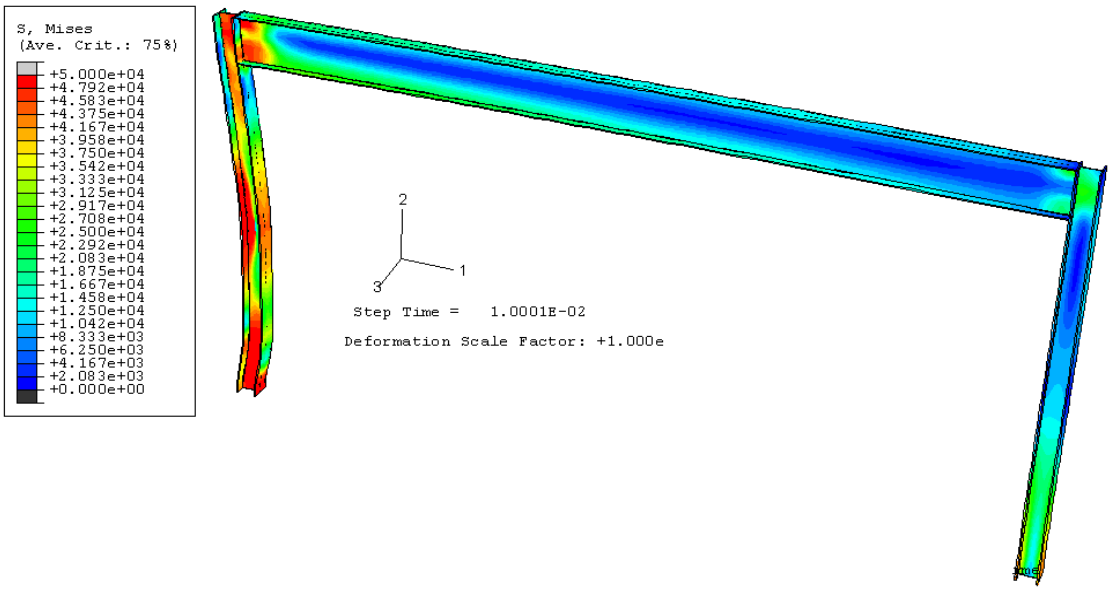

Fig. 3.11. Sample of von Mises stress distribution in the portal frame subjected to a 2,000 psi blast load at time t = 10 msec

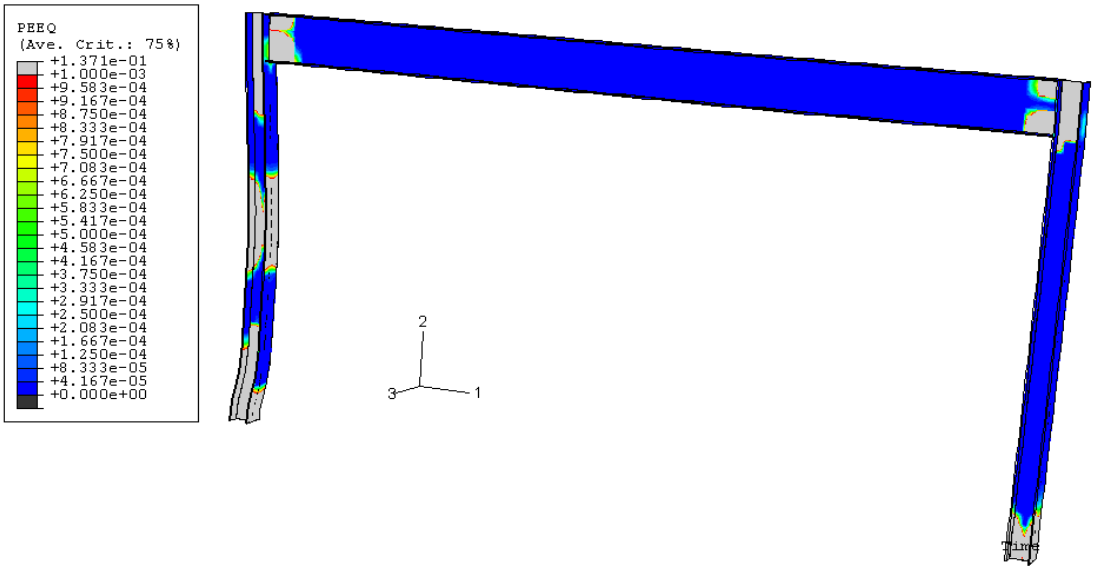

Fig. 3.12. Plastic deformation zones of the portal frame subjected to a 2,000 psi blast (no plastic deformation = blue) at time t = 0.25 sec

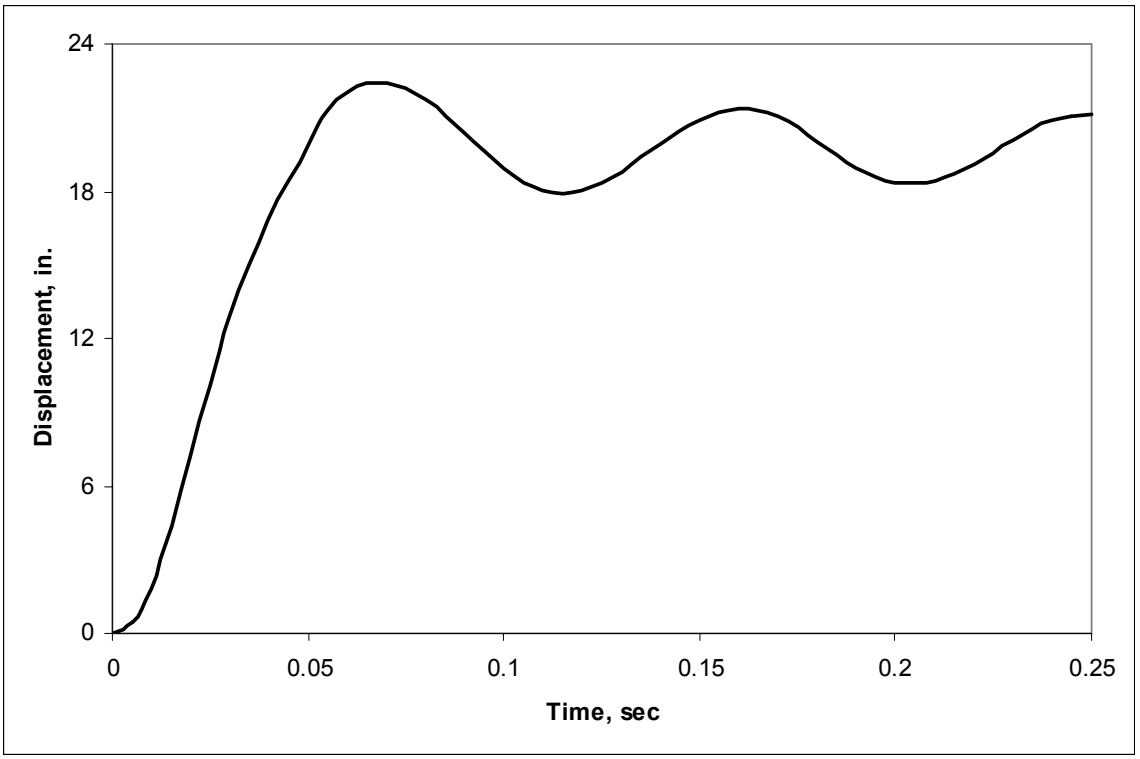

Fig. 3.13. Deflection time-history of node 405 for a 4,000 psi blast

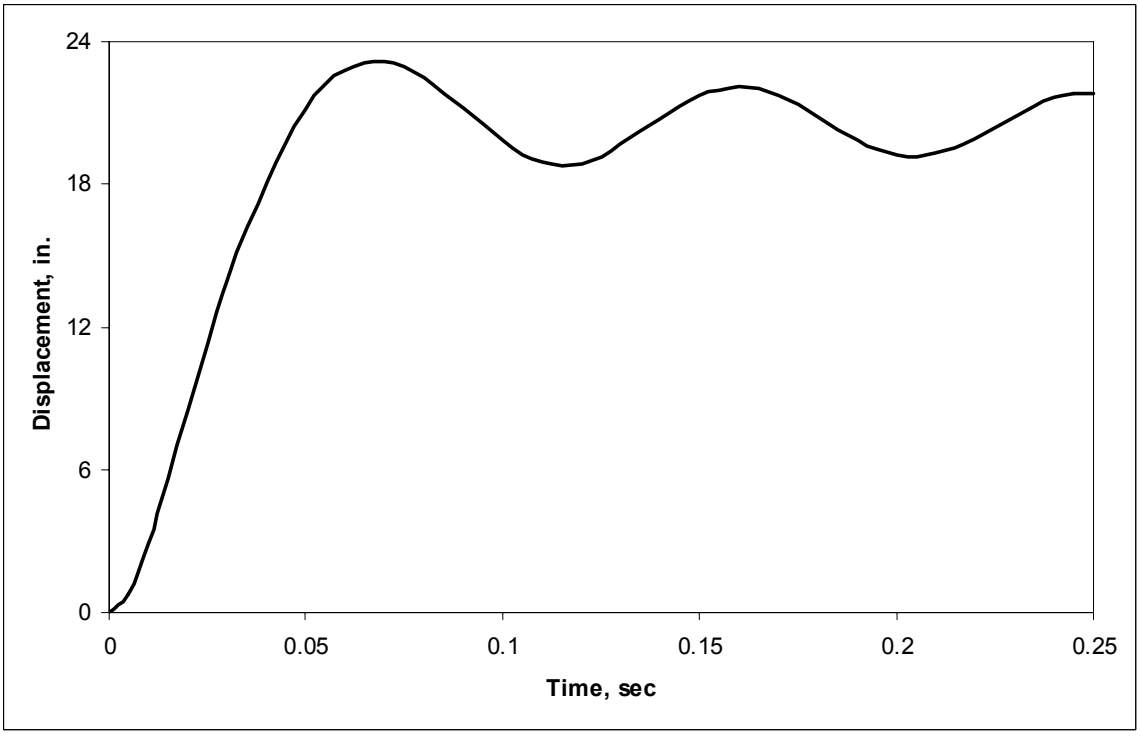

Fig. 3.14. Deflection time-history of node 11405 for a 4,000 psi blast

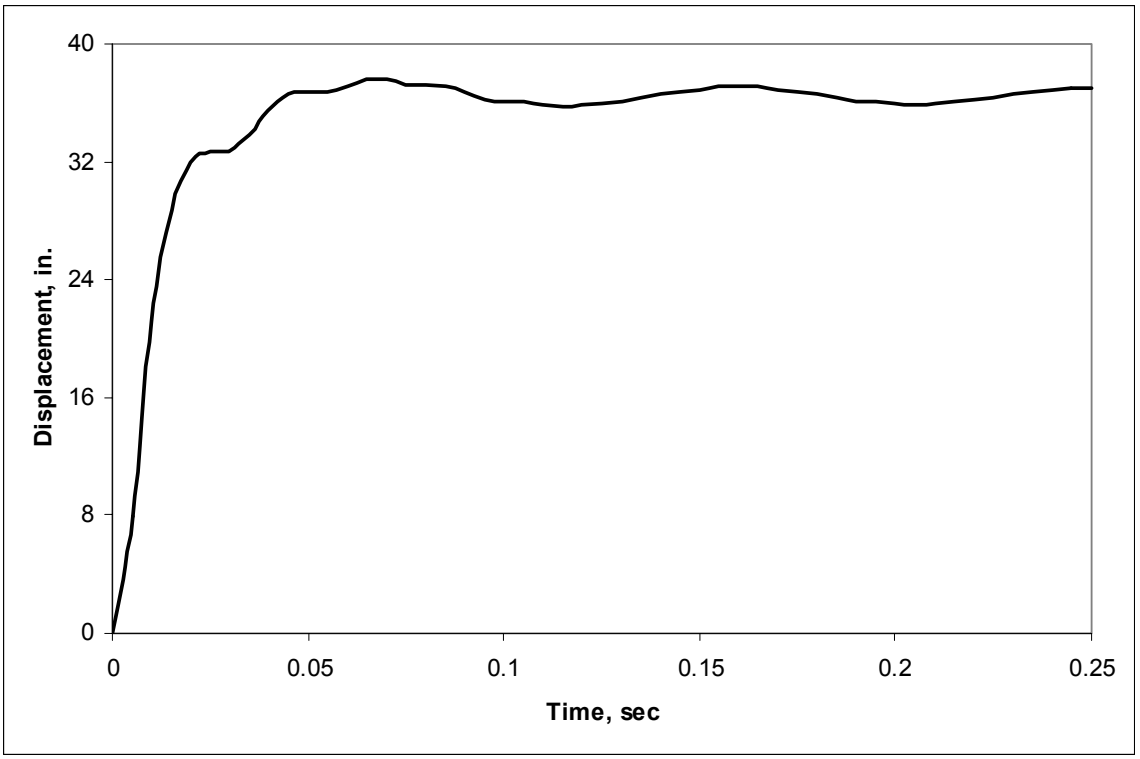

Fig. 3.15. Deflection time-history of node 205 for a 4,000 psi blast

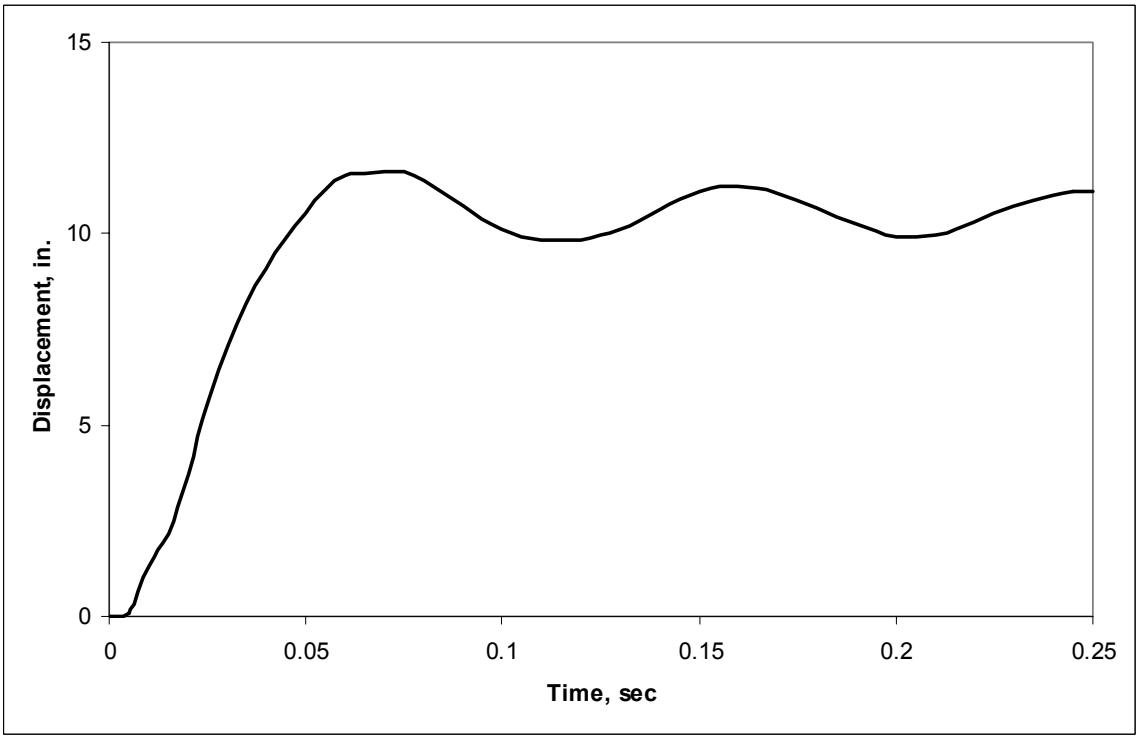

Fig. 3.16. Deflection time-history of node 11205 for a 4,000 psi blast

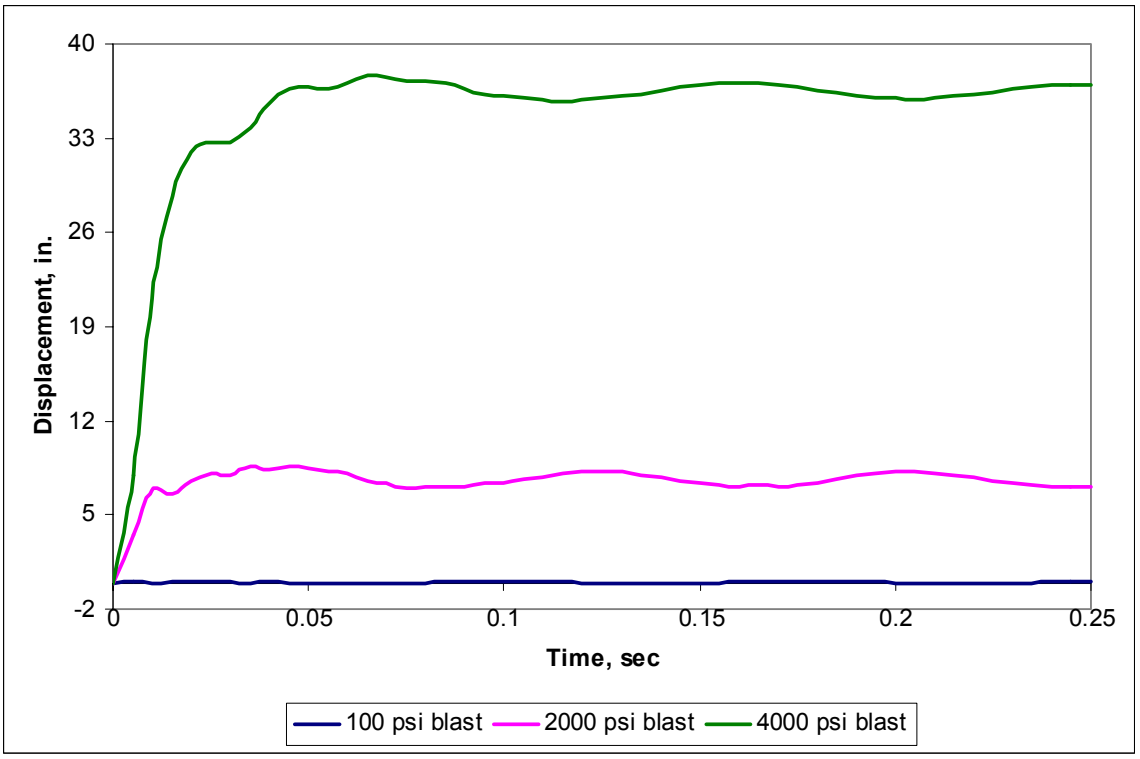

Fig. 3.17. Comparison of displacement time-histories at node 205 for different blasts

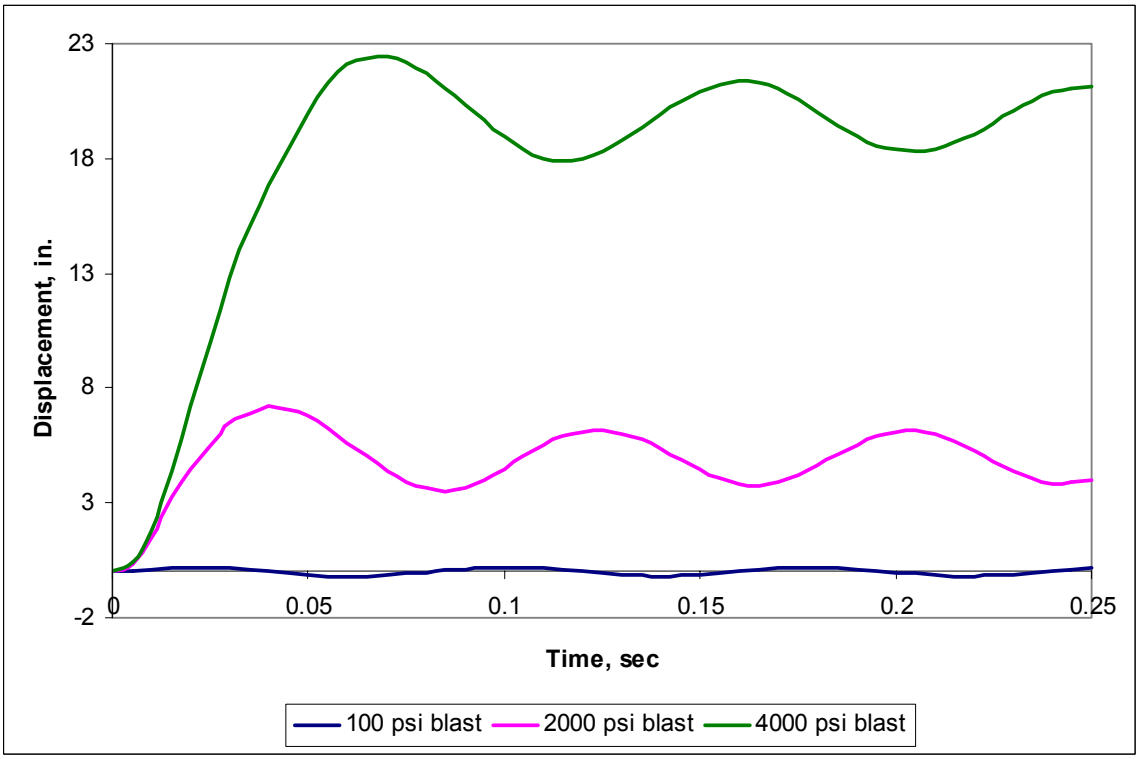

Fig. 3.18. Comparison of displacement time-histories at node 405 for different blasts

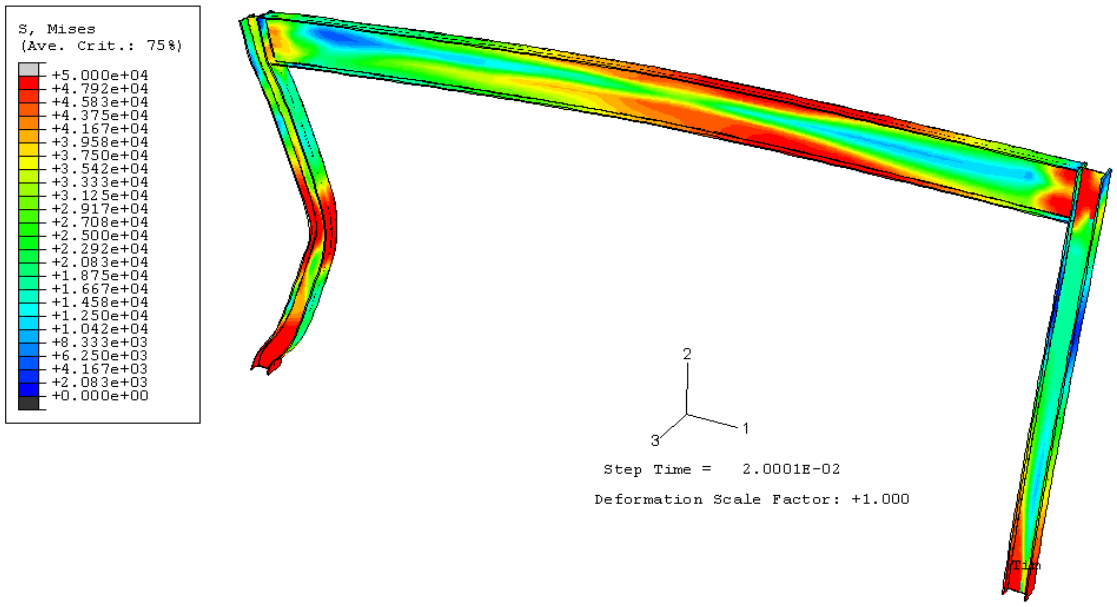

Fig. 3.19. Sample of von Mises stress distribution in the portal frame subjected to a 4,000 psi blast load at time t = 20 msec

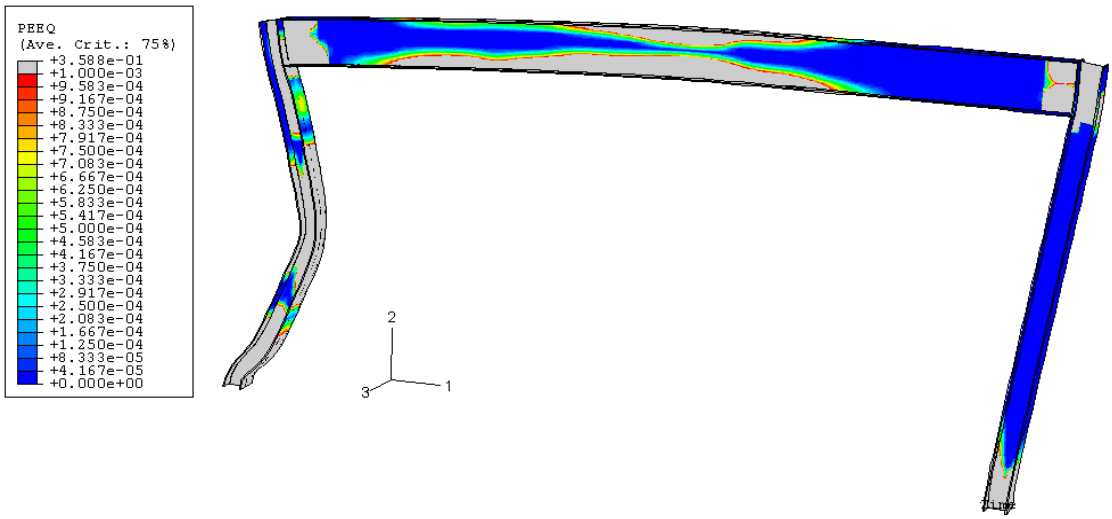

Fig. 3.20. Plastic deformation zones of the portal frame subjected to a 4,000 psi blast (no plastic deformation = blue) at time t = 0.25 sec

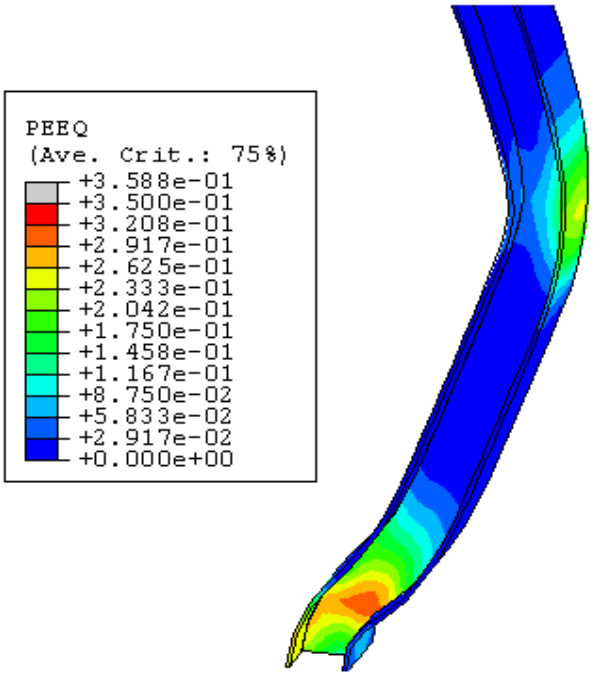

Fig. 3.21. Bending and equivalent plastic strain at the midspan and the support of the blast side column subjected to a 4,000 psi blast

Chapter 4

Effects of Bilinear Springs on the Models

4.1 SCEDs Modeled as Springs

Previous research by Pearson (2002) and Hennessey (2003) analyzed snapping-cable energy dissipators (SCEDs) as possible passive earthquake dampers. The research done to this point has focused on the properties of synthetic fiber ropes that are to be used as SCEDs. The results of the work thus far have shown that these ropes behave similarly to springs when in tension, but are not able to withstand any compressive force. This research studies the use of these ropes as a means to resist the effects of blast loads. Springs were introduced into the models by attaching them at the corners as an X-brace. Figure 4.1 shows the ABAQUS model of the springs attached to the frame. The shape of the springs is due to the fact that ABAQUS shapes the elements as coils. A more accurate representation of how the ropes being modeled would actually be placed in the frame can be seen in Fig. 4.2.

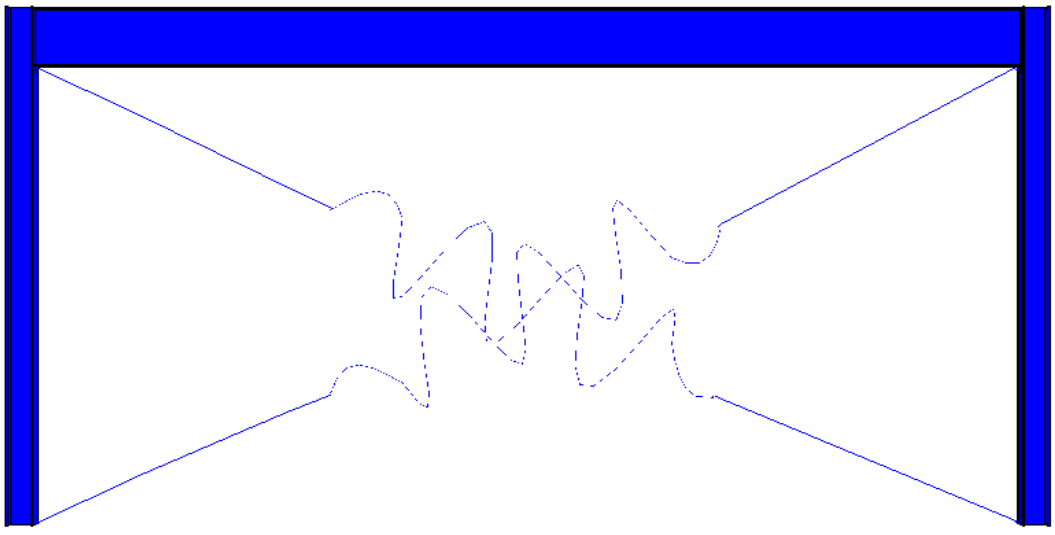

Fig. 4.1. ABAQUS representation of SCEDs introduced into the frame

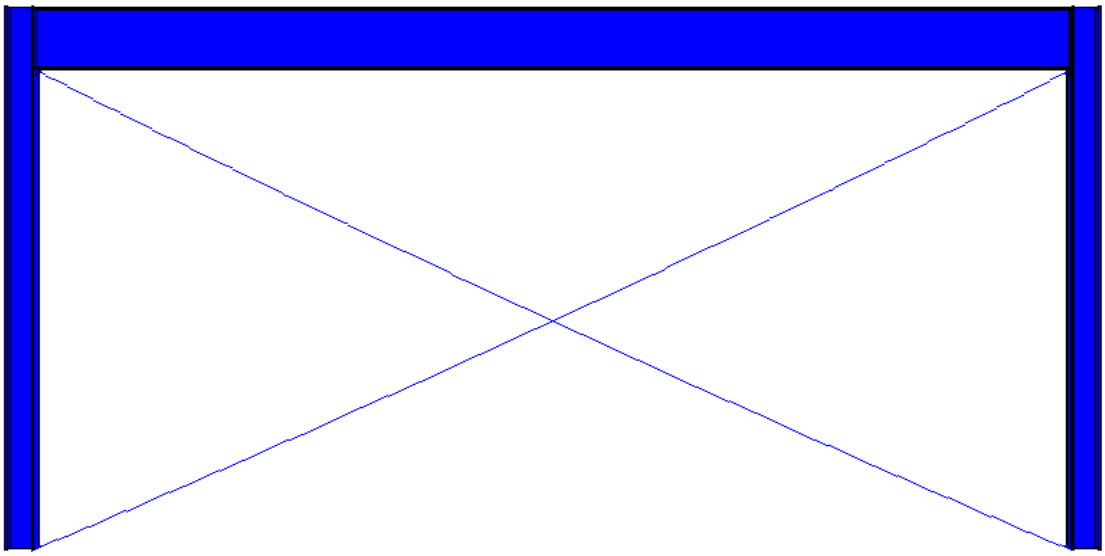

Fig. 4.2. Representation of how SCEDs would properly be placed into the frame

ABAQUS provides a *SPRING command that was used to model the springs. Coordinates were designated for spring force and spring displacement to provide a model for the spring constants. Bilinear springs were used for the initial test. Zero stiffness was provided for compression forces and no stiffness was given for the initial 1 in. of positive displacement to represent some slack in the ropes. One spring is connected to the frame at the midpoint of the inside flange of the blast side column at the support and at the midpoint of the bottom flange at the opposite of the beam. This spring is the primary spring for blast resistance in the following discussion. The spring was designed to have an initial length of 301.34 in., exactly 1 in. longer than the clear space of 300.34 in. between the connection points. Appendix A shows calculations for determining when the spring becomes taut. The displacement of the connection point of the primary spring to the beam coincides very closely with the horizontal displacement of node 11405. An orange line is placed on time histories of this displacement for the frame with springs attached. That line designates a global X-displacement of 1.10 in., the necessary displacement to relieve the slack in the spring. The other spring is connected to the frame in precisely the opposite manner as the primary spring. Only in very few instances did this spring exhibit any forces and they were small enough not to be considered. Constant springs stiffnesses of 5 kip/in., 10 kip/in., and 20 kip/in. were analyzed for spring

displacements larger than 1 in. A graph of these spring forces is seen in Fig. 4.3. It should also be noted that because of the initial 1 in. of zero stiffness, the frame subjected to a 100 psi blast was not analyzed for the inclusion of the ropes. Under the given parameters, the ropes did not become taut under a 100 psi blast; therefore, the frame did not experience any spring forces.

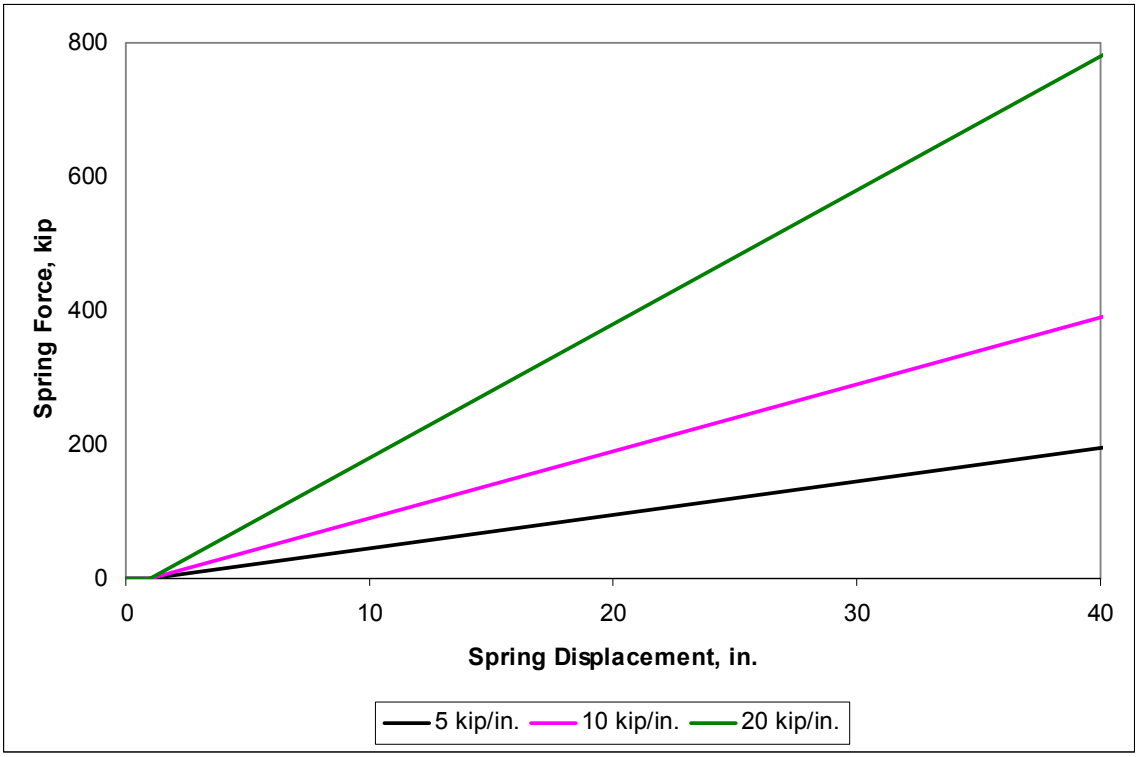

Fig. 4.3. Graph of spring stiffnesses

4.2 Effects of Springs on Displacements

4.2.1 Case II – 2,000 psi blast

The effect of the springs on the displacements of the key nodes was beneficial, especially at the connections. Figures 4.4, 4.5, 4.6, and 4.7 compare the displacement time histories of nodes 205, 405, 11205, and 11405, respectively. The effect of the springs at node 205, while noticeable, is much less substantial than the effect at nodes 405 and 11405. The reduction in total deflection at node 205 is most likely attributed to the reductions at

nodes 405 and 11405. In terms of global deflection, there is a correlation between the displacements at the midspan of a member relative to its end. The blast side column, however, still experiences significant bending at midspan. The behavior of the frame at nodes 405 and 11405 is positively affected by the springs. Table 4.1 shows a comparison of the maximum displacement and the dynamic behavior of the frame at node 405 after the blast load has ended. The time histories for nodes 405 and 11405 are nearly identical, therefore a summarization of node 405 only will suffice. Tables 4.2 and 4.3 contain similar data for nodes 205 and 11205 with the omission of period of vibration.

Spring Stiffness	Maximum Displacement	Maximum Displacement at Later Cycles of Motion	Period of Vibration
(kip/in.)	(in.)	(in.)	(sec)
No Springs	7.21	6.20	0.08
5	5.82	3.89	0.07
10	5.25	2.91	0.065
20	4.41	2.43	0.065

Table 4.1. Comparison of the structural behavior of the frame at node 405 with different bracing spring stiffnesses subjected to a blast load of 2,000 psi

Spring Stiffness	Maximum Displacement	Maximum Displacement at Later Cycles of Motion
(kip/in.)	(in.)	(in.)
No Springs	8.68	8.28
5	8.16	7.10
10	7.75	6.61
20	7.49	6.35

Table 4.2. Comparison of the structural behavior of the frame at node 205 with different bracing spring stiffnesses subjected to a blast load of 2,000 psi

Spring Stiffness	Maximum Displacement	Maximum Displacement at Later Cycles of Motion
(kip/in.)	(in.)	(in.)
No Springs	3.73	3.30
5	3.00	2.30
10	2.72	1.82
20	2.44	1.40

Table 4.3. Comparison of the structural behavior of the frame at node 11205 with different bracing spring stiffnesses subjected to a blast load of 2,000 psi

4.2.2 Case III – 4,000 psi blast

For case III, the springs had a much more significant effect. Figures 4.8, 4.9, 4.10, and 4.11 show the displacement time histories of the braced frame at each spring stiffness subjected to a 4,000 psi blast. Section 3.2.3 described the large deflections that occurred at the key nodes as a result of the 4,000 psi blast. The springs countered these large deflections much more effectively than they countered the smaller deflections that were caused by the 2,000 psi blast. Displacements were reduced by as much as 60% for the 20 kip/in. springs at nodes 405 and 11405. A large-scale reduction in the displacement of node 205 is not evident. Table 4.4 shows a comparison of the maximum displacement and the dynamic behavior of the frame at node 405 after the 4,000 blast load has ended. Tables 4.5 and 4.6 contain similar data for nodes 205 and 11205. An important aspect of the frame behavior with springs included is the high rate of reduction for the long-term displacements of nodes 405 and 11405. The amplitude of displacement for the long-term cycles of motion decreases by 80 percent, even for the 5 kip/in. spring.

Spring Stiffness	Maximum Displacement	Maximum Displacement at Later Cycles of Motion	Period of Vibration
(kip/in.)	(in.)	(in.)	(sec)
No Springs	22.43	21.36	0.09
5	13.3	4.4	0.085
10	10.89	3.38	0.08
20	8.67	3.62	0.075

Table 4.4. Comparison of the structural behavior of the frame at node 405 with different bracing spring stiffnesses subjected to a blast load of 4,000 psi

Spring Stiffness	Maximum Displacement	Maximum Displacement at Later Cycles of Motion
(kip/in.)	(in.)	(in.)
No Springs	37.61	37.15
5	34.35	29.17
10	33.35	28.84
20	32.49	29.27

Table 4.5. Comparison of the structural behavior of the frame at node 205 with different bracing spring stiffnesses subjected to a blast load of 4,000 psi

Spring Stiffness	Maximum Displacement	Maximum Displacement at Later Cycles of Motion
(kip/in.)	(in.)	(in.)
No Springs	11.63	11.23
5	7.3	2.71
10	6.12	1.97
20	4.99	2.26

Table 4.6. Comparison of the structural behavior of the frame at node 11205 with different bracing spring stiffnesses subjected to a blast load of 4,000 psi

4.3 Effect of Springs on Plasticity Spread

Analysis of the models following the addition of springs showed that the presence of the springs, even up to a spring stiffness of 20 kip/in., had no effect on the overall presence of permanent plasticity in the frame. Figure 4.12 shows the plastic deformation zones for the frame subjected to a 4,000 psi blast braced with 20 kip/in. springs. When compared to Fig. 3.21, the plastic deformation zones are almost identical. As mentioned previously, the overall plastic deformation of the frame was reduced, by as much as 50% in some instances, by the presence of the springs. However, the spread of plasticity in the frame concludes 3 msec into the model's run. Further analysis of Figs. 4.4 – 4.11 shows that the springs do not begin to aid in deflections until 2-3 msec into the analysis, after almost all of the permanent plasticity has occurred.

Note in Fig. 4.13 that the displacement at node 11405 for a bare frame does not reach 1.10 in.—the boundary for tension in the spring—until just after time t = 5 msec. It was previously noted that node 11405 will displace almost identically to the connection point of the tension spring. Figure 4.14 shows the plasticity in the frame at time t = 5 msec. When compared to Fig. 4.12, most of the plasticity spread in the blast side column has already occurred. It is also noted that almost no rebound occurs following the 4,000 psi blast, while a rebound between 10-15% takes place at nodes 405 and 11405 following the 2,000 psi blast.

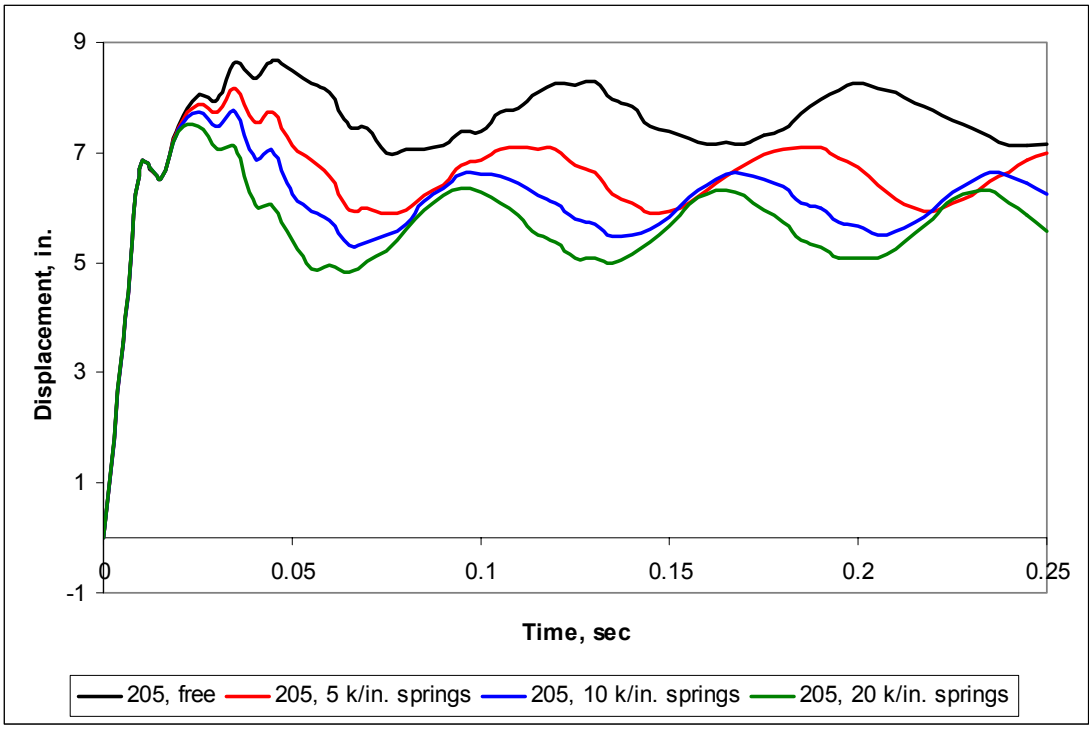

Fig. 4.4. Comparison of displacement time histories at node 205 for the frame subjected to a 2,000 psi blast

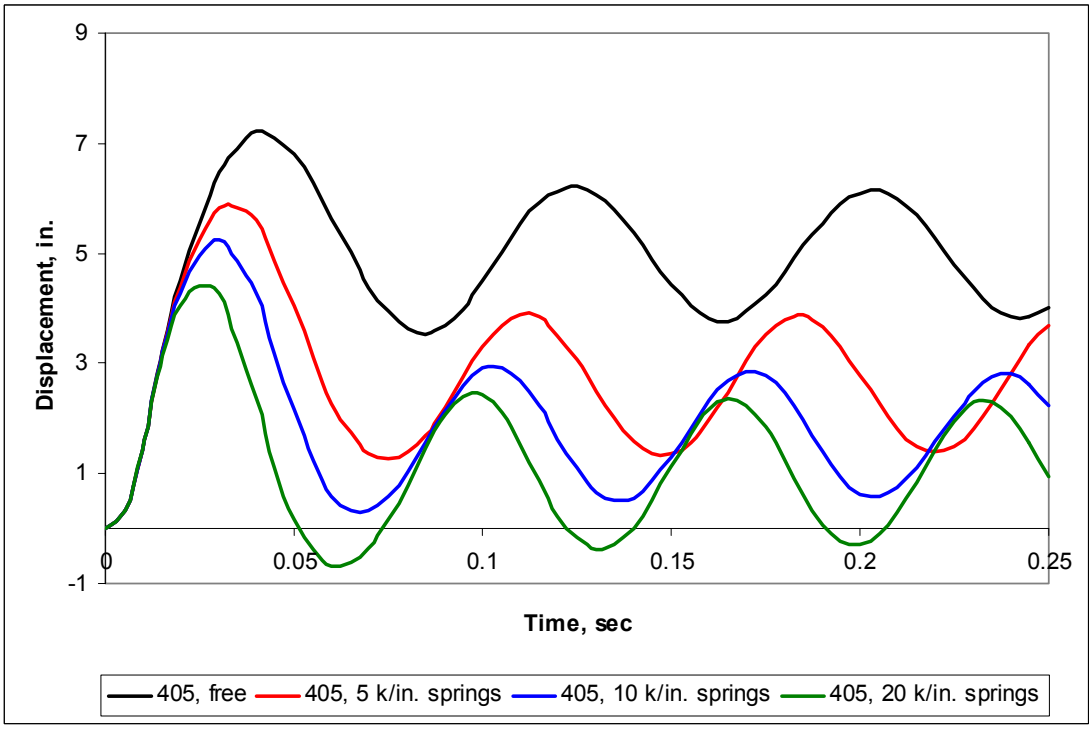

Fig. 4.5. Comparison of displacement time histories at node 405 for the frame subjected to a 2,000 psi blast

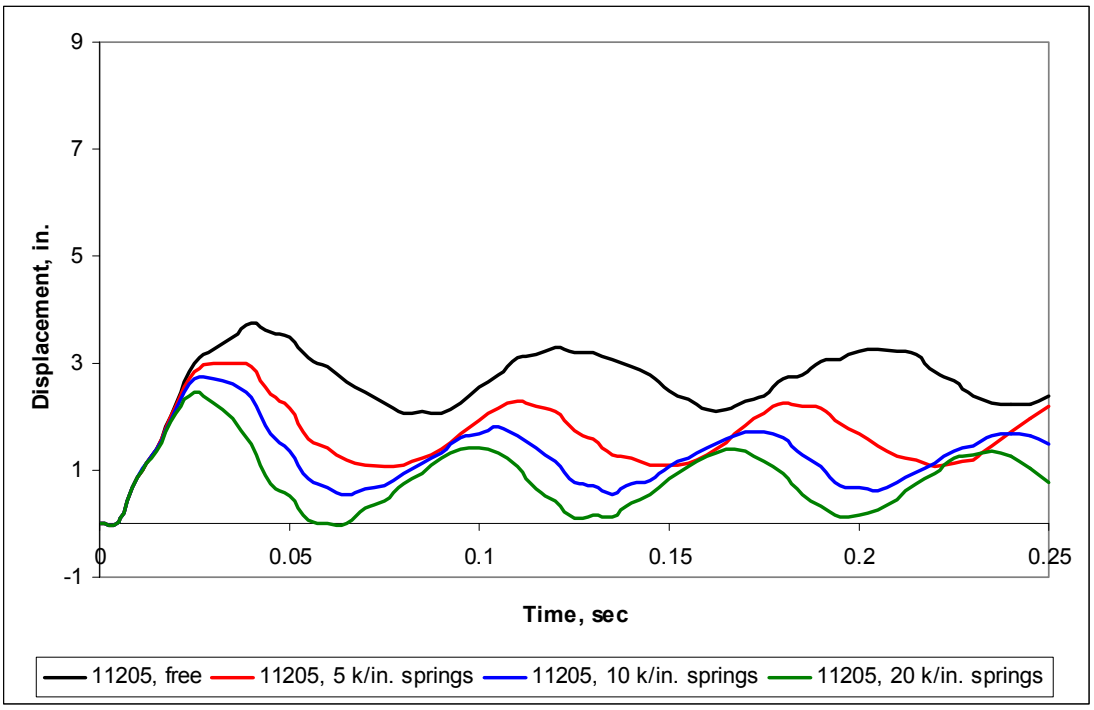

Fig. 4.6. Comparison of displacement time histories at node 11205 for the frame subjected to a 2,000 psi blast

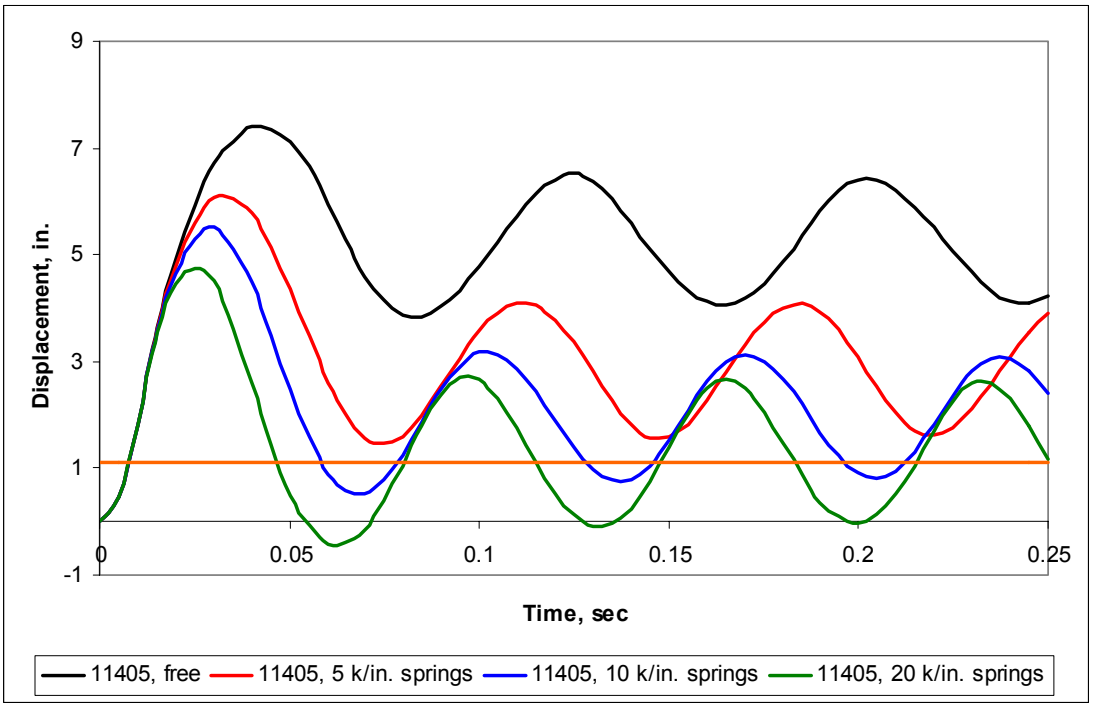

Fig. 4.7. Comparison of displacement time histories at node 11405 for the frame subjected to a 2,000 psi blast (orange line at 1.10 in. displacement signifies transition between slack and taut states for primary spring)

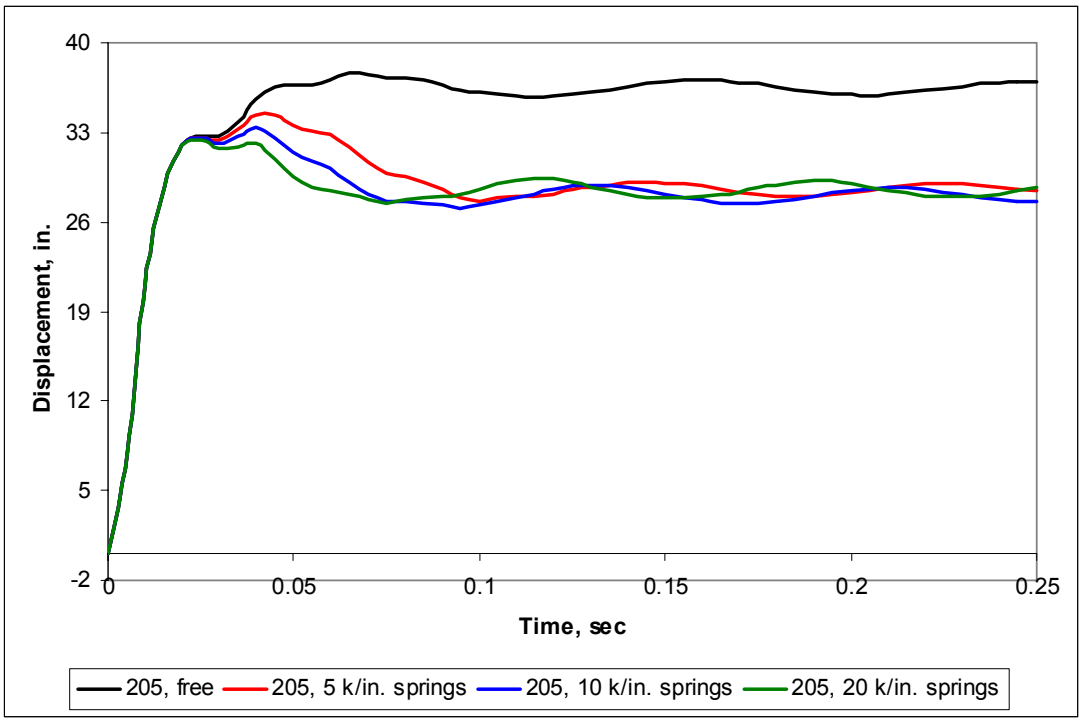

Fig. 4.8. Comparison of displacement time histories at node 205 for the frame subjected to a 4,000 psi blast

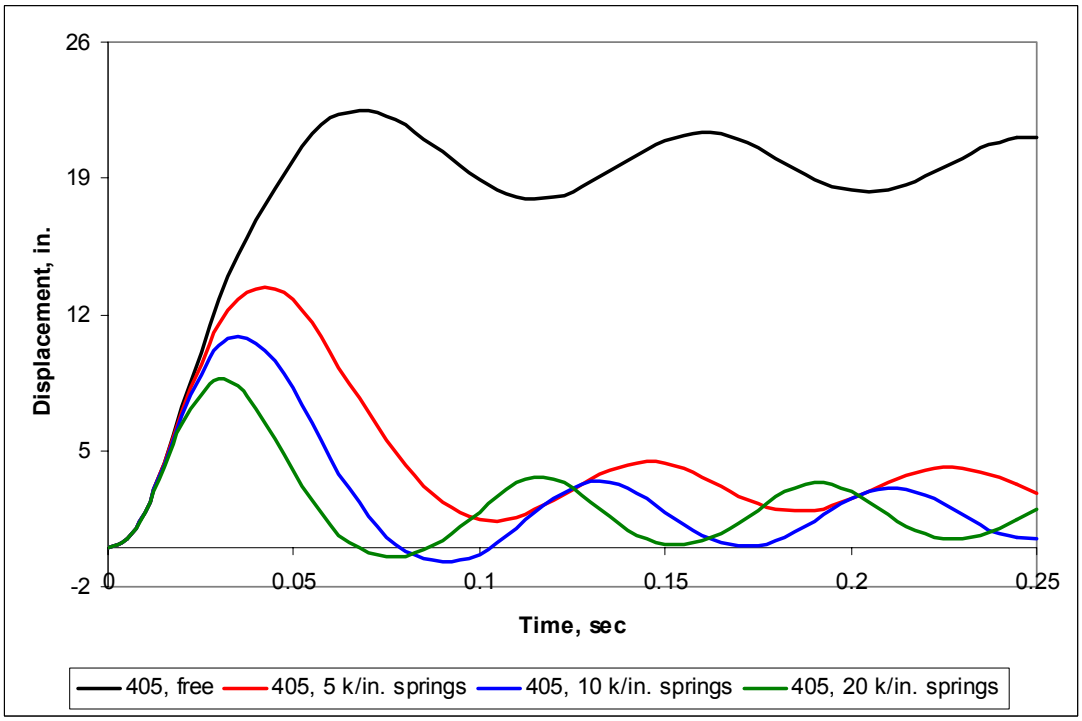

Fig. 4.9. Comparison of displacement time histories at node 405 for the frame subjected to a 4,000 psi blast

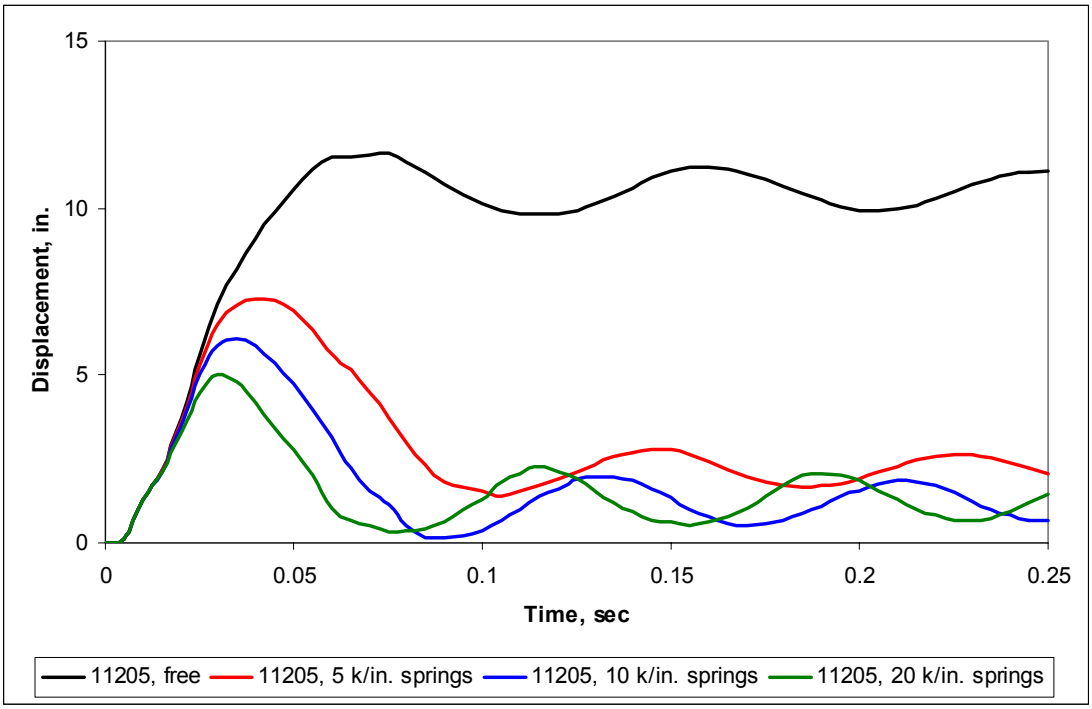

Fig. 4.10. Comparison of displacement time histories at node 11205 for the frame subjected to a 4,000 psi blast

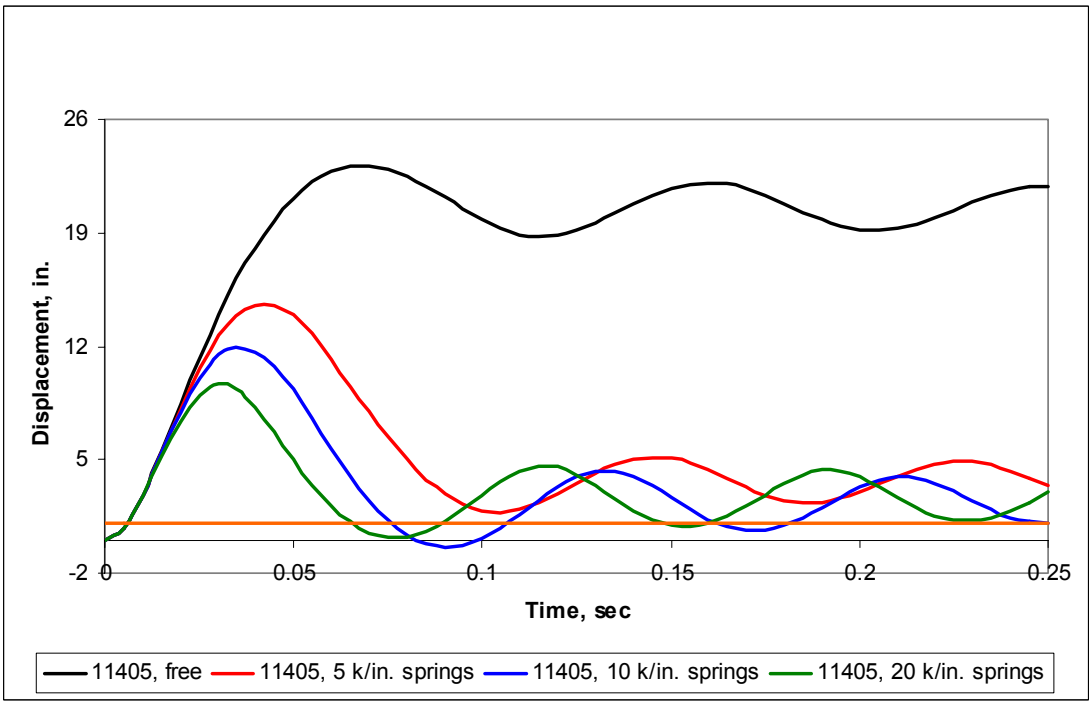

Fig. 4.11. Comparison of displacement time histories at node 11405 for the frame subjected to a 4,000 psi blast (orange line at 1.10 in. displacement signifies transition between slack and taut states for primary spring)

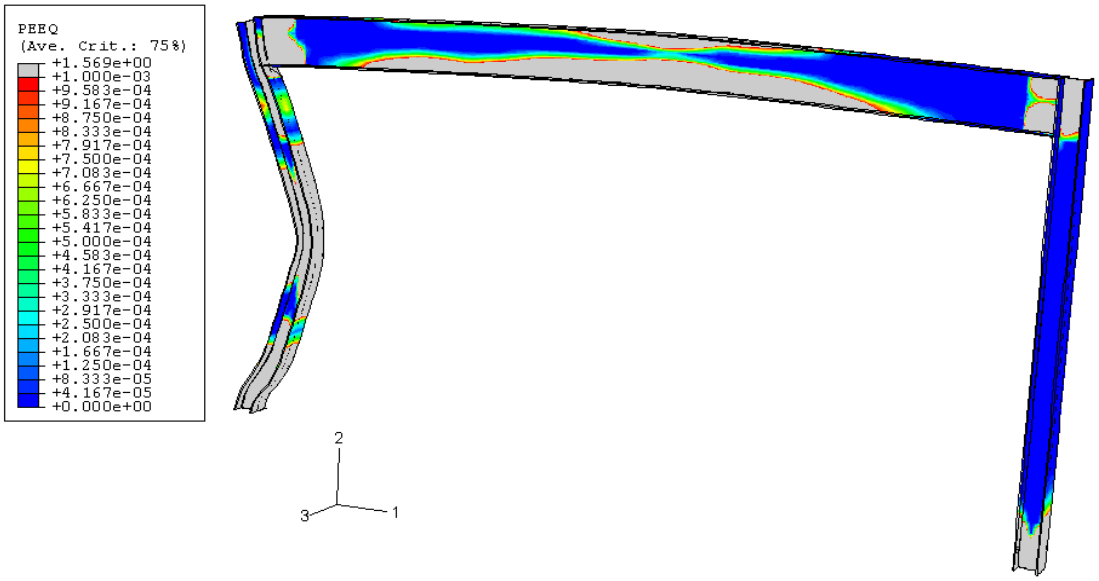

Fig. 4.12. Plastic deformation zones of the portal frame braced with 20 kip/in. springs subjected to a 4,000 psi blast (no plastic deformation = blue) at time t = 0.25 sec

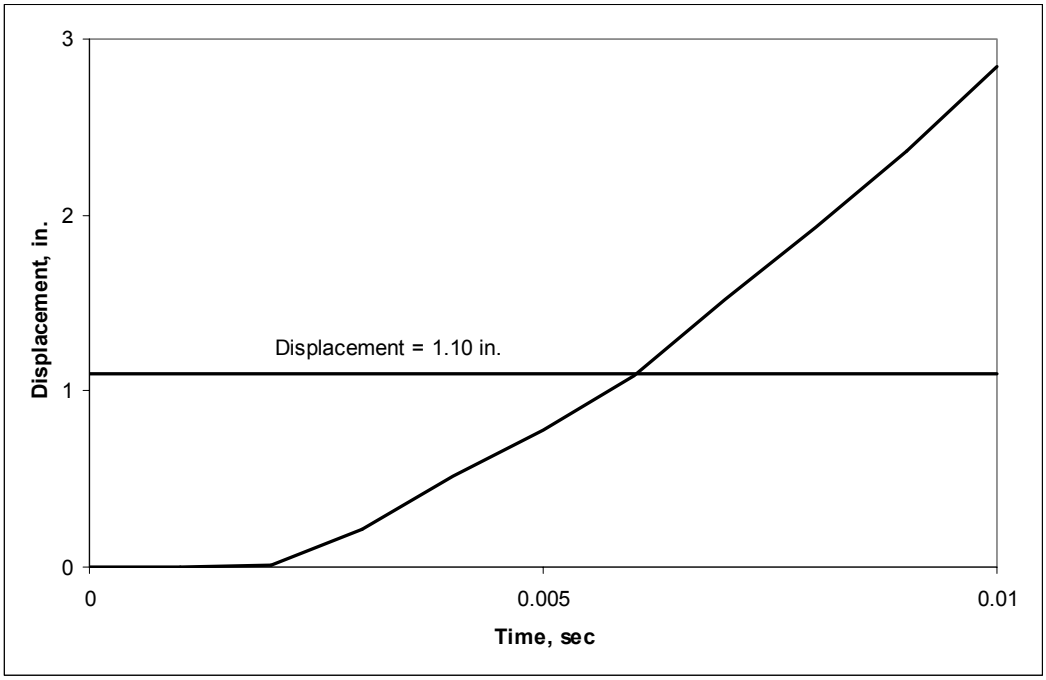

Fig. 4.13. Displacement time history of node 11405 with no springs for $0 < t < 0.01$ sec for a 4,000 psi blast

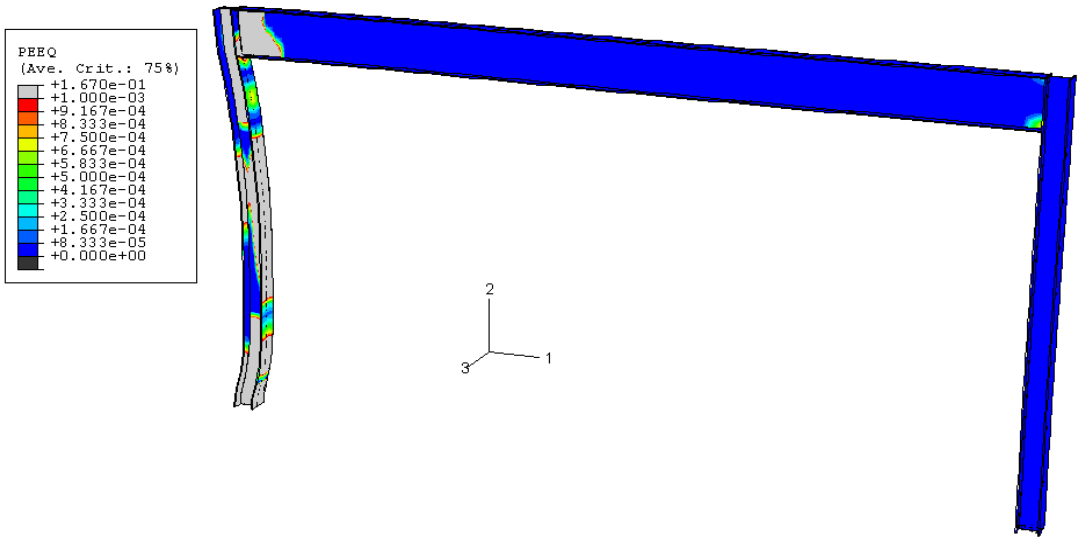

Fig. 4.14. Plastic deformation zones of the bare portal frame subjected to a 4,000 psi blast (no plastic deformation = blue) at time t = 5 msec

Chapter 5
Inclusion of Strain Rate Effects

5.1 Strain Rate Effects

The loading on a structure resulting from a blast has been discussed in detail thus far. The loads are much higher than most loads that a structure will experience, and occur over a much shorter time period. When a large dynamic load such as a blast load causes a material to begin to yield, it is common that the strain rate in the material will be higher than usual. Williams and Newell (1991) explain that materials loaded at high strain rates typically tend to exhibit higher yield strengths and greater ductilities than they would generally exhibit under a static load. Changes in values such as the modulus of elasticity and other material properties are negligible.

Shope and Plaut (1998) examined critical blast loads for compressed steel columns and determined that the inclusion of strain rate dependent yielding in their analysis resulted in an increase in critical blast impulse of approximately ten percent. Typically, when a structure is subjected to a loading that produces uniformly high material strain rates, a single dynamic increase factor is included. For the models analyzed by Shope and Plaut, strain rate effects were introduced based on a material model given in NAVFAC (1990) that is applicable for in-depth analyses with variations in dynamic increase factor (Eq. 5.1). A logarithmic increase is applied to the dynamic yield strength with an increase in strain rate. A similar tabulated rate dependent model was used for this research by inserting a *RATE DEPENDENT command into the material property section of the ABAQUS input file. This model can be seen in Fig. 5.1.

$$\text{Dynamic Increase Factor} = \frac{\sigma_{dy}}{\sigma_y} \tag{5.1}$$

where σ_{dy} = dynamic yield stress;

σ_y = static yield stress.

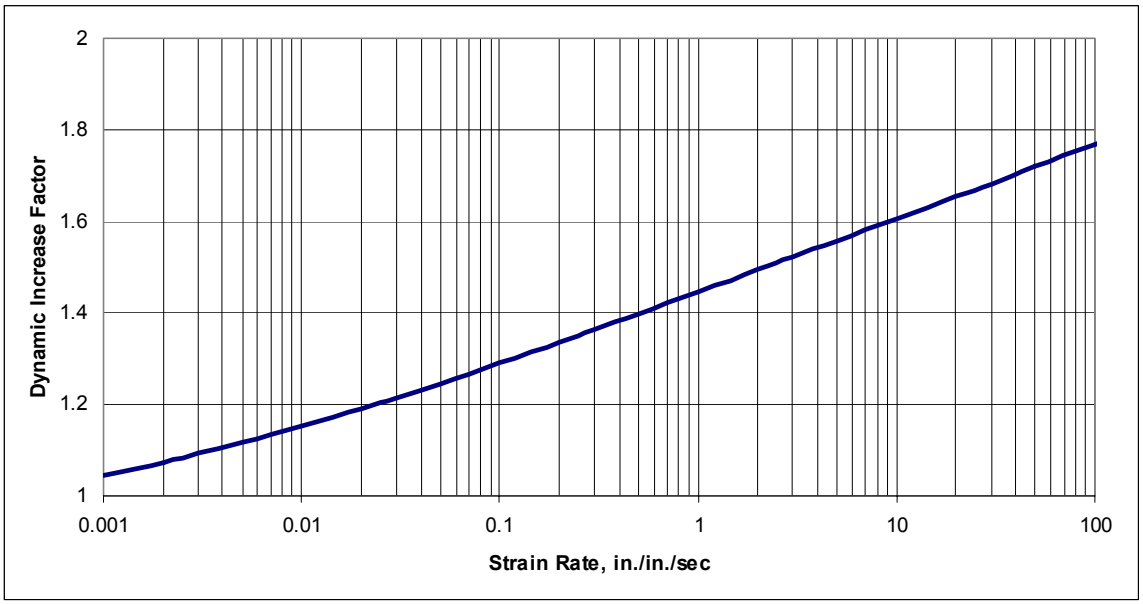

Fig. 5.1. Dynamic yield strength of the frame material based on strain rate

The effects of high strain rates were analyzed for cases II and III—the 2,000 psi and 4,000 psi blasts, respectively. The results of these analyses and a comparison of models with and without the inclusion of high strain rate effects can be found in sections 5.2-5.4. It should be noted that the 10 kip/in. bilinear spring was omitted from these analyses based on the results of the models from Chapter 4.

5.2 High Strain Rate Effects on Frame Displacements

5.2.1 Case II – 2,000 psi blast

Figures 5.2-5.13 compare displacement time histories for the frame subjected to a 2,000 psi blast with and without the inclusion of rate dependent yield effects. Figures 5.2-5.5 show the time histories of nodes 205, 405, 11205, and 11405, respectively with no springs on the frame. Figures 5.6-5.9 display the time histories of nodes 205, 405, 11205, and 11405, respectively, with 5 kip/in. springs bracing the frame. Figures 5.10-5.13 show the time histories of nodes 205, 405, 11205, and 11405, respectively, for the frame braced with 20 kip/in. springs. Figures showing displacement time histories for node

11405 contain the orange line marking the point where the "slack" is removed from the springs at 1.10 in. of displacement.

Initial analysis of these 12 figures shows that the higher strain rate effects clearly have a significant impact on the behavior of the system. Including the rate dependent yield effects increases the yield stress of the material, thereby decreasing the displacement of the system. With no springs included, the deflection of node 405 is higher than that of node 205, signifying a decrease in midspan bending in the blast side column. Comparisons of Figs. 5.2-5.5 and Figs. 5.6-5.13 show that the inclusion of springs diminishes the effects of higher strain rates, especially at nodes 405 and 11405. Figures 5.11-5.13 show that the 20 kip/in. spring nearly negates the effects of high strain rates at these nodes. The higher strain rates have similar effects on node 205 regardless of springs. The behavior of node 205 is based much more on the blast than on the total structural system that is in place. The springs do not restrict the displacement at node 205.

Tables 5.1-5.3 examine the inclusion of rate dependent yield effects on the structure. Note that strain rate effects have been designated SRE. Furthermore, note that the behavior of node 11405 is almost identical to that of node 405; therefore, it has been omitted from the tables.

	Maximum Displacement, No SRE (in.)	Maximum Displacement, SRE (in.)	Maximum Displacement at Later Cycles, No SRE (in.)	Maximum Displacement at Later Cycles, SRE (in.)
Node 205	8.68	5.59	8.28	5.02
Node 405	7.21	6.02	6.20	4.99
Node 11205	3.73	2.94	3.30	2.55

Table 5.1. Effects of the inclusion of rate dependent yield on the bare frame subjected to a 2,000 psi blast

	Maximum Displacement, No SRE (in.)	Maximum Displacement, SRE (in.)	Maximum Displacement at Later Cycles, No SRE (in.)	Maximum Displacement at Later Cycles, SRE (in.)
Node 205	8.16	5.36	7.10	4.35
Node 405	5.82	5.22	3.89	3.70
Node 11205	3.00	2.58	2.30	2.17

Table 5.2. Effects of the inclusion of rate dependent yield on the frame braced with 5 kip/in. springs subjected to a 2,000 psi blast

	Maximum Displacement, No SRE (in.)	Maximum Displacement, SRE (in.)	Maximum Displacement at Later Cycles, No SRE (in.)	Maximum Displacement at Later Cycles, SRE (in.)
Node 205	7.49	5.26	6.35	3.82
Node 405	4.41	4.33	2.43	2.67
Node 11205	2.44	2.16	1.40	1.45

Table 5.3. Effects of the inclusion of rate dependent yield on the frame braced with 20 kip/in. springs subjected to a 2,000 psi blast

5.2.2 Case III – 4,000 psi blast

Figures 5.14-5.25 compare displacement time histories for the frame subjected to a 4,000 psi blast with and without the inclusion of rate dependent yield effects, similar to those described in section 5.2.1. Figures 5.14-5.17 show the time histories of nodes 205, 405, 11205, and 11405, respectively with no springs on the frame. Figures 5.18-5.21 display the time histories of nodes 205, 405, 11205, and 11405, respectively, with 5 kip/in. springs bracing the frame. Figures 5.22-5.25 show displacement time histories of nodes 205, 405, 11205, and 11405, respectively, for the frame braced with 20 kip/in. springs. Figures that display displacement time histories for node 11405 contain the orange line marking the point where the "slack" is removed from the springs at 1.10 in. of displacement.

Investigation of these figures shows that the higher strain rate effects on the frame subjected to a 4,000 psi blast have a similar impact on the behavior of the system as in

the case of a 2,000 psi blast. Comparisons of Figs. 5.14-5.17 and Figs. 5.18-5.25 show that the inclusion of springs again diminishes the effects of higher strain rates. Tables 5.4-5.6 examine the inclusion of rate dependent yield effects on the structure.

	Maximum Displacement, No SRE (in.)	Maximum Displacement, SRE (in.)	Maximum Displacement at Later Cycles, No SRE (in.)	Maximum Displacement at Later Cycles, SRE (in.)
Node 205	37.61	23.49	37.15	22.63
Node 405	22.43	16.71	21.36	14.79
Node 11205	11.63	8.48	11.23	7.85

Table 5.4. Effects of the inclusion of rate dependent yield on the bare frame subjected to a 4,000 psi blast

	Maximum Displacement, No SRE (in.)	Maximum Displacement, SRE (in.)	Maximum Displacement at Later Cycles, No SRE (in.)	Maximum Displacement at Later Cycles, SRE (in.)
Node 205	34.35	21.28	29.17	18.39
Node 405	13.30	12.15	4.40	5.99
Node 11205	7.30	6.46	2.71	3.47

Table 5.5. Effects of the inclusion of rate dependent yield on the frame braced with 5 kip/in. springs subjected to a 4,000 psi blast

	Maximum Displacement, No SRE (in.)	Maximum Displacement, SRE (in.)	Maximum Displacement at Later Cycles, No SRE (in.)	Maximum Displacement at Later Cycles, SRE (in.)
Node 205	32.49	19.75	29.27	17.29
Node 405	8.67	8.25	3.62	3.94
Node 11205	4.99	4.94	2.26	2.27

Table 5.6. Effects of the inclusion of rate dependent yield on the frame braced with 20 kip/in. springs subjected to a 4,000 psi blast

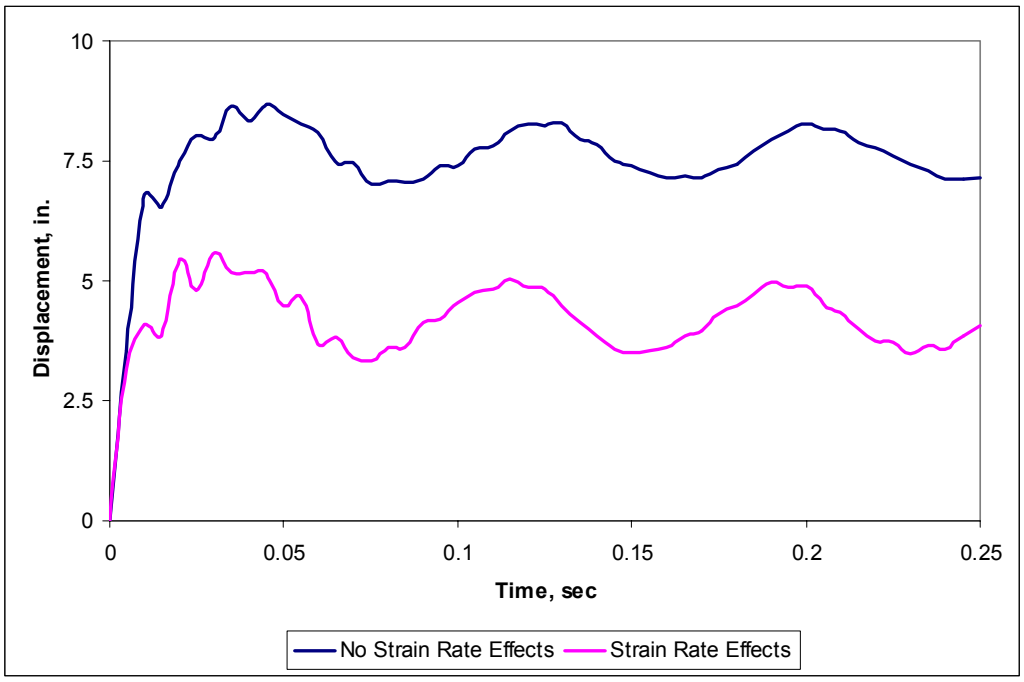

Fig. 5.2. Displacement time-histories with and without the inclusion of high strain rate effects at node 205 for the frame subjected to a 2,000 psi blast with no springs

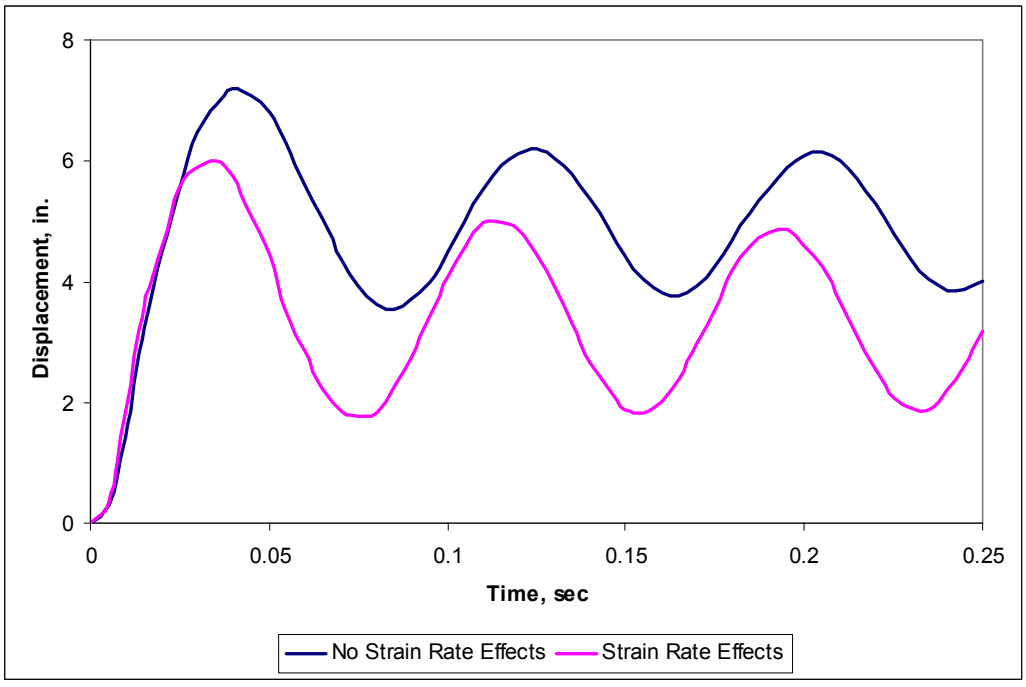

Fig. 5.3. Displacement time-histories with and without the inclusion of high strain rate effects at node 405 for the frame subjected to a 2,000 psi blast with no springs

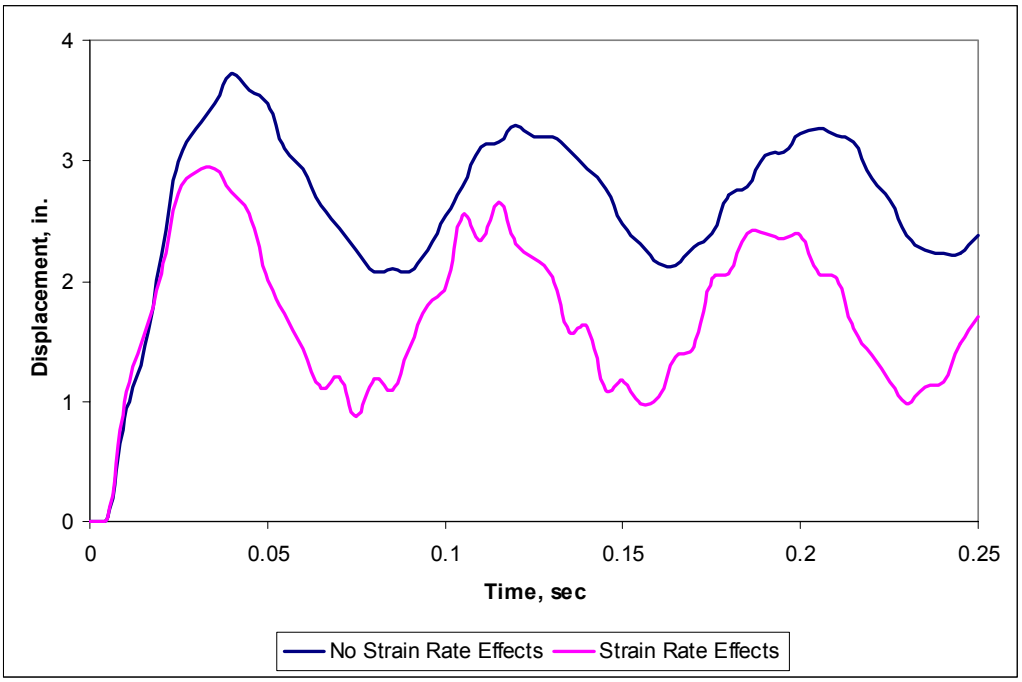

Fig. 5.4. Displacement time-histories with and without the inclusion of high strain rate effects at node 11205 for the frame subjected to a 2,000 psi blast with no springs

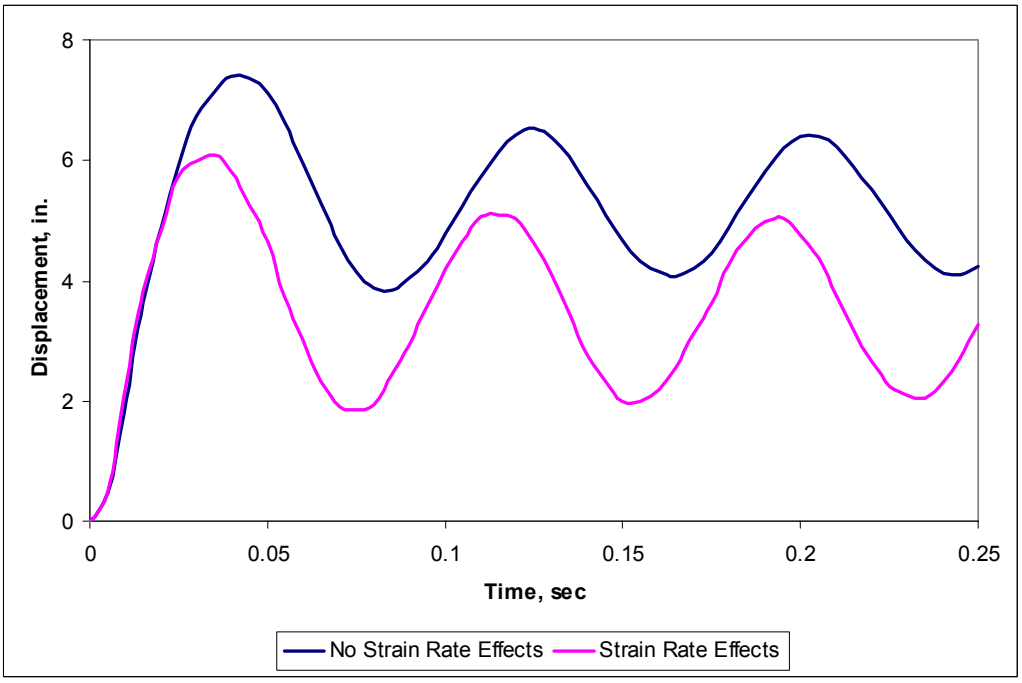

Fig. 5.5. Displacement time-histories with and without the inclusion of high strain rate effects at node 11405 for the frame subjected to a 2,000 psi blast with no springs

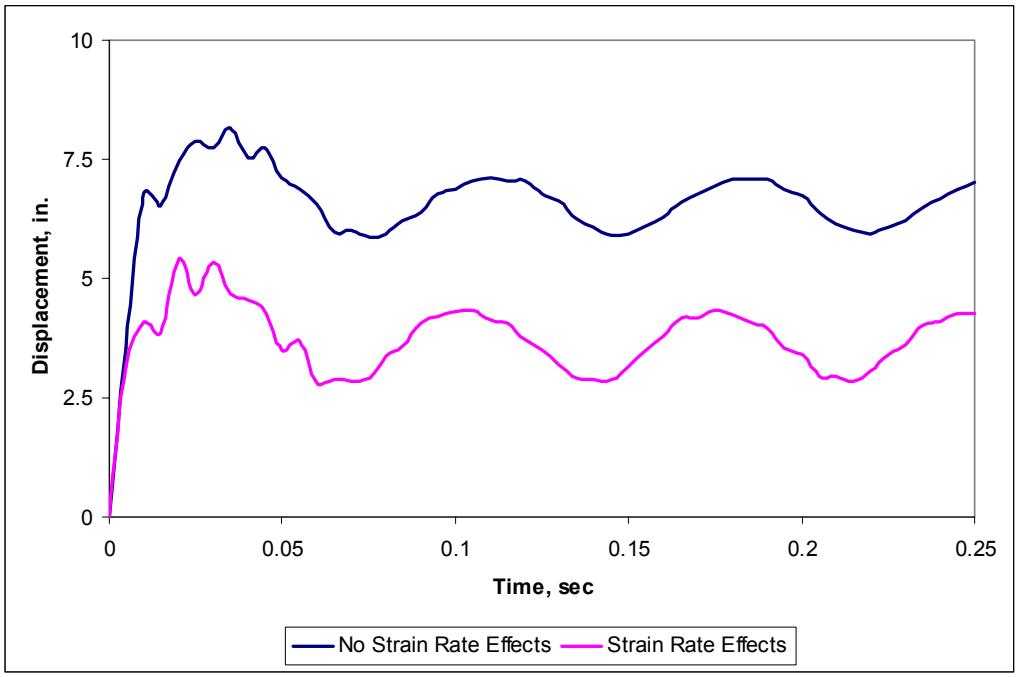

Fig. 5.6. Displacement time-histories with and without the inclusion of high strain rate effects at node 205 for the frame subjected to a 2,000 psi blast with 5 kip/in. bilinear springs

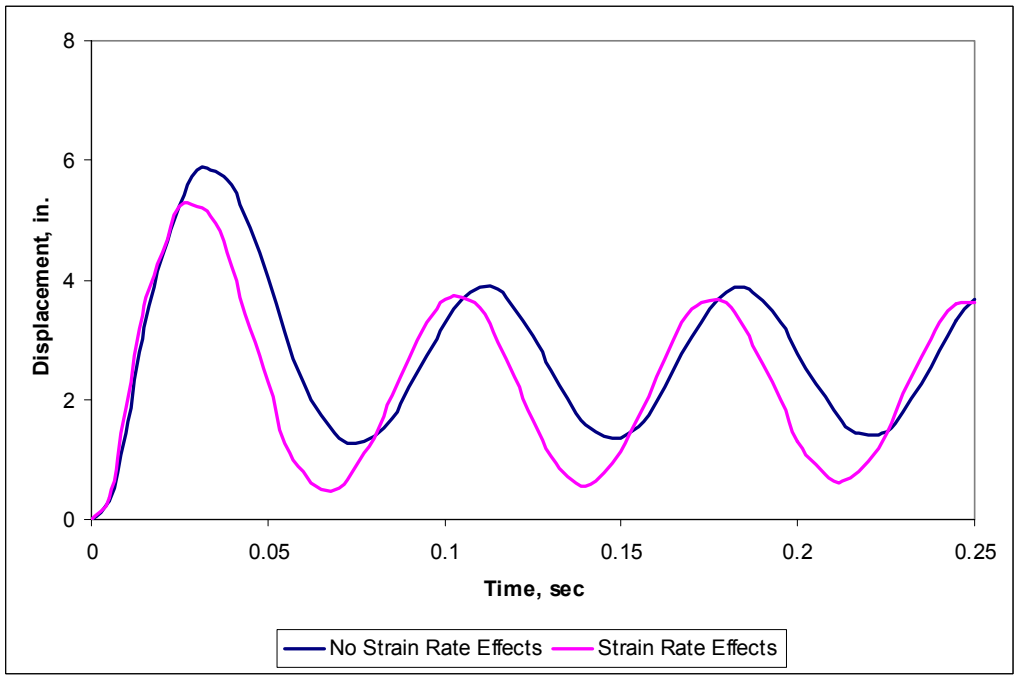

Fig. 5.7. Displacement time-histories with and without the inclusion of high strain rate effects at node 405 for the frame subjected to a 2,000 psi blast with 5 kip/in. bilinear springs

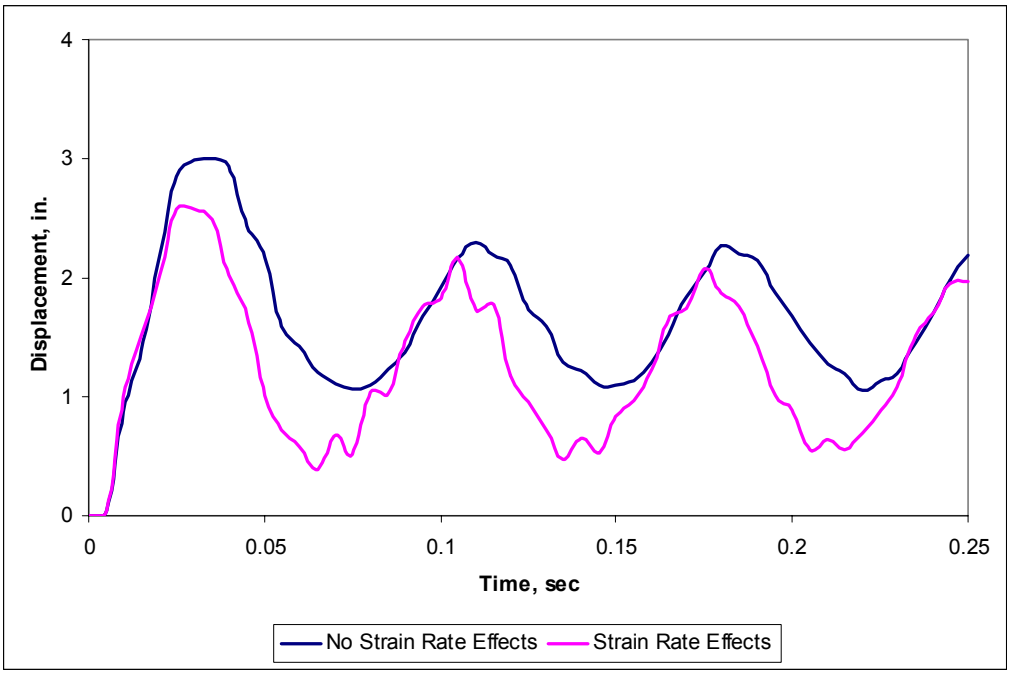

Fig. 5.8. Displacement time-histories with and without the inclusion of high strain rate effects at node 11205 for the frame subjected to a 2,000 psi blast with 5 kip/in. bilinear springs

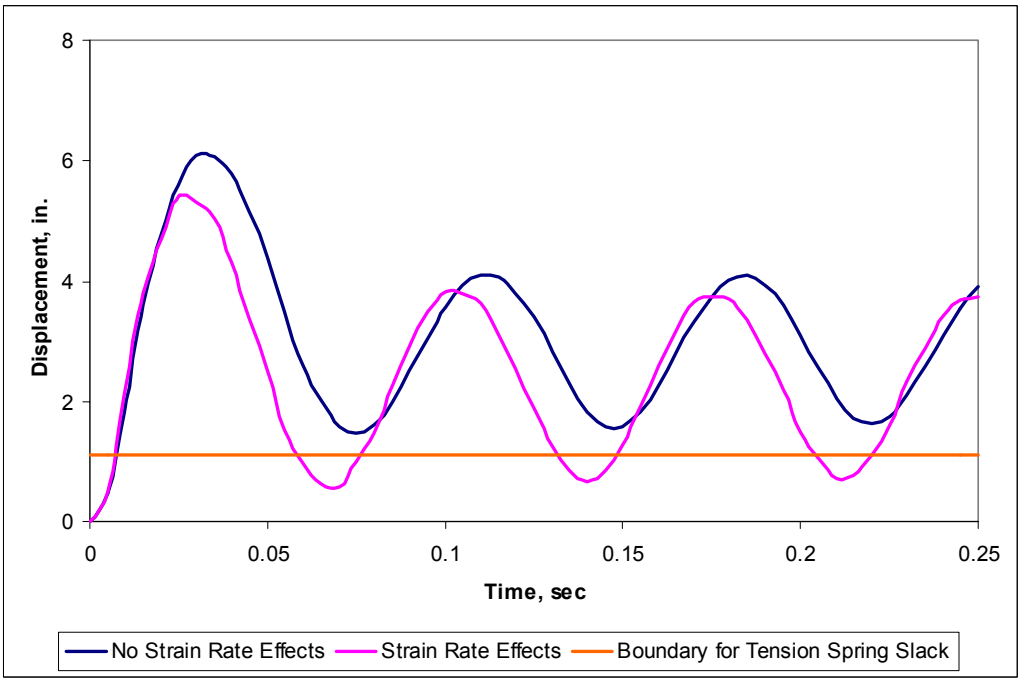

Fig. 5.9. Displacement time-histories with and without the inclusion of high strain rate effects at node 11405 for the frame subjected to a 2,000 psi blast with 5 kip/in. bilinear springs

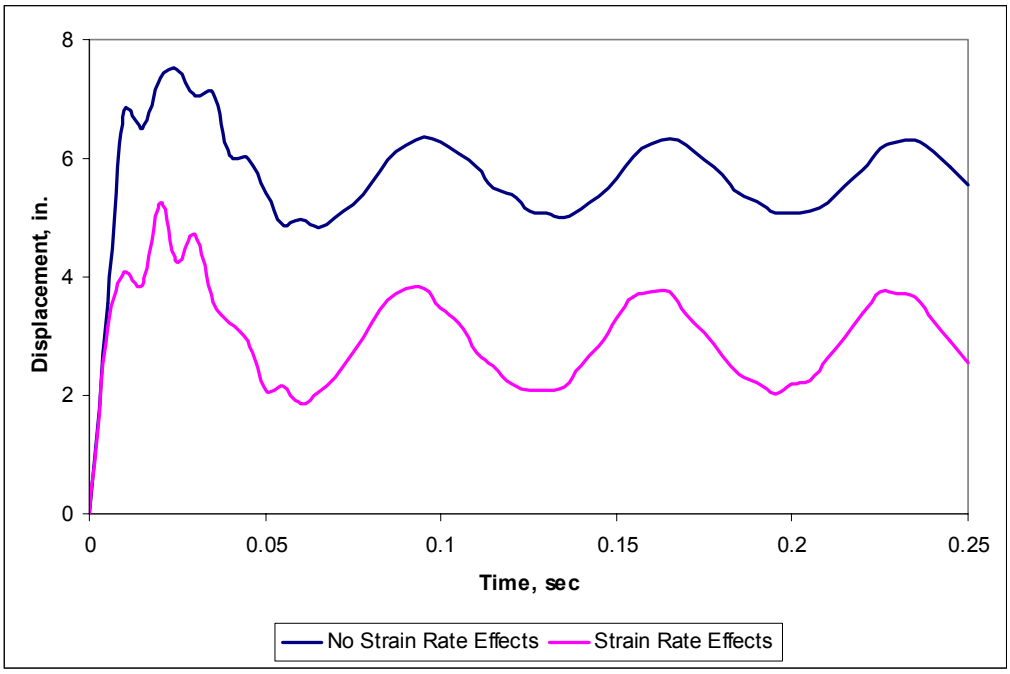

Fig. 5.10. Displacement time-histories with and without the inclusion of high strain rate effects at node 205 for the frame subjected to a 2,000 psi blast with 20 kip/in. bilinear springs

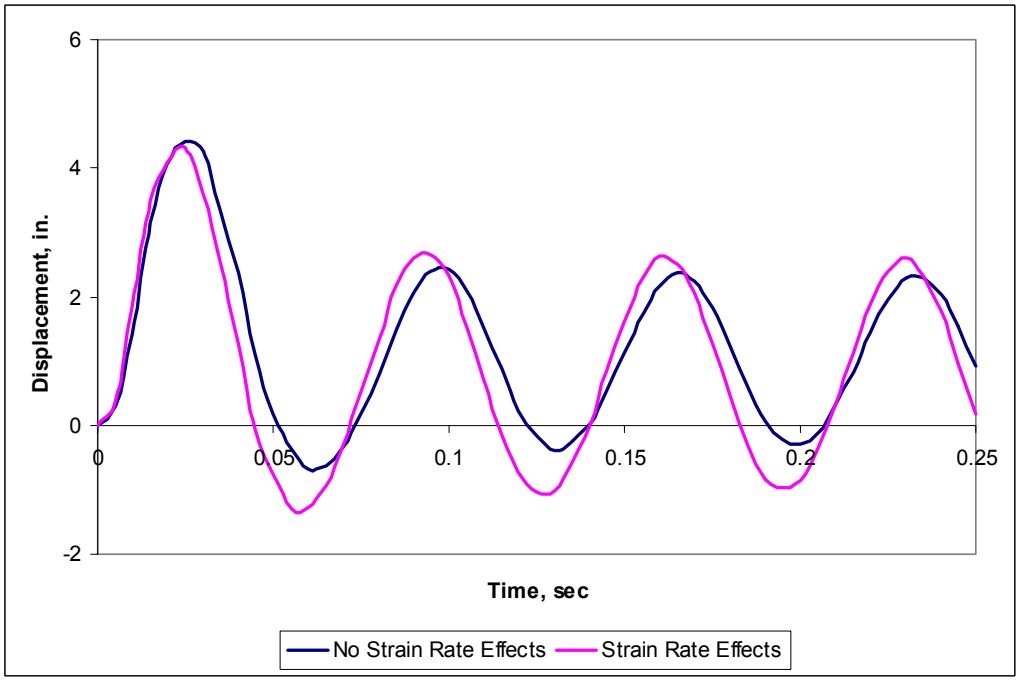

Fig. 5.11. Displacement time-histories with and without the inclusion of high strain rate effects at node 405 for the frame subjected to a 2,000 psi blast with 20 kip/in. bilinear springs

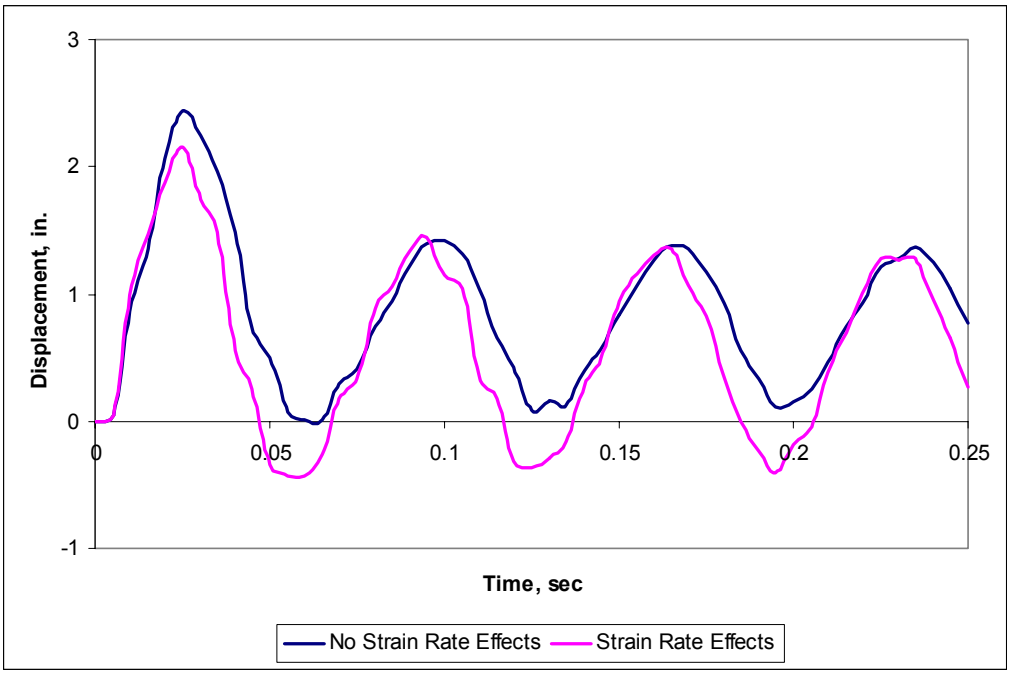

Fig. 5.12. Displacement time-histories with and without the inclusion of high strain rate effects at node 11205 for the frame subjected to a 2,000 psi blast with 20 kip/in. bilinear springs

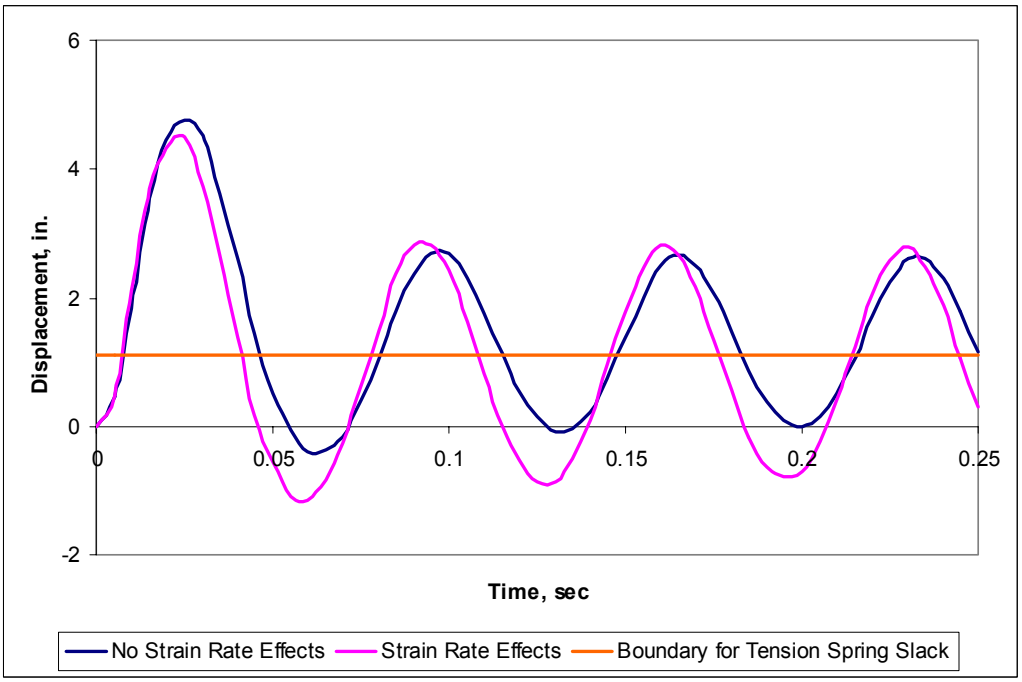

Fig. 5.13. Displacement time-histories with and without the inclusion of high strain rate effects at node 11405 for the frame subjected to a 2,000 psi blast with 20 kip/in. bilinear springs

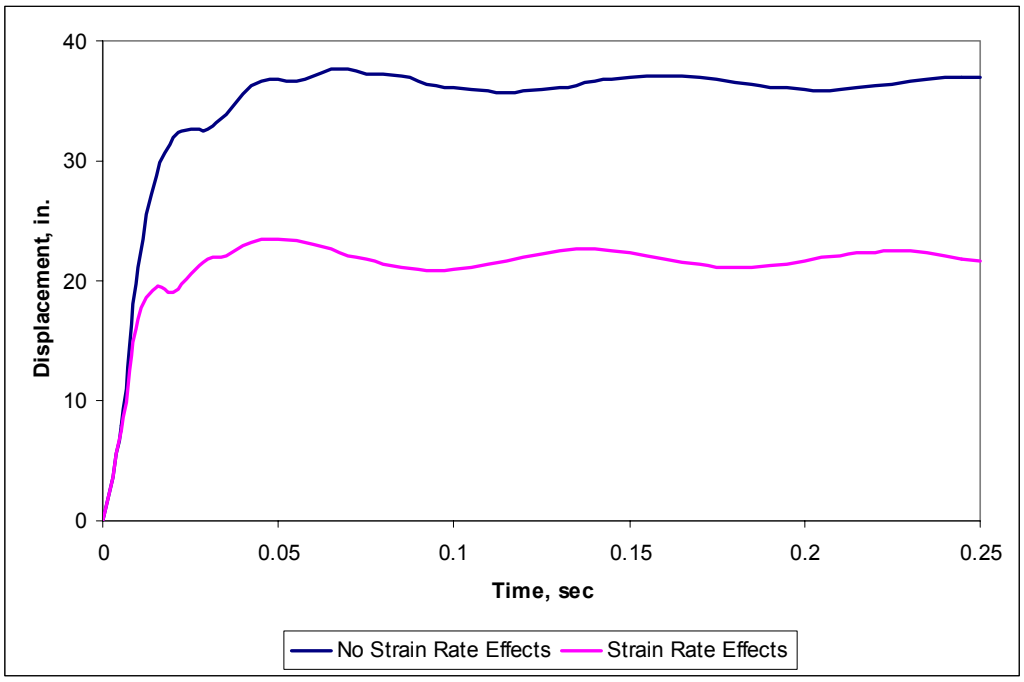

Fig. 5.14. Displacement time-histories with and without the inclusion of high strain rate effects at node 205 for the frame subjected to a 4,000 psi blast with no springs

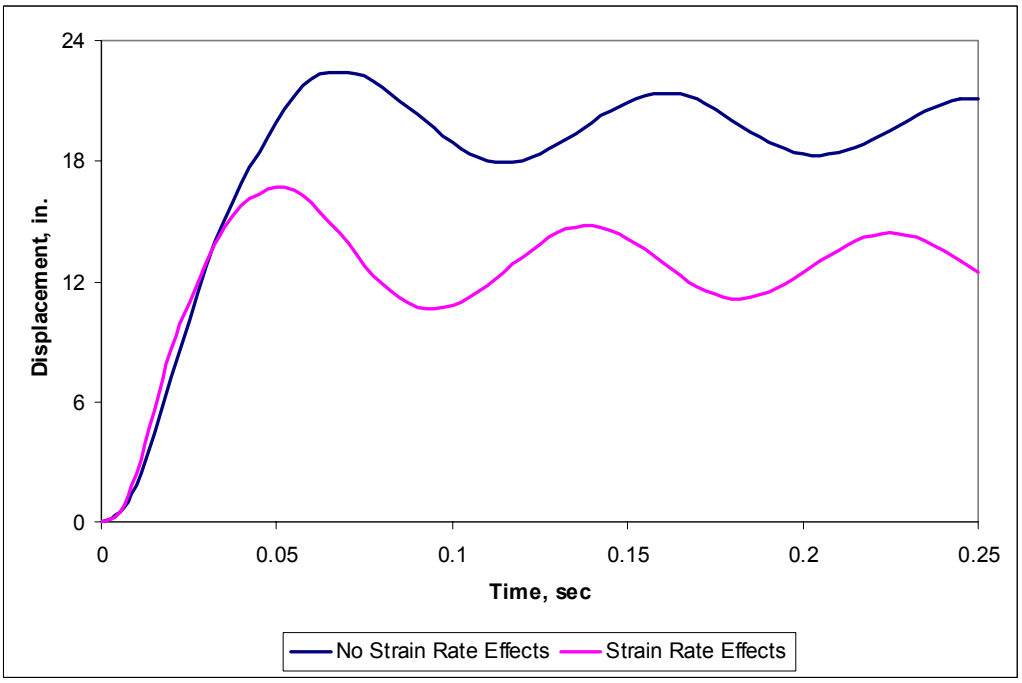

Fig. 5.15. Displacement time-histories with and without the inclusion of high strain rate effects at node 405 for the frame subjected to a 4,000 psi blast with no springs

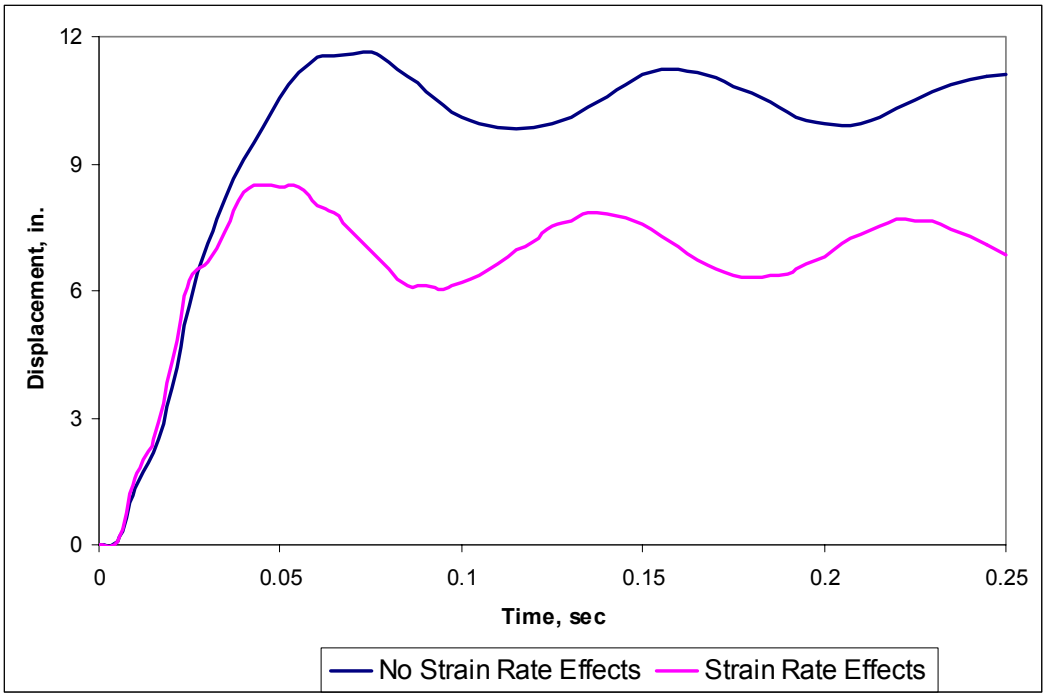

Fig. 5.16. Displacement time-histories with and without the inclusion of high strain rate effects at node 11205 for the frame subjected to a 4,000 psi blast with no springs

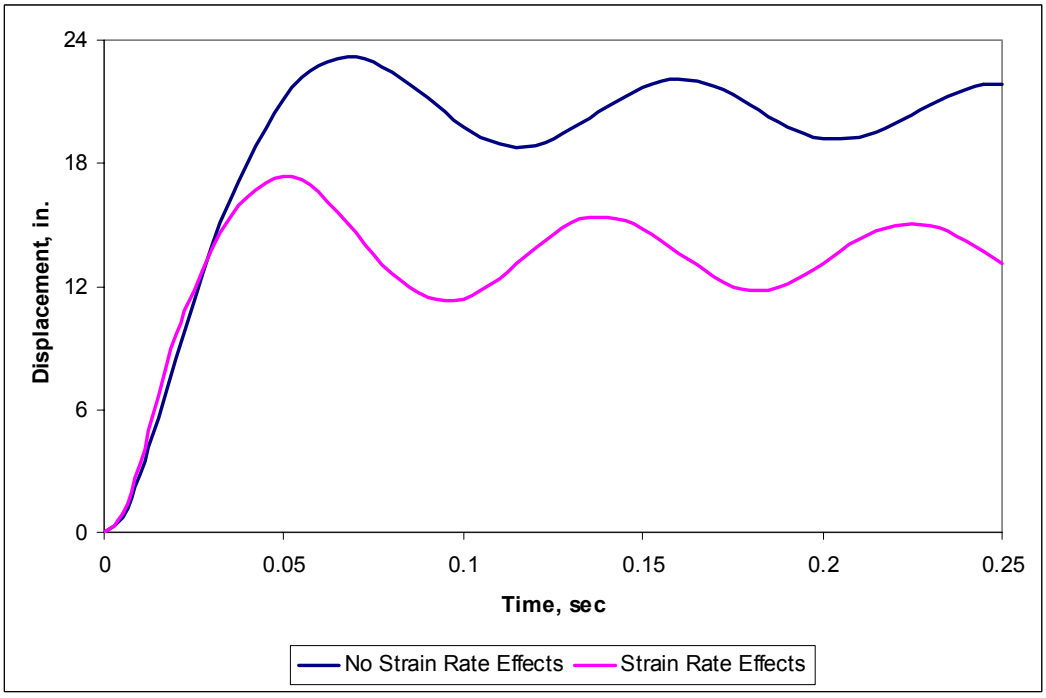

Fig. 5.17. Displacement time-histories with and without the inclusion of high strain rate effects at node 11405 for the frame subjected to a 4,000 psi blast with no springs

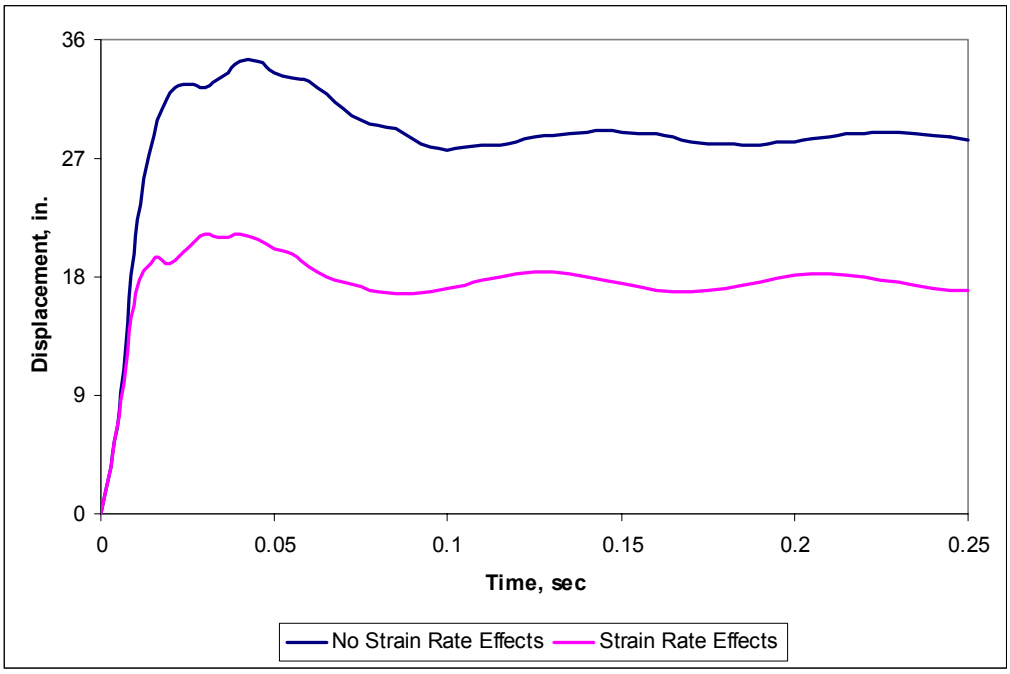

Fig. 5.18. Displacement time-histories with and without the inclusion of high strain rate effects at node 205 for the frame subjected to a 4,000 psi blast with 5 kip/in. bilinear springs

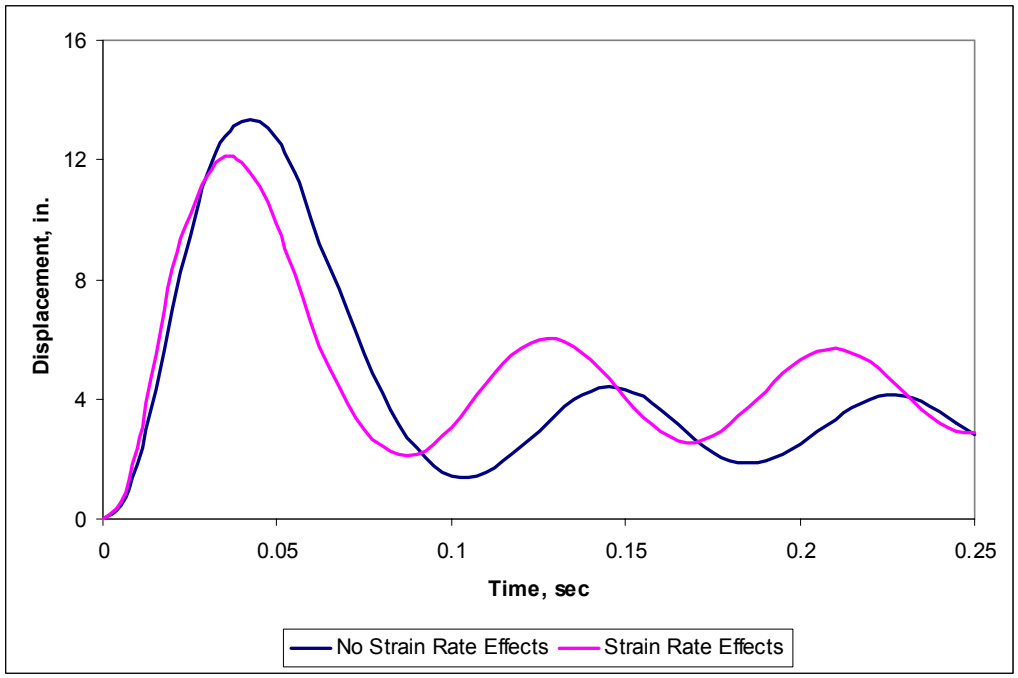

Fig. 5.19. Displacement time-histories with and without the inclusion of high strain rate effects at node 405 for the frame subjected to a 4,000 psi blast with 5 kip/in. bilinear springs

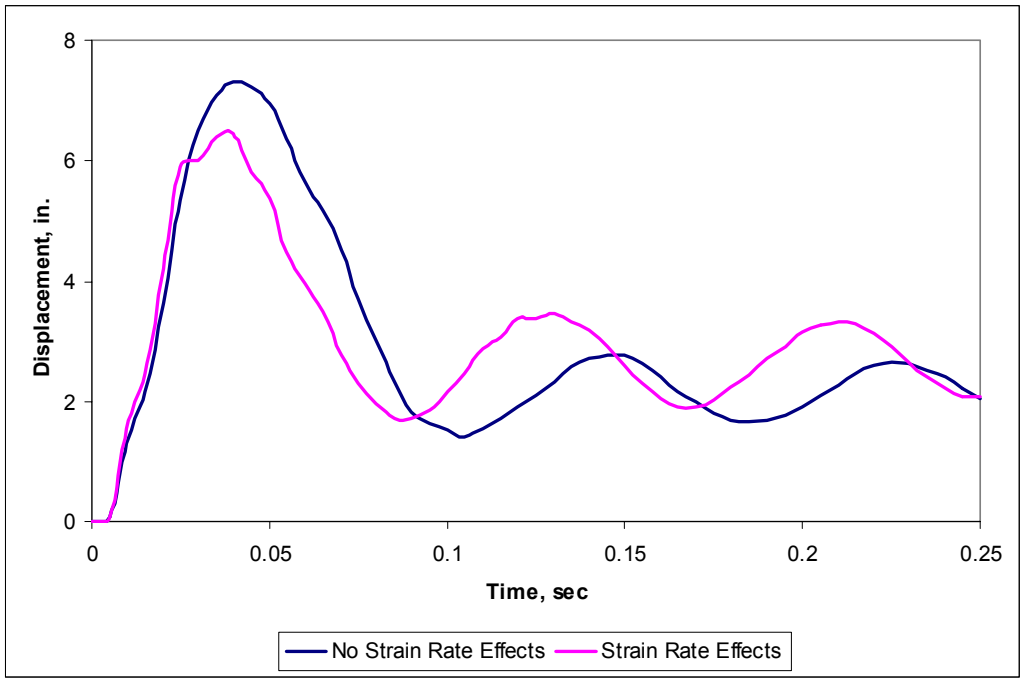

Fig. 5.20. Displacement time-histories with and without the inclusion of high strain rate effects at node 11205 for the frame subjected to a 4,000 psi blast with 5 kip/in. bilinear springs

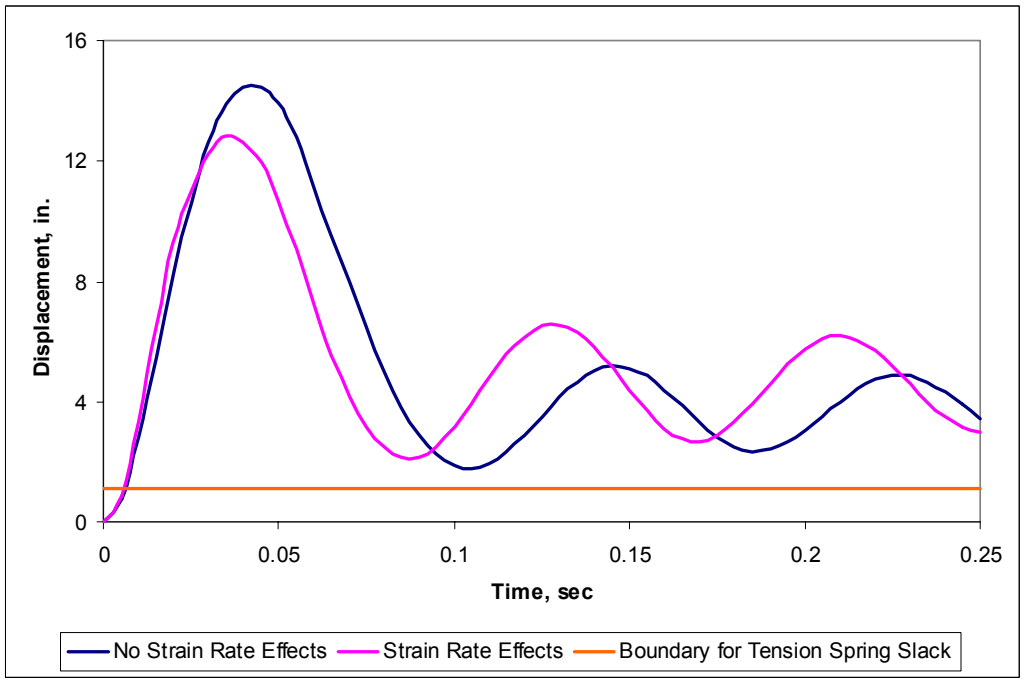

Fig. 5.21. Displacement time-histories with and without the inclusion of high strain rate effects at node 11405 for the frame subjected to a 4,000 psi blast with 5 kip/in. bilinear springs

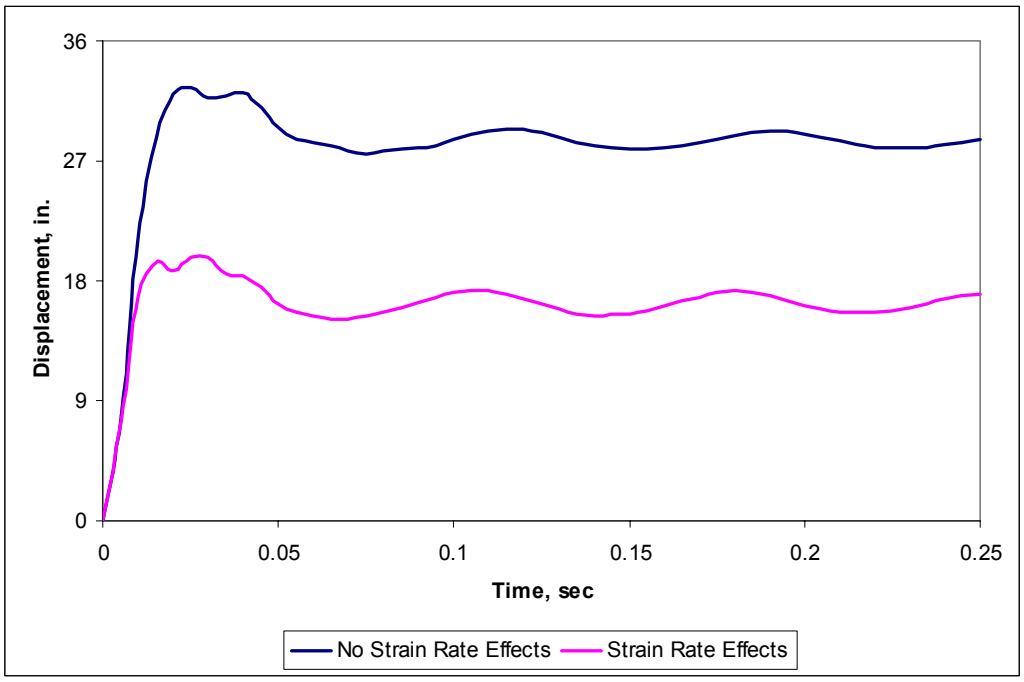

Fig. 5.22. Displacement time-histories with and without the inclusion of high strain rate effects at node 205 for the frame subjected to a 4,000 psi blast with 20 kip/in. bilinear springs

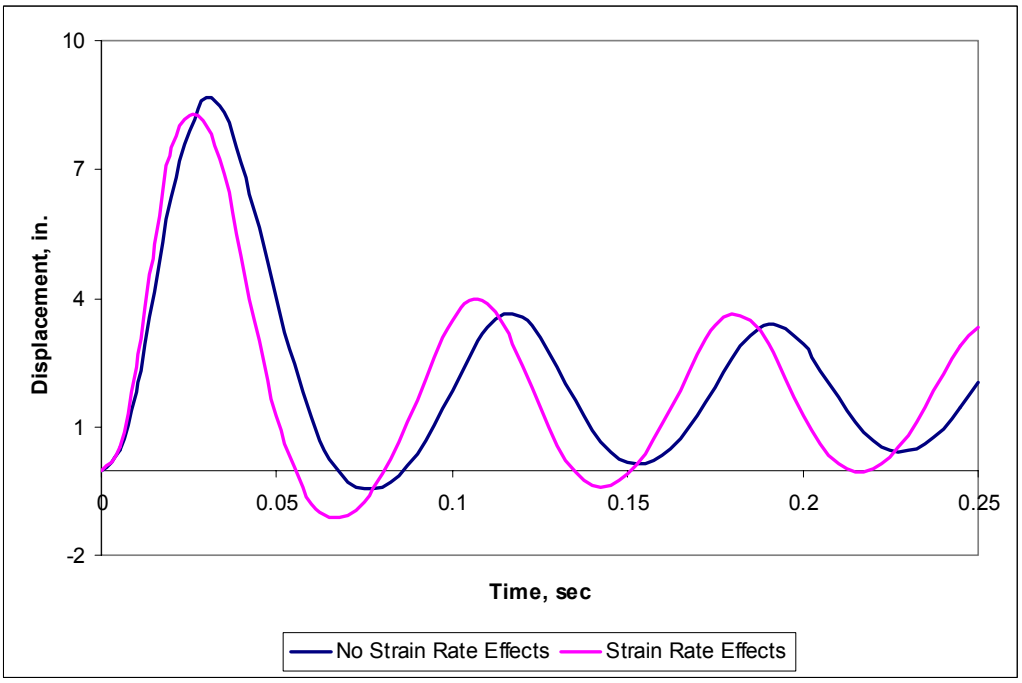

Fig. 5.23. Displacement time-histories with and without the inclusion of high strain rate effects at node 405 for the frame subjected to a 4,000 psi blast with 20 kip/in. bilinear springs

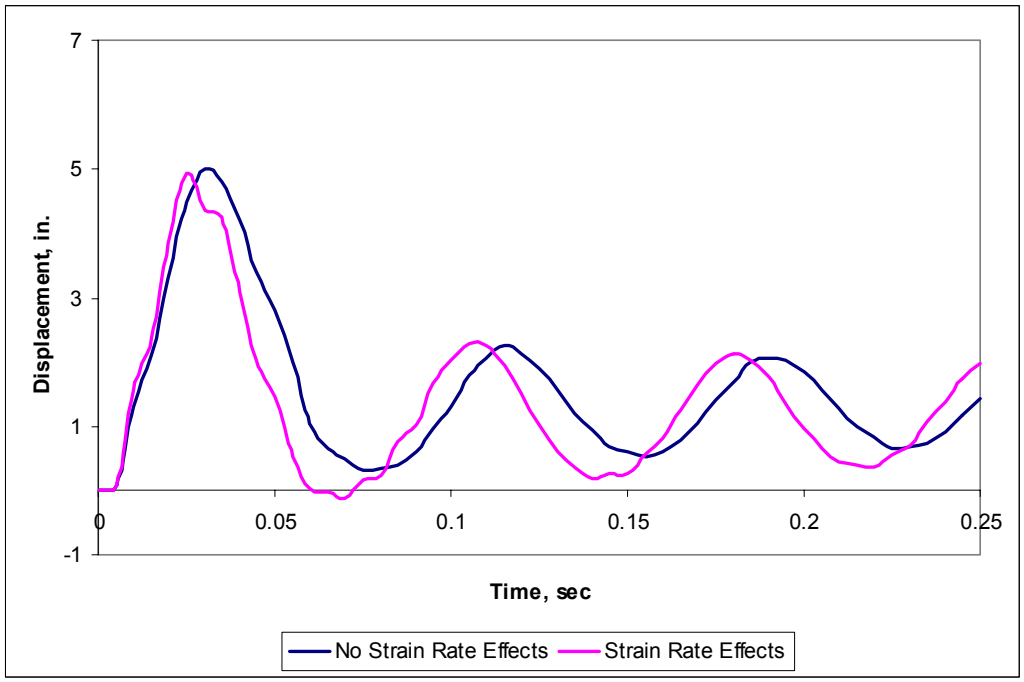

Fig. 5.24. Displacement time-histories with and without the inclusion of high strain rate effects at node 11205 for the frame subjected to a 4,000 psi blast with 20 kip/in. bilinear springs

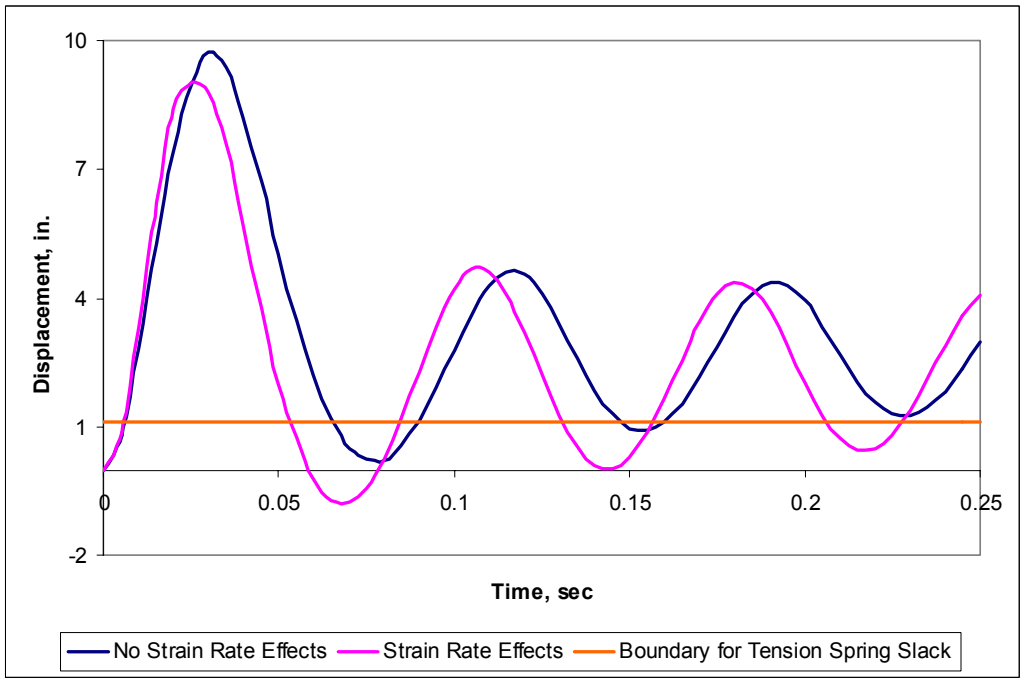

Fig. 5.25. Displacement time-histories with and without the inclusion of high strain rate effects at node 11405 for the frame subjected to a 4,000 psi blast with 20 kip/in. bilinear springs

5.3 High Strain Rate Effects on Material Stresses

An elastic-perfectly plastic constitutive material relationship with a material yield stress of 50 ksi was used for these analyses. Because of the bilinear nature of such a material relationship, the stresses in the models do not exceed the yield stress throughout the duration of the analysis, regardless of plastic strain. This is evident in Figs. 3.12 and 3.20. The inclusion of rate dependent yield in the models increases the material yield stress by a dynamic increase factor relative to the strain rate (Fig. 5.1). The material behavior beyond the yield point, however, remains constant the same way it would with a dynamic increase factor of 1.0. This relationship is shown in Fig. 5.26.

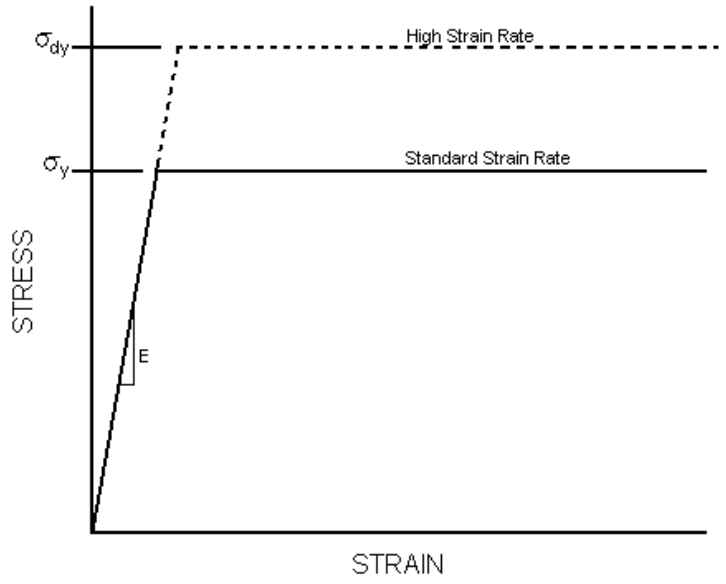

Fig. 5.26. Stress-strain relationship with and without a dynamic increase factor

Based on these properties, stresses in the frame reached values much higher than 50 ksi, depending upon the strain rate. Sample images of the von Mises stresses in a bare frame with 2,000 psi and 4,000 psi blast loadings are shown in Figs. 5.27 and 5.28, respectively. Noting the scale on the left hand side of the figures, stresses are as high as 84 ksi, corresponding to a dynamic increase factor of 1.68 and a strain rate of about 30 in./in./sec (see Fig. 5.1). The inclusion of springs again had little effect on the stresses in the frame (Fig. 5.29). This was discussed in Chapter 4.

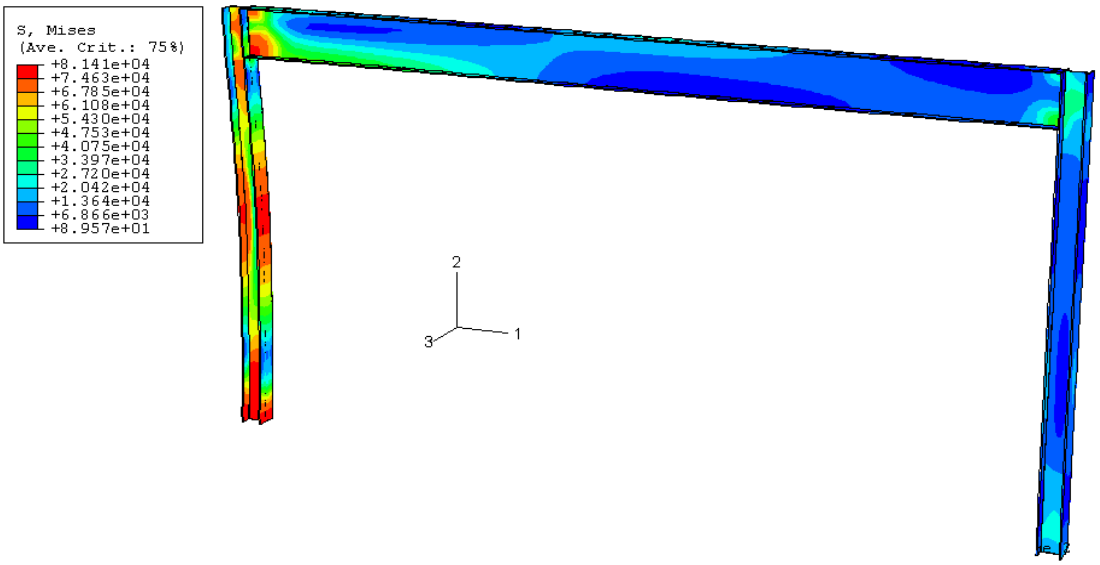

Fig. 5.27. von Mises stresses at time t = 5 msec in the bare frame subjected to a 2,000 psi blast load with rate dependent yielding

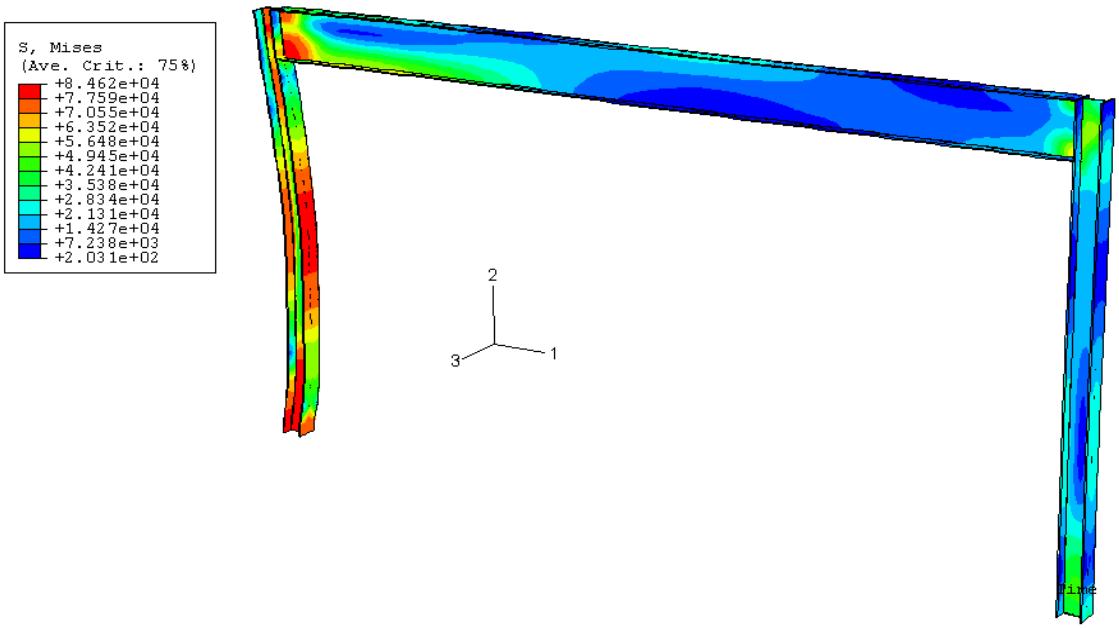

Fig. 5.28. von Mises stresses at time t = 5 msec in the bare frame subjected to a 4,000 psi blast load with rate dependent yielding

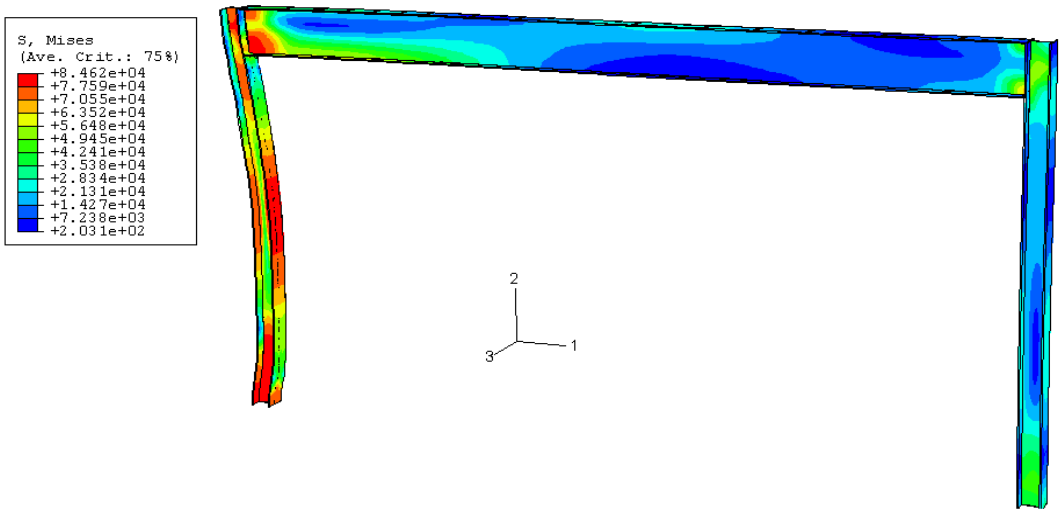

Fig. 5.29. von Mises stresses at time t = 5 msec in the frame braced with 20 kip/in. springs subjected to a 4,000 psi blast load with rate dependent yielding

5.4 High Strain Rate Effects on Material Plasticity

The spread of plasticity in the frame was again unaffected by the introduction of springs into the model. Figures 5.30 and 5.31 show the plastic deformation zones in the frame subjected to a 2,000 psi blast without springs and with 20 kip/in. springs, respectively. Figures 5.32 and 5.33 show similar models subjected to a 4,000 psi blast. Note that the stresses are nearly identical with and without springs.

The rate dependent yield effects, however, did produce lower levels of permanent plastic deformation in the frames. Comparisons of Figs. 5.30, 5.32, and 5.33 to Figs. 3.12, 3.20, and 4.12, respectively, show that there is a considerable decrease in the percentage of the frame that experiences permanent equivalent plastic strain. Figure 5.34 shows the equivalent plastic strain in the lower half of the blast side column. The model shows a maximum of 0.23 in./in. of strain, compared to a maximum value of 0.31 in./in. of strain seen in Fig. 3.21. This coincides with the information in section 5.2 regarding the reduced displacement resulting from the inclusion of rate dependent yield effects.

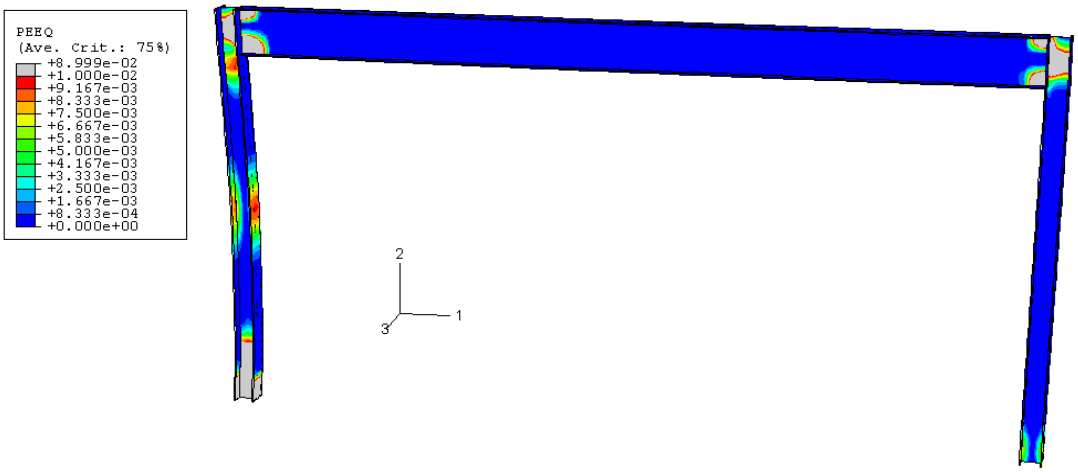

Fig. 5.30. Plastic deformation zones of the bare portal frame subjected to a 2,000 psi blast (no plastic deformation = blue) at time t = 0.25 sec

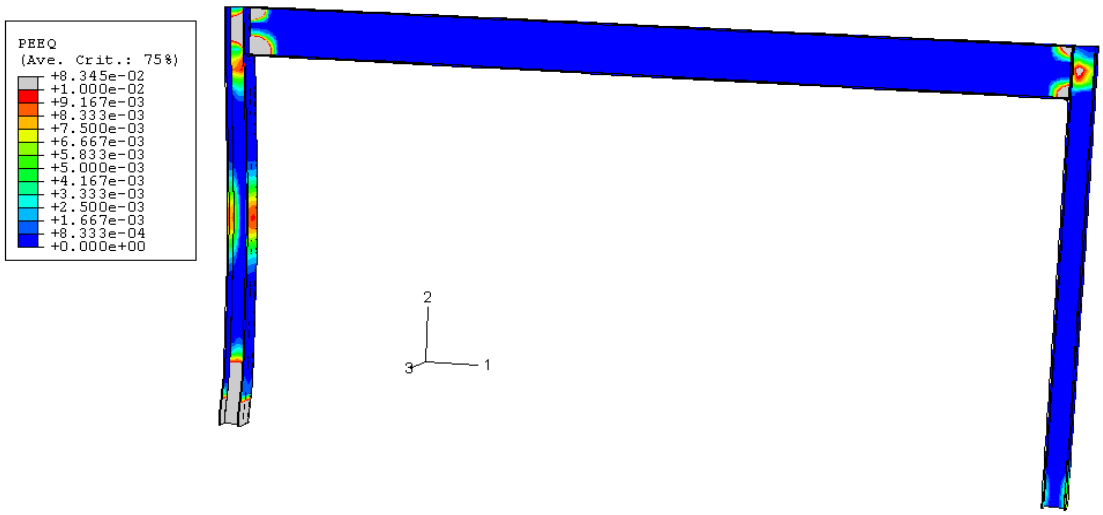

Fig. 5.31. Plastic deformation zones of the portal frame braced with 20 kip/in. springs subjected to a 2,000 psi blast (no plastic deformation = blue) at time t = 0.25 sec

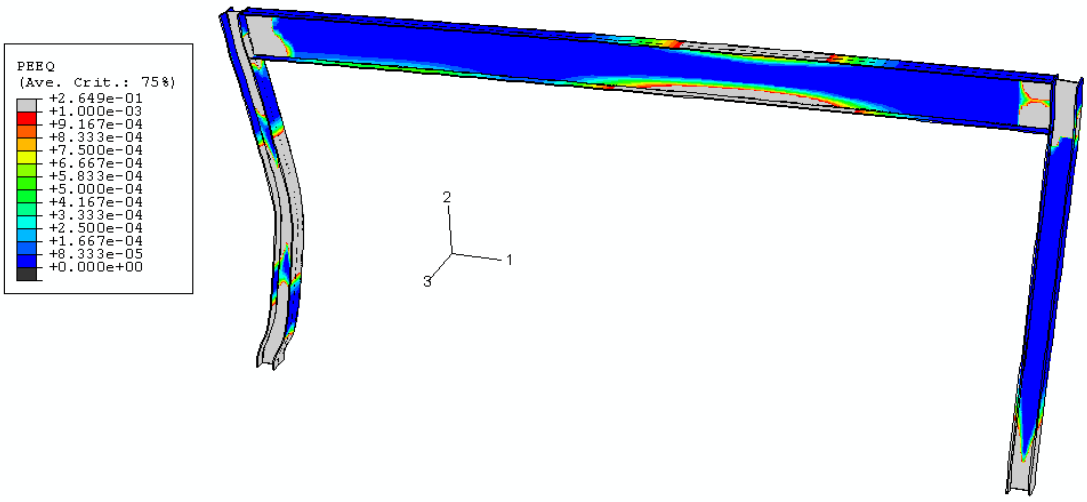

Fig. 5.32. Plastic deformation zones of the bare portal frame subjected to a 4,000 psi blast (no plastic deformation = blue) at time t = 0.25 sec

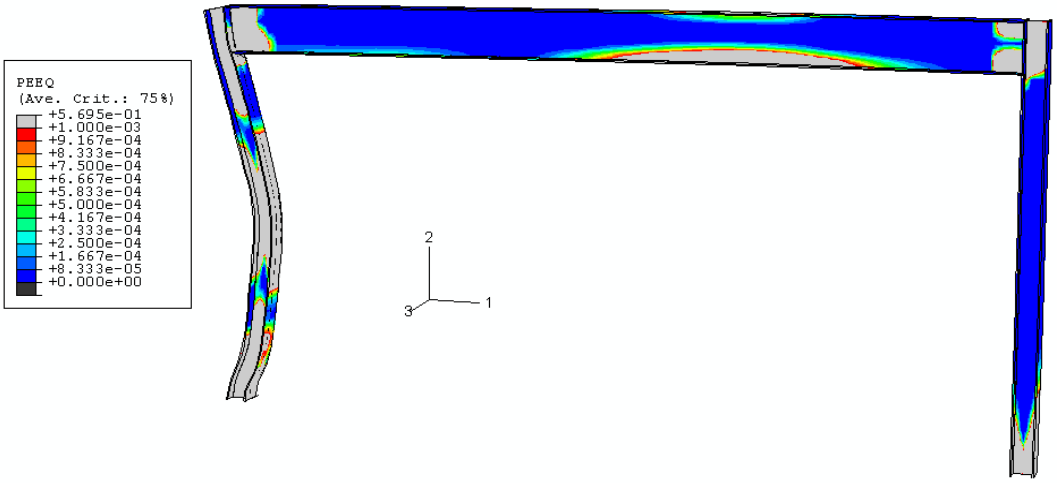

Fig. 5.33. Plastic deformation zones of the portal frame braced with 20 kip/in. springs subjected to a 4,000 psi blast (no plastic deformation = blue) at time t = 0.25 sec

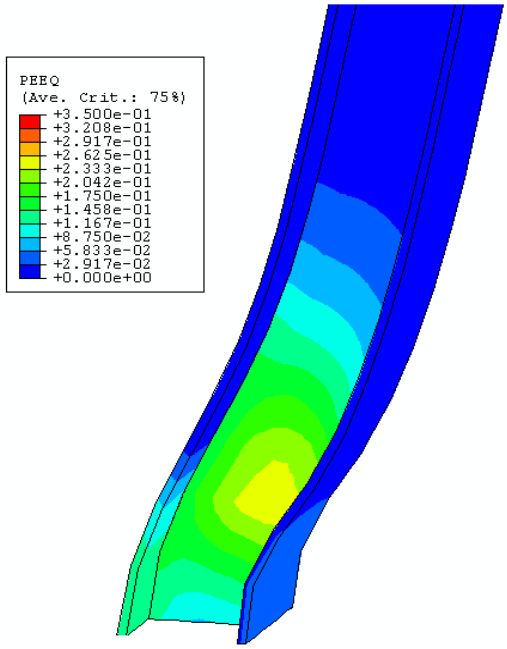

Fig. 5.34. Bending and equivalent plastic strain at the midspan and the support of the blast side column subjected to a 4,000 psi blast, with high strain rate effects included

Chapter 6
Nonlinear Springs

6.1 Nonlinear Spring Properties

This research has examined the blast resistant effects of bilinear springs on portal frames. Parallel research has been conducted regarding the material properties of the synthetic ropes used as snapping cable energy dissipators (SCEDs) that the springs are modeling. Initial tests of these ropes have suggested that the true force in the spring can be approximated via the following equation:

$$F = kx^{1.3} \tag{6.1}$$

where k = spring stiffness (kip/(in.$^{1.3}$))

x = axial displacement of the spring after the spring becomes taut

Spring models were created for this research using Eq. 6.1 and compared to the bilinear results. Because the stiffnesses cannot directly coincide, several models were analyzed. The bilinear spring stiffnesses of 5 kip/in. and 20 kip/in. were evaluated and, through trial and error, spring stiffnesses in kip/(in.$^{1.3}$) units were developed for comparisons. Two means of comparison were developed—one where the bilinear spring stiffness was more of an average of the nonlinear stiffness and another where the bilinear spring stiffness was nearly tangent to the nonlinear stiffness at low displacements and never exceeds the value of the nonlinear stiffness. Figures 6.1 and 6.2 show these comparisons.

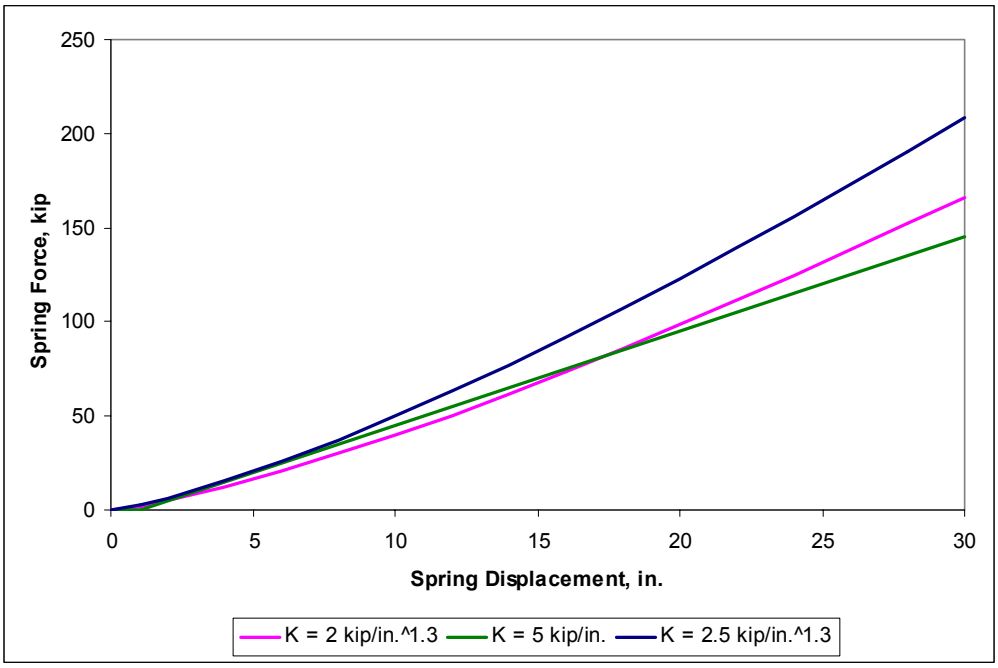

Fig. 6.1. Bilinear and nonlinear spring force vs. displacement plots based on bilinear 5 kip/in. spring

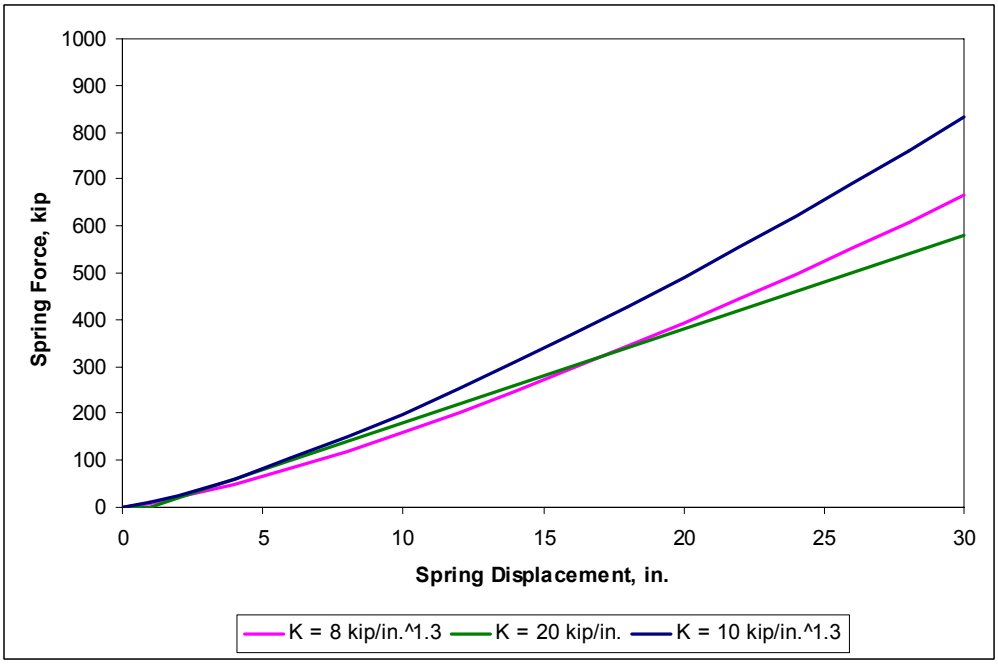

Fig. 6.2. Bilinear and nonlinear spring force vs. displacement plots based on bilinear 20 kip/in. spring

It should be noted that the goal of this chapter was to compare effects of springs with bilinear stiffnesses (bilinear springs) and nonlinear stiffnesses (nonlinear springs) on the behavior of the frame system. This was done by ensuring that the nonlinear spring stiffnesses were as close as possible to the bilinear spring stiffnesses. It was noted in chapters 4 and 5 that the spring stiffnesses had little effect on the plasticity spread and the stresses in the system. Analysis of the nonlinear springs showed that the stresses in the system and the plasticity spread were nearly identical for the comparisons, as would be expected. It should also be noted that rate dependent yield effects were considered in the following analysis. The high strain rates caused by blast loads necessitate such consideration for a more realistic analysis.

6.2 Displacement Comparisons

The subsections that follow detail the comparisons between bilinear and nonlinear springs. The research discussed in the previous sections compared the structural behavior of the frame subjected to varying blast loads, specifically 100 psi, 2,000 psi, and 4,000 psi blasts. For the purpose of comparing the bilinear and nonlinear springs, the 4,000 psi blast was considered based on the higher displacements and more spring activity. These higher spring forces make for a better means of comparison. Comparisons of the time histories of the bilinear and nonlinear spring forces can be found in Appendix C.

6.2.1 Spring Case I – 5 kip/in. bilinear springs and corresponding nonlinear springs

The first step for comparing the bilinear and nonlinear springs was selecting the proper nonlinear spring constants. Figure 6.1 shows a spring force vs. displacement diagram for the 5 kip/in. bilinear spring. Nonlinear spring constants of 2 kip/in.$^{1.3}$ and 2.5 kip/in.$^{1.3}$ were selected for comparisons. The 2 kip/in.$^{1.3}$ nonlinear spring has a lower spring stiffness up to an axial displacement of 17.4 in., while the 2.5 kip/in.$^{1.3}$ nonlinear spring has a greater spring stiffness than the 5 kip/in. bilinear spring for all displacements. The

2.5 kip/in.$^{1.3}$ nonlinear spring is nearly tangent to the 5 kip/in. bilinear spring at a displacement of just under 4 in.

Figures 6.3-6.6 show displacement time histories at nodes 205, 405, 11205, and 11405, respectively. These figures compare the system displacements for frames subjected to 4,000 psi blasts with each of the three different springs included. It is easily noted that there is very little difference between the time histories for each of the three spring stiffnesses, bilinear or nonlinear. The 2 kip/in.$^{1.3}$ spring had slightly less effect on the frame than the 5 kip/in. bilinear spring, while the 2.5 kip/in.$^{1.3}$ showed slightly more effect on the frame. This behavior would be expected since displacements do not exceed 17 in. at the nodes except in the case of node 205, which, as previously discussed, is least affected by the springs. Table 6.1 compares maximum displacements for the key nodes of the frame with different spring stiffnesses. Table 6.2 evaluates maximum displacements at later cycles.

	5 kip/in. bilinear spring	2 kip/in.$^{1.3}$ nonlinear spring	2.5 kip/in.$^{1.3}$ nonlinear spring
Node 205	21.39	21.37	21.14
Node 405	12.19	12.42	11.89
Node 11205	6.49	6.66	6.29
Node 11405	12.88	13.11	12.57

Table 6.1. Maximum displacements at key nodes in the frame subjected to a 4,000 psi blast and braced with springs with noted stiffnesses (base unit = inch)

	5 kip/in. bilinear spring	2 kip/in.$^{1.3}$ nonlinear spring	2.5 kip/in.$^{1.3}$ nonlinear spring
Node 205	18.42	18.86	18.45
Node 405	5.91	6.98	6.18
Node 11205	3.45	3.90	3.36
Node 11405	6.33	7.70	6.73

Table 6.2. Maximum displacements at later cycles at key nodes in the frame subjected to a 4,000 psi blast and braced with springs with noted stiffnesses (base unit = inch)

6.2.2 Spring Case II – 20 kip/in. bilinear springs and corresponding nonlinear springs

Figure 6.2 shows a spring force vs. displacement diagram for the 20 kip/in. bilinear spring. Based on the fact that the 20 kip/in. bilinear spring is 4 times stiffer than the 5 kip/in. bilinear spring, corresponding nonlinear spring constants of 8 kip/in.$^{1.3}$ and 10 kip/in.$^{1.3}$ were selected for comparisons. Similarly, the 8 kip/in.$^{1.3}$ nonlinear spring has a lower spring stiffness up to an axial displacement near 17.4 in., while the 10 kip/in.$^{1.3}$ nonlinear spring has a higher spring stiffness than the 20 kip/in. bilinear spring for all displacements. The 10 kip/in.$^{1.3}$ nonlinear spring is nearly tangent to the 20 kip/in. bilinear spring at a displacement of just under 4 in.

Figures 6.7-6.10 show displacement time histories at nodes 205, 405, 11205, and 11405, respectively, comparing the system displacements for frames subjected to the same 4,000 psi blasts with each of the three different springs included. Note that there is again very little difference between the time histories for each of the three spring stiffnesses, bilinear or nonlinear. The difference for this set of comparisons is less than for the comparisons made in the previous subsection. The 8 kip/in.$^{1.3}$ spring had slightly less effect on the frame than the 20 kip/in. bilinear spring, while the 10 kip/in.$^{1.3}$ spring had slightly more effect on the frame. Table 6.3 compares maximum displacements for the key nodes of the frame with different spring stiffnesses. Table 6.4 shows maximum displacements at later cycles of motion.

	20 kip/in. bilinear spring	8 kip/in.$^{1.3}$ nonlinear spring	10 kip/in.$^{1.3}$ nonlinear spring
Node 205	19.86	20.00	19.66
Node 405	8.26	8.52	8.03
Node 11205	4.95	5.08	4.83
Node 11405	9.06	9.27	8.81

Table 6.3. Maximum displacements at key nodes in the frame subjected to a 4,000 psi blast and braced with springs with noted stiffnesses (base unit = inch)

	20 kip/in. bilinear spring	8 kip/in.$^{1.3}$ nonlinear spring	10 kip/in.$^{1.3}$ nonlinear spring
Node 205	17.43	17.41	17.24
Node 405	4.13	4.07	3.78
Node 11205	2.32	2.23	2.11
Node 11405	4.82	4.57	4.38

Table 6.4. Maximum displacements at later cycles at key nodes in the frame subjected to a 4,000 psi blast and braced with springs with noted stiffnesses (base unit = inch)

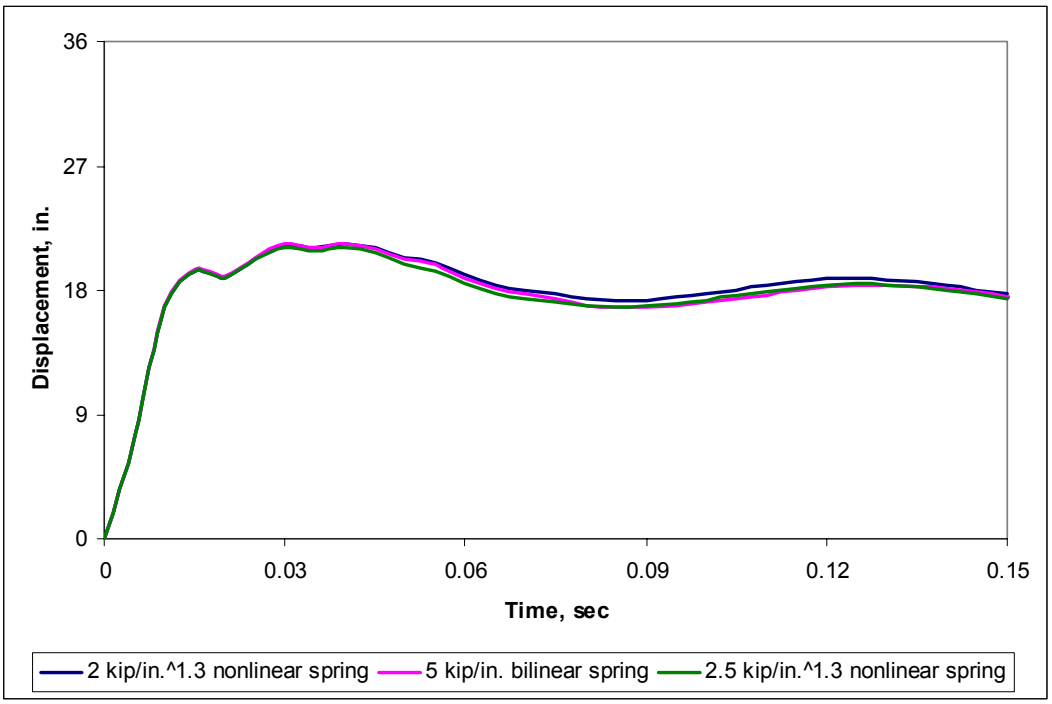

Fig. 6.3. Displacement time-histories for 5 kip/in. bilinear springs and corresponding nonlinear springs for node 205 of the frame subjected to a 4,000 psi blast

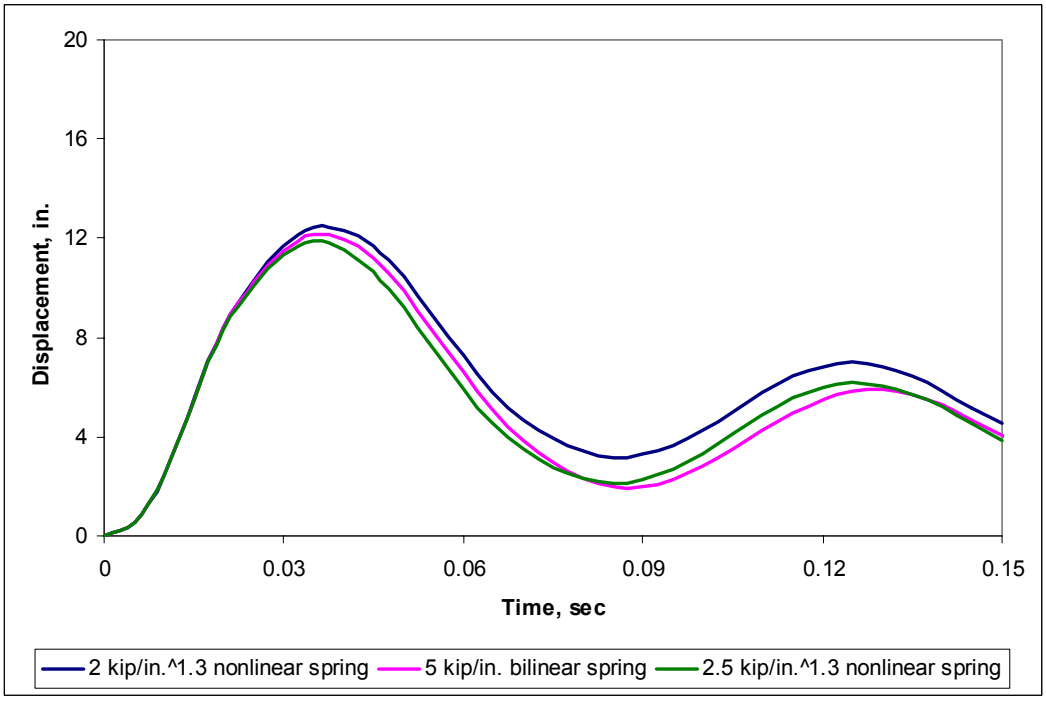

Fig. 6.4. Displacement time-histories for 5 kip/in. bilinear springs and corresponding nonlinear springs for node 405 of the frame subjected to a 4,000 psi blast

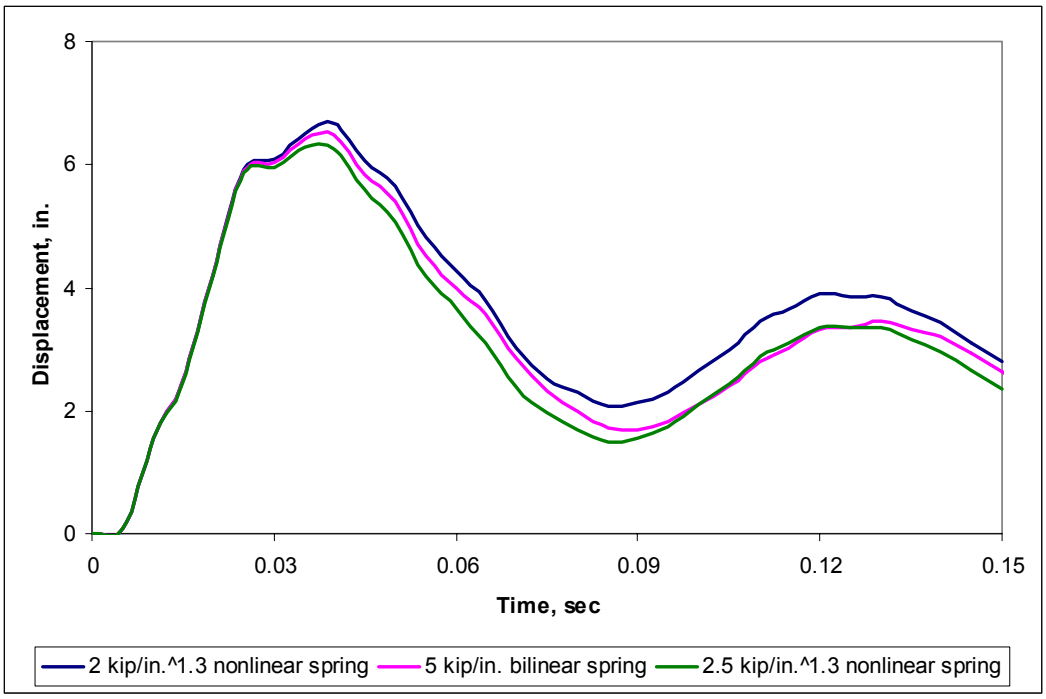

Fig. 6.5. Displacement time-histories for 5 kip/in. bilinear springs and corresponding nonlinear springs for node 11205 of the frame subjected to a 4,000 psi blast

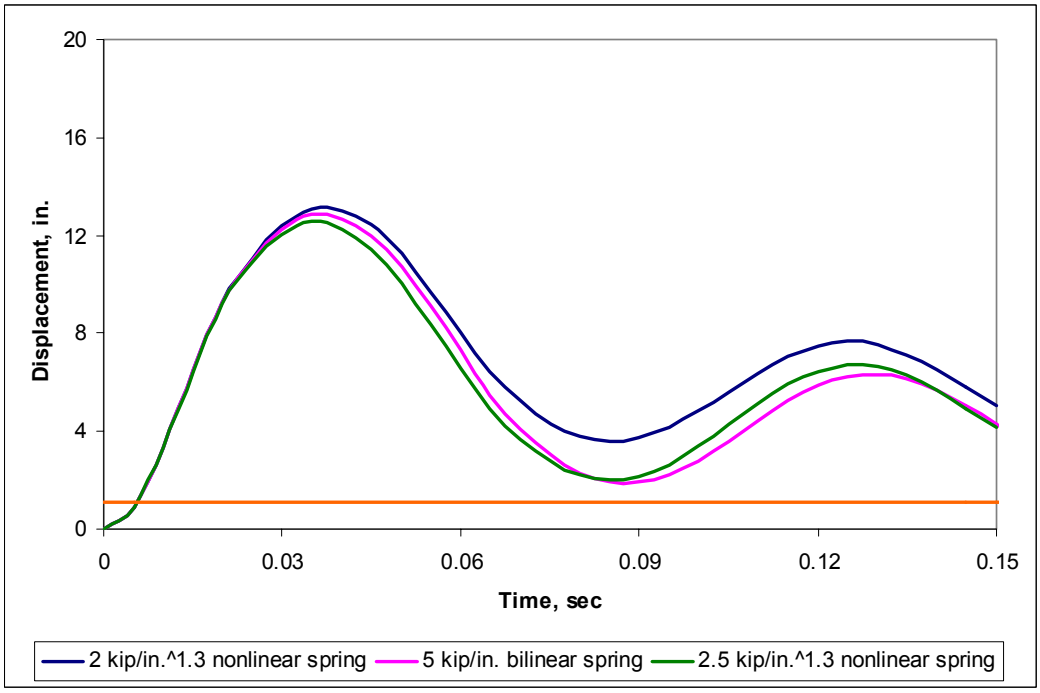

Fig. 6.6. Displacement time-histories for 5 kip/in. bilinear springs and corresponding nonlinear springs for node 11405 of the frame subjected to a 4,000 psi blast

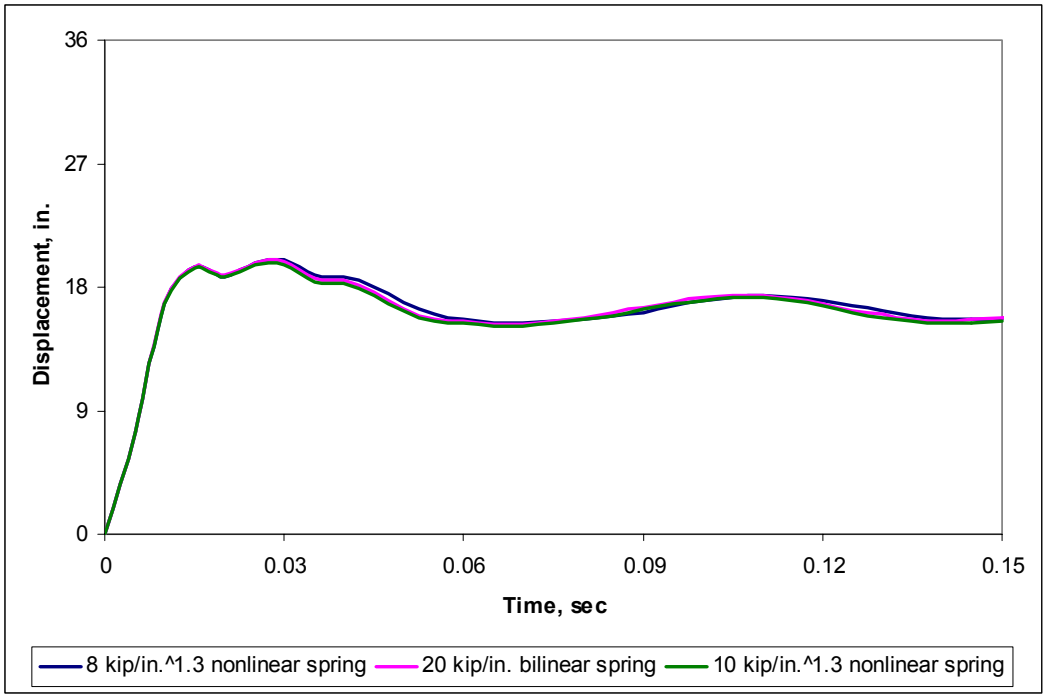

Fig. 6.7. Displacement time-histories for 20 kip/in. bilinear springs and corresponding nonlinear springs for node 205 of the frame subjected to a 4,000 psi blast

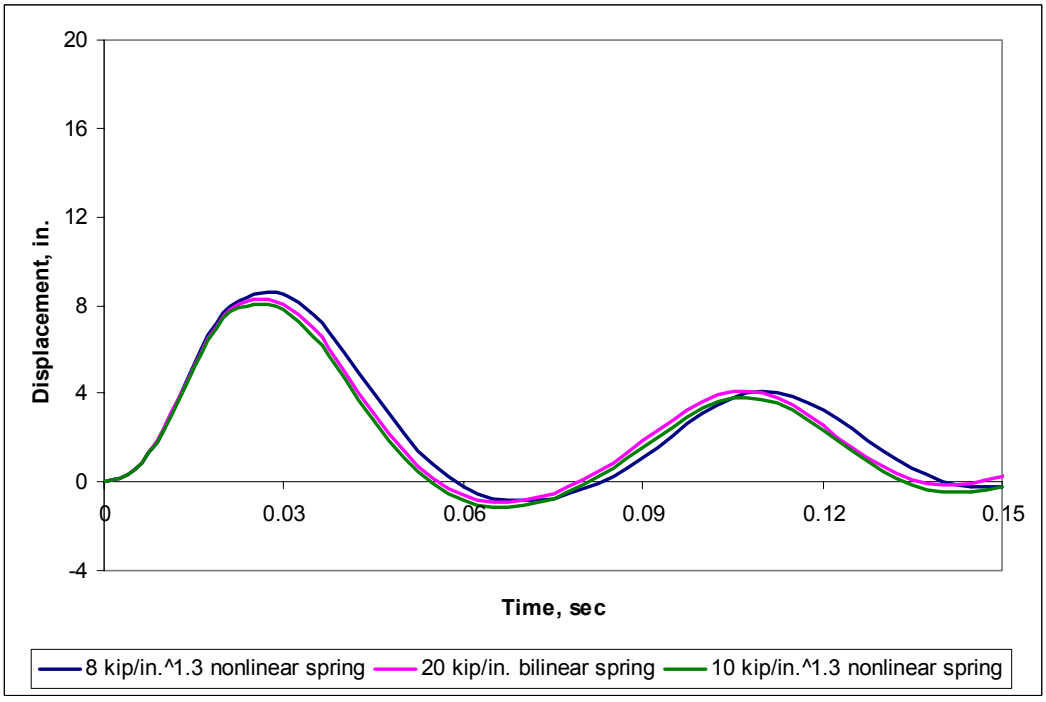

Fig. 6.8. Displacement time-histories for 20 kip/in. bilinear springs and corresponding nonlinear springs for node 405 of the frame subjected to a 4,000 psi blast

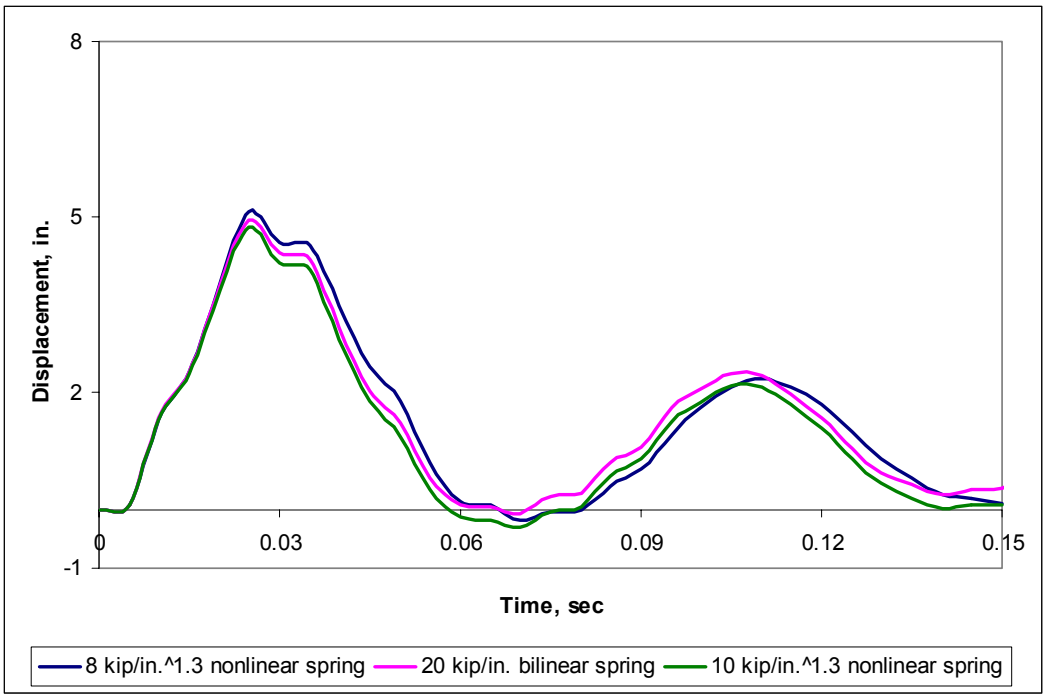

Fig. 6.9. Displacement time-histories for 20 kip/in. bilinear springs and corresponding nonlinear springs for node 11205 of the frame subjected to a 4,000 psi blast

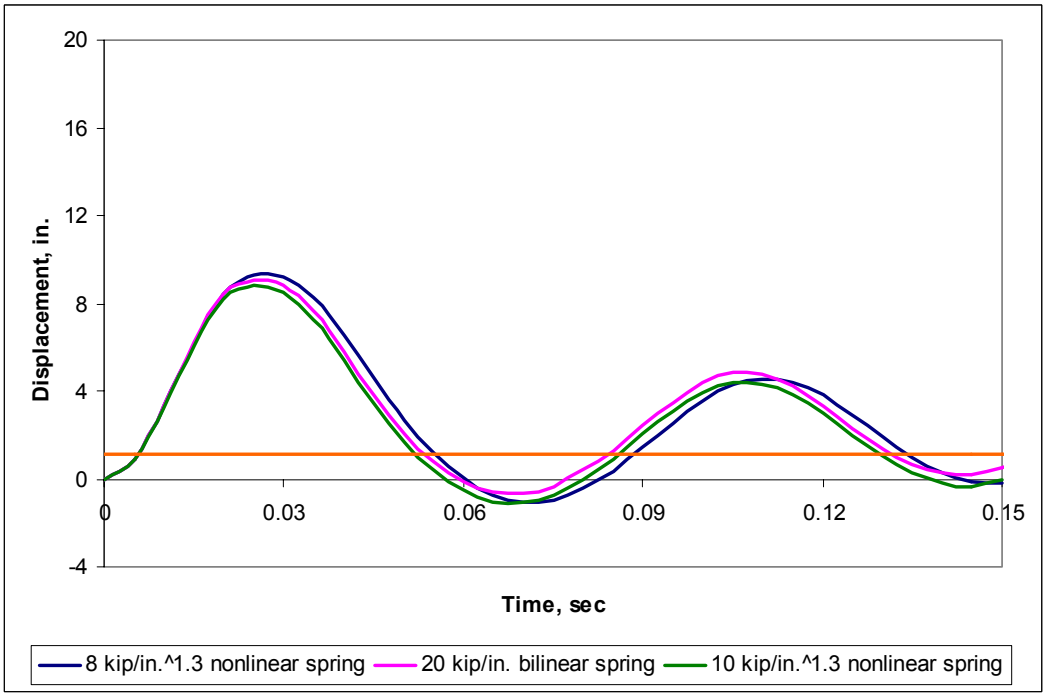

Fig. 6.10. Displacement time-histories for 20 kip/in. bilinear springs and corresponding nonlinear springs for node 11405 of the frame subjected to a 4,000 psi blast

Chapter 7
Conclusions and Recommendations for Future Research

7.1 Summary and Conclusions

This research examined blast loads on portal frames and focused on methods of reducing the effects of these loads. When an explosive device is detonated, a high-speed pressure wave is created that can produce very high loads on a structure over very short time spans. Many structures are not properly designed to resist these high loads; therefore, research is underway to develop new methods of alleviating the effects of these loads. This research is part of a multi-stage research project examining synthetic fiber ropes as a means of lateral load resistance against seismic, blast, and wind loads. The long-term goal of the project is to develop these ropes as Snapping-Cable Energy Dissipators (SCEDs) that can be used as a structural element in a lateral load-resisting system.

The initial stages of this research project focused on the dynamic and material behavior of the synthetic fiber ropes. Pearson (2002) and Hennessey (2003) studied these ropes through experimental tests and analytical models. Their research is currently being continued to better understand the exact behavior of the ropes. As the data from the ropes are collected, alternate models are being developed to analyze the possible effects of the ropes in structural systems. This thesis studied the effects of the ropes as blast resistant structural elements through finite element analysis of blast loads on portal frames. The commercial finite element program ABAQUS was used in all of the finite element modeling, and both static and dynamic verification exercises were developed to ensure the results of the models.

The frame models were created using 7,200 three-dimensional brick elements forming a portal frame consisting of three steel I-beams with fixed supports and rigid connections. An ideal unit blast curve was developed based on the Friedlander equation (Eq. 1.1) with a maximum amplitude that can be modified in the ABAQUS input file to create varying

blast loads on the structure. The behavior of the frame subject to blast loads of 100, 2,000, and 4,000 psi was analyzed and key points of response were determined to exist at the midspan and the top of each column. These key points were defined in Table 3.2 as nodes 205, 405, 11205, and 11405. Time histories of displacements at the key nodes were shown for each structural system that was analyzed as the primary form of comparison. Initial tests of the blasts on the frame provided several important results. First, the 100 psi blast proved to have very little effect overall on the structure, with maximum displacements of about 0.2 in. at the corners of the frame. The 2,000 and 4,000 psi blasts showed substantial permanent displacement at each of the key points of the structure, as high as 37 in. at the midspan of the blast side column. Equivalent plastic strains in the web of the blast side column neared the point of failure. These are the effects that the synthetic ropes are meant to resist.

The ropes were introduced into the model by developing bilinear springs as cross braces. Physical models of the ropes in the frame would inherently have a small amount of slack in the ropes. This was modeled by providing the spring zero stiffness to a displacement of 1.0 in. Appendix A shows calculations to determine the necessary global X-displacement for the transition between the slack and taut states in the ropes. Because of the necessary displacement of 1.10 in. at node 11405, the 100 psi blast was not modeled with springs. The first braced frame models were developed using bilinear springs with stiffnesses of 5, 10, and 20 kip/in. The springs were shown to have a positive effect on the displacement of the system at each of the key points of the frame. The effects of the springs were more evident at nodes 405 and 11405—the tops of the columns—based on the fact that the springs were connected to the frame at those points and had a more direct effect there. Furthermore, the springs had much more effect on the system for the 4,000 psi blast than the 2,000 psi blast, most likely because the higher blast resulted in higher displacements in the system. The springs were also shown to reduce the permanent deformation at the key nodes by as much as 80% in some instances. The springs did not have much effect on the maximum stresses and permanent plasticity in the system. Most of the plasticity spread in the frame occurred before the springs became taut. However, the level of equivalent plastic strain was positively affected by the stronger springs.

Blasts produce very large loads over short time periods; therefore, they result in high strain rates. Because the structure cannot yield at the same rate as the load is applied, rate dependent yield affects the behavior of the structure and a dynamic increase factor can be applied to the yield stress of the material. This dynamic increase factor increases logarithmically with the increase in strain rate (see Fig. 5.1). The dynamic increase factor was proven to be integral for this research. Significant reductions in displacement occurred following the introduction of rate dependent yield effects into the unbraced system, specifically at the midspans of the columns relative to the tops of the columns. However, the analysis showed that the inclusion of springs in the models reduced the effects of high strain rates at nodes 405 and 11405. The 20 kip/in. bilinear spring nearly negated the effects of rate dependent yield. Stresses in the material reached 84 ksi, corresponding to a dynamic increase factor of 1.68 and a strain rate near 30 in./in./sec. The corresponding critical strain points in the web of the base of the blast side column showed significant reduction of strain of nearly 30%.

Parallel research showed that the spring forces based on displacement resulted in nonlinear stiffnesses of kip/(in.$^{1.3}$) instead of the bilinear stiffness in kip/in. Nonlinear spring stiffnesses were used for comparison with the bilinear springs. Two nonlinear models were developed for each bilinear model—one where the bilinear stiffness was more of a trend line for the nonlinear stiffness and another where the bilinear stiffness was nearly a tangent for the nonlinear stiffness (see Figs. 6.1 and 6.2). The data showed that the behavior of the frame braced with nonlinear springs coincided very closely with the behavior of the frame braced with bilinear springs.

The results of this research are promising. The springs that were modeled had a definitively positive impact on the behavior of the frame. Large displacements lead to failures that can be both costly and dangerous. Reducing these displacements is crucial in the protection of the structure from blasts. The models provided in this research can be valuable tools for determining the effects of the synthetic fiber ropes on the behavior of a structure. The bilinear spring models were shown to closely coincide with the initial

models of the actual nonlinear behavior of the springs. For the models where the bilinear spring stiffness was tangent to the nonlinear spring stiffness, the bilinear spring models gave a slightly conservative method of accurately determining the behavior of the system.

7.2 Recommendations for Future Research

As previously mentioned, this is the third stage of a multi-stage research project. The possibility of SCEDs as a means of lateral load resistance brings about the potential for an adequate method of blast resistance that would be more cost-effective than designing laterally braced structural systems or retrofitting existing buildings. To sufficiently understand the effects that synthetic fiber ropes could have on structures, several steps must be taken in future stages of this research.

First and foremost, the exact behavior of the ropes must be determined. Parallel research is underway in developing the material properties of the ropes and their dynamic behavior. The models developed for this research can easily be adapted for future research by changing the commands within the ABAQUS input file. The models that were analyzed in this research show that springs can be effective for reducing blast response.

Second, to be able to apply these ropes to more realistic structural systems, large-scale finite element modeling is recommended. Increasing the number of bays and creating a three-dimensional model is feasible for the next level of this research. Models could also be developed with various locations of the springs, alternative to X-bracing, to find the system that most effectively mitigates the blast loads and reduces their effects.

The most beneficial research would be physical tests that could be run with scale models of the frames. Currently scale model tests are being conducted to determine the behavior of the synthetic ropes during seismic activity. Developing physical tests to analyze blast loads is not a practical undertaking; however, the data that could be retrieved from these tests would be invaluable to determining the nature of the rope behavior under such high

loads. Finally, additional uses of the SCEDs should be considered. More parallel research is currently being developed for possible uses of the synthetic ropes for mitigating bridge deflections and stabilizing towers. These types of applications could lead to further use of SCEDs as a cost-effective means of bracing a structural system.

References

AISC (2001). *Load and Resistance Factor Design Specification for Structural Steel Buildings*, AISC, Chicago, IL.

Baker, W.E. (1973). *Explosions in Air*. University of Texas Press, Austin, TX.

Barker, D.D. (1997). "Dynamic Material Behavior," *Building to Last, Proceedings of Structures Congress XV*, ASCE, Portland, OR, pp. 614-623.

Beshara, F.B.A. (1994). "Modeling of Blast Loading on Aboveground Structures—I. General Phenomenology and External Blast," *Computers & Structures*, Vol. 51, No. 5, pp. 585-596.

Chopra, A.K. (2001). *Dynamics of Structures: Theory and Applications to Earthquake Engineering, Second Edition*. Prentice-Hall, Upper Saddle River, NJ.

Conrath, E.J., Krauthammer, T., Marchand, K.A., and Mlakar, P.F. (1999). *Structural Design for Physical Security: State of the Practice*. ASCE, Reston, VA.

Dharaneepathy, M.V., Keshava Rao, M.N., and Santhakumar, A.R. (1995). "Critical Distance for Blast-Resistant Design," *Computers & Structures*, Vol. 54, No. 4, pp. 587-595.

Fung, T.C. and Chow, S.K. (1999). "Responses of Blast Loading by Complex Time Step Method," *Journal of Sound and Vibration*, Vol. 223, No. 1, pp. 23-48.

Hennessey, C.M. (2003). "Analysis and Modeling of Snap Loads on Synthetic Fiber Ropes," M.S. Thesis. Virginia Polytechnic Institute and State University, Blacksburg, VA. http://scholar.lib.vt.edu/theses/available/etd-11092003-135228/.

Krauthammer, T. (1999). "Blast-resistant Structural Concrete and Steel Connections," *International Journal of Impact Engineering*, Vol. 22, No. 9-10, pp. 887-910.

Longinow, A. and Mniszewski, K.R. (1996). "Protecting Buildings Against Vehicle Bomb Attacks," *Practice Periodical on Structural Design and Construction*, Vol. 1, No. 1, pp. 51-54.

Miyamoto, H.K. and Taylor, D. (2000). "Structural Control of Dynamic Blast Loading," *Advanced Technology in Structural Engineering, Proceedings from Structures Congress 2000*, ASCE, Reston, VA, CD-ROM.

Mlakar, P.F. (1996). "Structural Design for Vehicular Bombs," *Building an International Community of Structural Engineers*, Vol. 2, pp. 1269-1276.

NAVFAC (1990). *Structures to Resist the Effects of Accidental Explosions*, Revision 1. Dept. of the Navy Publication NAVFAC P-397, Dept. of the Army Technical Manual TM-1300, Dept. of the Air Force Manual AFM 88-22, U.S. Depts. Of the Army, Navy, and Air Force, Washington, DC.

Pearson, N.J. (2002). "Experimental Snap Loading of Synthetic Fiber Ropes," M.S. Thesis. Virginia Polytechnic Institute and State University, Blacksburg, VA. http://scholar.lib.vt.edu/theses/available/etd-01132003-105300/.

Shope, R.L. and Plaut, R.H. (1998). "Critical Blast Loads for Compressed Steel Columns," *Engineering Mechanics: A Force for the 21st Century*, H. Murakami and J.E. Luco, eds., ASCE, Reston, VA, pp. 712-715

Shope, R.L. and Plaut, R.H. (1999). "Critical Blast Loads for Two-Span Compressed Steel Columns, *Proceedings of the 13th Engineering Mechanics Division Conference*, N.P. Jones and R.G. Ghanem, eds.

Williams, M.S. and Newell, J.P. (1991). "Methods for the Assessment of the Blast Response of Engineering Structures," *Earthquake, Blast, and Impact: Measurement and Effects of Vibration*, Society for Earthquake and Civil Engineering Design, E & F N Spon, London, pp. 176-185.

Appendix A

Calculation of the Necessary Frame Displacement for Transformation of the Springs from Slack to Taut State

A.1 Calculation of Global X-Displacement Boundary for Transition Between Slack and Taut States of the Primary Spring

$$Spring\_Length_{x\_direction} = 300in$$

$$Beam\_Depth = 17.7in$$

$$Spring\_Length_{y\_direction} = 156in - Beam\_Depth = 138.3in$$

$$Spring\_Length = \sqrt{Spring\_Length_{x\_direction}^{2} + Spring\_Length_{y\_direction}^{2}} = 330.34in$$

$$Slack = 1.0in$$

$$Spring\_Extension = Spring\_Length + Slack = 331.34in$$

$$X\_Displacement_{Node\_11405} = \sqrt{Spring\_Extension^{2} - Spring\_Length_{y\_direction}^{2}} = 1.10in$$

Appendix B

Sample ABAQUS Input File

B.1 4,000 psi Blast on a Frame Braced with 8 kip/in.$^{1.3}$ Nonlinear Springs with Strain Rate Effects Included

```
*Heading
 UNIFORM BLAST 8 KLI^1.3 NONLIN SPRINGS
 BASE UNITS: IN, LB, SEC
** Job name: UNIFORMBLAST
**E=29000000
**
*Node
1,-8.25,0,-4.035
10,-8.25,0,4.035
401,-8.25,156,-4.035
410,-8.25,156,4.035
100001,-7.69,0,-0.18
100010,-0.56,0,-0.18
100401,-7.69,156,-0.18
100410,-0.56,156,-0.18
200001,0,156,-3.0
200010,0,156,3.0
200801,300,156,-3.0
200810,300,156,3.0
300010,0,155.575,-0.15
300001,0,138.725,-0.15
300810,300,155.575,-0.15
300801,300,138.725,-0.15
*NGEN, NSET=BOT
1,10,1
*NGEN, NSET=TOP
401,410,1
*NGEN, NSET=BOTW
100001,100010,1
*NGEN, NSET=TOPW
100401,100410,1
*NGEN, NSET=LBF
200001,200010,1
*NGEN, NSET=RBF
200801,200810,1
*NGEN, NSET=LBW
300001,300010,1
*NGEN, NSET=RBW
300801,300810,1
*NFILL, NSET=OUTEDGE
BOT,TOP,40,10
*NFILL, NSET=OUTWEB
BOTW,TOPW,40,10
*NFILL, NSET=TOPBF
LBF,RBF,80,10
*NFILL, NSET=BW
LBW,RBW,80,10
**
*NCOPY, SHIFT, CHANGE NUMBER=1000, OLD SET=OUTEDGE
```

```
0.28,0,0
0,0,0,0,0,0
*NCOPY, SHIFT, CHANGE NUMBER=2000, OLD SET=OUTEDGE
0.56,0,0
0,0,0,0,0,0
*NCOPY, SHIFT, CHANGE NUMBER=3000, OLD SET=OUTEDGE
7.69,0,0
0,0,0,0,0,0
*NCOPY, SHIFT, CHANGE NUMBER=4000, OLD SET=OUTEDGE
7.97,0,0
0,0,0,0,0,0
*NCOPY, SHIFT, CHANGE NUMBER=5000, OLD SET=OUTEDGE
8.25,0,0
0,0,0,0,0,0
*NCOPY, SHIFT, CHANGE NUMBER=6000, OLD SET=OUTEDGE
308.25,0,0
0,0,0,0,0,0
*NCOPY, SHIFT, CHANGE NUMBER=7000, OLD SET=OUTEDGE
308.53,0,0
0,0,0,0,0,0
*NCOPY, SHIFT, CHANGE NUMBER=8000, OLD SET=OUTEDGE
308.81,0,0
0,0,0,0,0,0
*NCOPY, SHIFT, CHANGE NUMBER=9000, OLD SET=OUTEDGE
315.94,0,0
0,0,0,0,0,0
*NCOPY, SHIFT, CHANGE NUMBER=10000, OLD SET=OUTEDGE
316.22,0,0
0,0,0,0,0,0
*NCOPY, SHIFT, CHANGE NUMBER=11000, OLD SET=OUTEDGE
316.5,0,0
0,0,0,0,0,0
*NCOPY, SHIFT, CHANGE NUMBER=1000, OLD SET=OUTWEB
0,0,0.36
0,0,0,0,0,0
*NCOPY, SHIFT, CHANGE NUMBER=2000, OLD SET=OUTWEB
308.25,0,0
0,0,0,0,0,0
*NCOPY, SHIFT, CHANGE NUMBER=3000, OLD SET=OUTWEB
308.25,0,0.36
0,0,0,0,0,0
*NCOPY, SHIFT, CHANGE NUMBER=1000, OLD SET=TOPBF
0,-0.2125,0
0,0,0,0,0,0
*NCOPY, SHIFT, CHANGE NUMBER=2000, OLD SET=TOPBF
0,-0.425,0
0,0,0,0,0,0
*NCOPY, SHIFT, CHANGE NUMBER=3000, OLD SET=TOPBF
0,-17.275,0
0,0,0,0,0,0
*NCOPY, SHIFT, CHANGE NUMBER=4000, OLD SET=TOPBF
0,-17.4875,0
0,0,0,0,0,0
*NCOPY, SHIFT, CHANGE NUMBER=5000, OLD SET=TOPBF
0,-17.7,0
0,0,0,0,0,0
*NCOPY, SHIFT, CHANGE NUMBER=1000, OLD SET=BW
```

```
0,0,0.30
0,0,0,0,0,0
*ELEMENT, TYPE=C3D8R
1,1,11,12,2,1001,1011,1012,1002
2001,3001,3011,3012,3002,4001,4011,4012,4002
10001,100001,100011,101011,101001,100002,100012,101012,101002
200001,200001,200011,200012,200002,201001,201011,201012,201002
202001,203001,203011,203012,203002,204001,204011,204012,204002
300001,300001,300002,301002,301001,300011,300012,301012,301011
*ELEMENT, TYPE=SPRINGA
500001,205005,6005
500002,5005,205805
*ELGEN, ELSET=LCOL
1, 9,1,1, 40,10,10, 2,1000,1000
2001, 9,1,1, 40,10,10, 2,1000,1000
*ELGEN, ELSET=LWEB
10001, 1,1,1, 40,10,1, 9,1,100
*ELGEN, ELSET=BFLANGE
200001, 9,1,1, 80,10,10, 2,1000,1000
202001, 9,1,1, 80,10,10, 2,1000,1000
*ELGEN, ELSET=BWEB
300001, 1,1,1, 9,1,1, 80,10,10
*ELCOPY, OLDSET=LCOL, ELEMENT SHIFT=4000, SHIFT NODES=6000, NEW
SET=RCOL
*ELCOPY, OLDSETS=LWEB, ELEMENT SHIFT=1000, SHIFT NODES=2000, NEW
SET=RWEB
*ELSET, ELSET=COLUMNS
LCOL,RCOL,LWEB,RWEB
*ELSET, ELSET=BEAM
BFLANGE,BWEB
*ELSET, ELSET=SPRING
500001,500002
*SPRING, ELSET=SPRING, NONLINEAR

0.0, 0.0, ,
8000, 1.0, ,
19700, 2.0, ,
48500, 4.0, ,
82160, 6.0, ,
119430, 8.0, ,
159620, 10.0, ,
202310, 12.0, ,
247200, 14.0, ,
294070, 16.0, ,
342720, 18.0, ,
393030, 20.0, ,
444880, 22.0, ,
498160, 24.0, ,
552780, 26.0, ,
608690, 28.0, ,
665810, 30.0, ,
*SOLID SECTION, ELSET=COLUMNS, MATERIAL=COLSTEEL
*SOLID SECTION, ELSET=BEAM, MATERIAL=BEAMSTEEL
**
*Nset, nset=SUPPORTS, GENERATE
1,10,1
1001,1010,1
```

```
2001,2010,1
3001,3010,1
4001,4010,1
5001,5010,1
6001,6010,1
7001,7010,1
8001,8010,1
9001,9010,1
10001,10010,1
11001,11010,1
100002,100009,1
101002,101009,1
102002,102009,1
103002,103009,1
*Elset, elset=BLASTSIDE, GENERATE
1,9,1
11,19,1
21,29,1
31,39,1
41,49,1
51,59,1
61,69,1
71,79,1
81,89,1
91,99,1
101,109,1
111,119,1
121,129,1
131,139,1
141,149,1
151,159,1
161,169,1
171,179,1
181,189,1
191,199,1
201,209,1
211,219,1
221,229,1
231,239,1
241,249,1
251,259,1
261,269,1
271,279,1
281,289,1
291,299,1
301,309,1
311,319,1
321,329,1
331,339,1
341,349,1
351,359,1
361,369,1
371,379,1
381,389,1
391,399,1
*ELSET, ELSET=LCFO, GENERATE
1005,1395,10
```

```
*ELSET, ELSET=LCWL, GENERATE
10001,10040,1
*ELSET, ELSET=LCWR, GENERATE
10801,10840,1
*ELSET, ELSET=LCFI, GENERATE
2005,2395,10
*ELSET, ELSET=RCFI, GENERATE
5005,5395,10
*ELSET, ELSET=RCWL, GENERATE
11001,11040,1
*ELSET, ELSET=RCWR, GENERATE
11801,11840,1
*ELSET, ELSET=RCFO, GENERATE
6005,6395,10
*ELSET, ELSET=BTF, GENERATE
201005,201795,10
*ELSET, ELSET=BWT, GENERATE
300009,300799,10
*ELSET, ELSET=BWB, GENERATE
300001,300791,10
*ELSET, ELSET=BBF, GENERATE
202005,202795,10
*ELSET, ELSET=LCON, GENERATE
3355,3395,10
*ELSET, ELSET=LB, GENERATE
300002,300008,1
*ELSET, ELSET=RB, GENERATE
300792,300798,1
*ELSET, ELSET=RCON, GENERATE
4355,4395,10
*SURFACE, NAME=LCFO
LCFO, S2
*SURFACE, NAME=LCWL
LCWL, S1
*SURFACE, NAME=LCWR
LCWR, S2
*SURFACE, NAME=LCFI
LCFI, S1
*SURFACE, NAME=RCFI
RCFI, S2
*SURFACE, NAME=RCWL
RCWL, S1
*SURFACE, NAME=RCWR
RCWR, S2
*SURFACE, NAME=RCFO
RCFO, S1
*SURFACE, NAME=BTF
BTF, S2
*SURFACE, NAME=BWT
BWT, S4
*SURFACE, NAME=BWB
BWB, S6
*SURFACE, NAME=BBF
BBF, S1
*SURFACE, NAME=LCON
LCON, S2
*SURFACE, NAME=LB
```

```
LB, S1
*SURFACE, NAME=RB
RB, S2
*SURFACE, NAME=RCON
RCON, S1
*TIE, NAME=BUILDSECTIONS
LCWL,LCFO
LCWR,LCFI
RCWL,RCFI
RCWR,RCFO
BWT,BTF
BWB,BBF
*TIE, NAME=CONNECTIONS
LB,LCON
RB,RCON
**
*AMPLITUDE, NAME=Blast, DEFINITION=TABULAR
0.0E-3, 0.0000, 1.0E-3, 1.0000, 2.0E-3, 0.7009, 3.0E-3, 0.4852
4.0E-3, 0.3307, 5.0E-3, 0.2207, 6.0E-3, 0.1433, 7.0E-3, 0.0893
8.0E-3, 0.0521, 9.0E-3, 0.0271, 10.0E-3, 0.0105, 11.0E-3, 0.0000
12.0E-3, -0.0064, 13.0E-3, -0.0100, 14.0E-3, -0.0116, 15.0E-3, -0.0121
16.0E-3, -0.0121, 17.0E-3, -0.0118, 18.0E-3, -0.0110, 19.0E-3, -0.0100
20.0E-3, -0.0089, 21.0E-3, -0.0078, 22.0E-3, -0.0067, 23.0E-3, -0.0058
24.0E-3, -0.0049, 25.0E-3, -0.0041, 26.0E-3, -0.0035, 27.0E-3, -0.0028
28.0E-3, -0.0021, 29.0E-3, -0.0014, 30.0E-3, -0.0007, 31.0E-3, -0.0000
**
** MATERIALS
**
*Material, name=COLSTEEL
*Density
0.0007379
*Elastic
29000000, 0.3
*Plastic
50000, 0.0000
*RATE DEPENDENT,TYPE=YIELD RATIO
1.000,0.000000
1.046,0.001
1.074,0.002
1.092,0.003
1.116,0.005
1.153,0.01
1.192,0.02
1.216,0.03
1.247,0.05
1.291,0.10
1.337,0.20
1.364,0.30
1.399,0.50
1.447,1
1.495,2
1.523,3
1.558,5
1.605,10
1.655, 20
1.683, 30
1.718, 50
```

```
1.767, 100
1.815, 200
1.843, 300
**
*Material, name=BEAMSTEEL
*Density
0.0007334
*Elastic
29000000, 0.3
*Plastic
50000, 0.0000
*RATE DEPENDENT,TYPE=YIELD RATIO
1.000,0.000000
1.046,0.001
1.074,0.002
1.092,0.003
1.116,0.005
1.153,0.01
1.192,0.02
1.216,0.03
1.247,0.05
1.291,0.10
1.337,0.20
1.364,0.30
1.399,0.50
1.447,1
1.495,2
1.523,3
1.558,5
1.605,10
1.655, 20
1.683, 30
1.718, 50
1.767, 100
1.815, 200
1.843, 300
**
** STEP: Blast
** BOUNDARY CONDITIONS
**
** Name: Fixed Support
**
*STEP, NLGEOM=YES
Blast Load
*DYNAMIC, EXPLICIT
 , 0.25, , 0.001
*Boundary
SUPPORTS, ENCASTRE
*DLOAD, AMPLITUDE=Blast
BLASTSIDE, BX, 4000
**
** OUTPUT REQUESTS
**
*OUTPUT, FIELD, VARIABLE=PRESELECT, NUMBER INTERVAL=50
*OUTPUT, HISTORY, VARIABLE=PRESELECT
*END STEP
```

Appendix C

Comparison of Time Histories of the Bilinear and Nonlinear Spring Forces Resulting from a 4,000 psi Blast

C.1 Comparison of Time Histories of Bilinear and Nonlinear Spring Forces

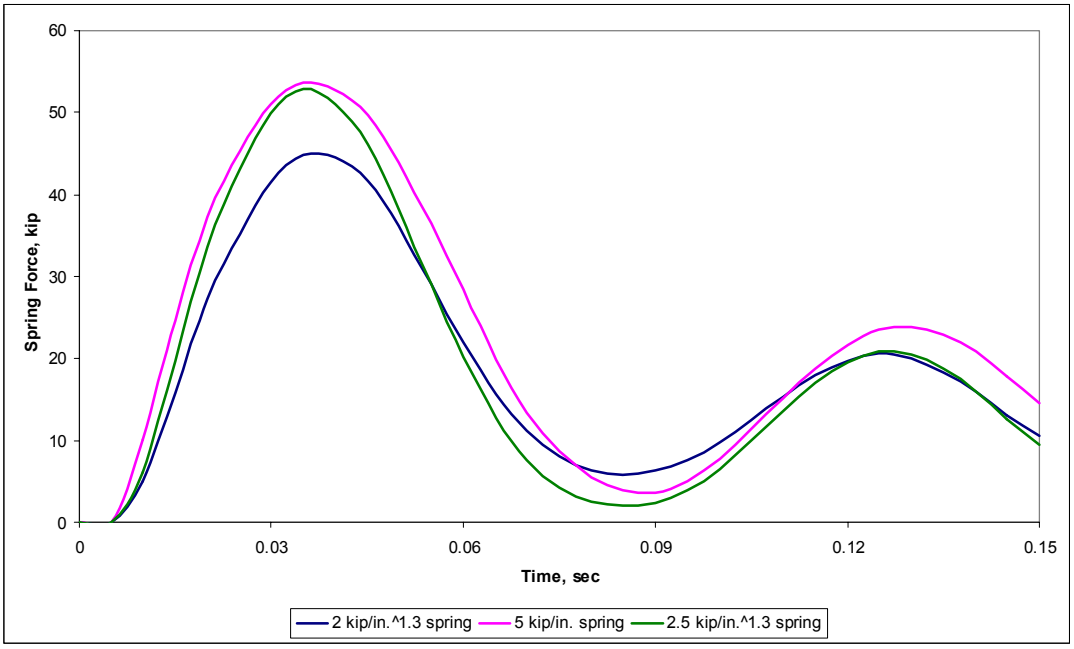

Fig. C.1. Comparison of time histories of 5 kip/in. bilinear and corresponding nonlinear spring forces for frame subjected to a 4,000 psi blast

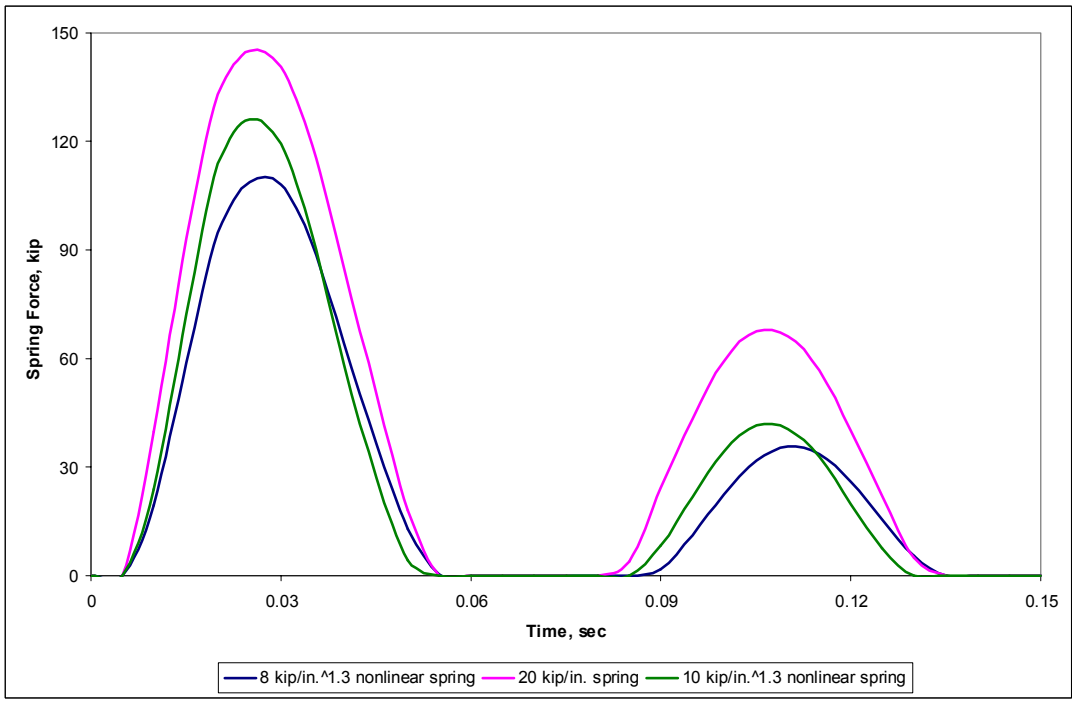

Fig. C.2. Comparison of time histories of 20 kip/in. bilinear and corresponding nonlinear spring forces for frame subjected to a 4,000 psi blast

Vita

Michael Rembert Motley was born in Charleston, South Carolina on April 20, 1982, where he lived for the duration of his youth, graduating from St. Andrew's Parish High School in June 1999. He attended The Citadel in Charleston from 1999 to 2003 where he received his Bachelor of Science Degree in Civil and Environmental Engineering. He moved on to Virginia Polytechnic Institute and State University as a Via Fellow in the summer of 2003 where he continued his studies in pursuit of a Master of Science Degree in Structural Engineering in the Via Department of Civil and Environmental Engineering. He completed his Master's Degree program in December of 2004.

_____

Michael R. Motley